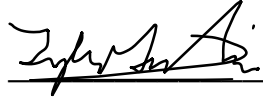


Aircraft Design for the 2023 AIAA DBF Competition

A Major Qualifying Project Report
Submitted to the Faculty of the
WORCESTER POLYTECHNIC INSTITUTE
in Partial Fulfillment of the Requirements for the
Degree of Bachelor of Science
in Aerospace Engineering

by:



Tyler Guertin



Nickolas Pellegrini



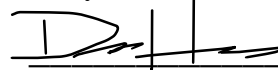
Noah Cook



Nicholas Fiorenza



Dylan Gerisch



Drake Hamblin



Newton Le



Joseph Salvato

April 25, 2023

Approved by: _____



David J. Olinger, Advisor

Associate Professor, Aerospace Engineering Program

WPI

Abstract

A remote-controlled 'jamming aircraft' has been developed for the 2023 AIAA DBF Competition. The modular aircraft, which fits disassembled in a specified shipping box, features an airfoil shaped fuselage and twin tail booms with a novel control surface linkage design. The empty aircraft was able to complete three laps of a required flight course with a flight speed of 55 miles per hour. In a second mission, the aircraft carried 32 percent of its gross weight of 7.825 lbs as an 'electronics payload' and completed twelve flight laps. In a third mission, a 5.75-inch long, PVC pipe 'jamming antenna' was carried on one wingtip while completing three flight laps in 69 seconds. The aircraft supported 5.5 lbs of added test weight when its 55-inch wingspan was hung between two wingtip fixtures.

Certain materials are included under the fair use exemption of the U.S. Copyright Law and have been prepared according to the fair use guidelines and are restricted from further use

Acknowledgements

The MQP team would like to thank the following individuals for their help and support throughout the entirety of this project:

- Project Advisor Professor David Olinger for his support and critique of the project work.
- Financial Administrator, Joanne Tripp, for her help in providing the logistics to the travel team.
- Competition Pilot Tim Dickey for giving his time in Tucson to fly the aircraft.
- Underclass Team Member Melina Iannacchione for offering her support in the competition.
- Central Massachusetts Radio Control Modelers for offering the use of their field and providing their experience in building RC aircraft.
- Randy Holtgreffe for his guidance and critique of the aircraft, as well as the material donations he has given for our airplane.

Table of Authorship

Section	Author(s)
1. Introduction	NP
1.1 Background and Literature Review	JS
1.2 Project Goals	NP
1.3 Project Design Requirements, Constrains, and Other Considerations	NP
1.4 Project Management	NP
1.5 MQP Objectives, Methods, and Standards	NP
1.5.1 MATLAB	NP
1.5.2 XFRL5	NP
1.5.3 Fusion 360	NP
1.5.4 MotoCalc8	NP
1.6 MQP Tasks and Timetable	NP
1.6.1 Final Aircraft	DH
2 Conceptual Design Approach	NP
2.1 Mission Requirements	NP
2.2 Sub-System Requirements	NP
2.3 Scoring Sensitivity Analysis	NL
2.4 Design Configurations Considered	NP
2.4.1 Wing Planform Shape	NP
2.4.2 Wing Vertical Position	NP
2.4.3 Fuselage Shape	NP
2.4.4 Tail Boom	NP
2.4.5 Tail Configuration	NP
2.4.6 Motor Configuration	NL
2.4.7 Landing Gear	NF
2.5 Resulting Aircraft Configuration	NP
3 Preliminary Design	TG
3.1 Design and Analysis Methodology	NP
3.2 Initial Aircraft Sizing	TG
3.3 Propulsion System	NL
3.3.1 Electric Motor Selection	NL
3.3.2 Battery	NL
3.4 Aerodynamics	TG
3.4.1 Required Coefficient of Lift	TG
3.4.2 Wing Aerodynamics	TG
3.4.3 Tail Aerodynamics	TG
3.4.4 Drag Analysis	TG
3.4.5 Wing-tip Antenna	TG
3.4.6 Predicted Take-Off Distance	TG
3.5 Stability and Controls	n/a

3.5.1	Flight Controllers	NL
3.5.2	Actuators	NP
3.5.3	Static Stability	TG
3.5.4	Center of Gravity and Neutral Point Comparison	TG, NL
3.5.5	Dynamic Stability	NL
3.6	Structural Analysis	TG, DG
3.6.1	Fuselage	JS
3.6.2	Tail Attachment Structure	NC
3.6.3	Wing Attachment Structure	NC
3.6.4	Landing Gear	NF
3.6.5	Wing Structure	TG
3.6.6	Electronics Payload	JS
3.7	Predicted Flight Performance	NF
3.8	Mission Uncertainty	NL
4	Detailed Design	TG
4.1	Summary of Aircraft Parameters	TG
4.2	Final Sub-System Architectures	DG
4.2.1	Propulsion System	NL
4.2.2	Flight Control System	NL
4.3	Structure	TG, DG
4.4	Aircraft Weight and Balance	NF
4.5	Final Aircraft Performance	NL
4.6	Predicted Mission Performance	NF
4.7	Drawing Package	DH
4.8	Ground Test Hardware	MI
5	Manufacturing Plan	NL
5.1	Processes	NL
5.1.1	Balsa Construction	NL
5.1.2	3D Printing	NC
5.1.3	Adhesives	DH
5.1.4	Hardware	JS, DH
5.1.5	Metal Component Manufacturing	JS, DH
5.2	Manufacturing Selection	NL
5.2.1	Wing Construction	NL, JS
5.2.2	Fuselage Construction	NL
5.2.3	Landing Gear	NL, JS
5.2.4	Tail and Tail Boom	NL
5.2.5	Payloads	JS
5.2.6	Ground Test Fixture	MI
6	The Testing Plan	TG
6.1	Ground Testing	TG
6.1.1	Propulsion Test	TG
6.1.2	Wind-Tunnel Test	TG
6.1.3	Ground Mission Test	TG
6.1.4	Range Test	NL

6.2	Glide Tests	TG
6.3	Flight Testing	TG
6.3.1	Prototype 1 Testing	TG
6.3.2	Prototype 2 Testing	TG
6.4	Check Lists	JS, TG
6.5	Testing Schedule	TG
7	Performance Results	TG
7.1	Ground Testing Results	NF, NL
7.1.1	Range Testing Results	NL
7.1.2	Wind Tunnel Testing Results	NF, TG
7.2	Flight Testing Results	NL
7.2.1	Glider Performance – “The Ukraine”	NL
7.2.2	Prototype 1 Performance- “The Lizard”	TG, JS
7.2.3	Prototype 2 Performance – “Flappy Bird”	DG
7.2.4	Final Aircraft Performance – “Beluga”	NF
8	Conclusion	n/a
8.1	Summary	NP
8.2	Conclusions	NP
8.3	Recommendations for Future Work	DH
8.4	Project Broader Impacts	NL

Table of Contents

1	Introduction.....	11
1.1	Background and Literature Review.....	13
1.2	Project Goals	14
1.3	Project Design Requirements, Constrains, and Other Considerations	15
1.4	Project Management.....	16
1.5	MQP Objectives, Methods, and Standards	18
1.5.1	MATLAB.....	18
1.5.2	XFLR5	19
1.5.3	Fusion 360.....	19
1.5.4	MotoCalc8.....	19
1.6	MQP Tasks and Timetable.....	19
1.6.1	Final Aircraft.....	21
2	Conceptual Design Approach	22
2.1	Mission Requirements.....	22
2.2	Sub-System Requirements	24
2.3	Scoring Sensitivity Analysis	27
2.4	Design Configurations Considered	29
2.4.1	Wing Planform Shape	30
2.4.2	Wing Vertical Position.....	31
2.4.3	Fuselage Shape.....	32
2.4.4	Tail Boom	33
2.4.5	Tail Configuration.....	33
2.4.6	Motor Configuration	34
2.4.7	Landing Gear	35
2.5	Resulting Aircraft Configuration	36
3	Preliminary Design	37
3.1	Design and Analysis Methodology	37
3.2	Initial Aircraft Sizing	38
3.3	Propulsion System.....	41
3.3.1	Electric Motor Selection	41
3.3.2	Battery.....	43

3.4	Aerodynamics.....	43
3.4.1	Required Coefficient of Lift.....	44
3.4.2	Wing Aerodynamics	45
3.4.3	Tail Aerodynamics.....	49
3.4.4	Drag Analysis.....	50
3.4.5	Wing-tip Antenna.....	52
3.4.6	Predicted Take-Off Distance.....	55
3.5	Stability and Controls.....	56
3.5.2	Flight Controllers	56
3.5.2	Actuators	57
3.5.3	Static Stability.....	58
3.5.4	Center of Gravity and Neutral Point Comparison.....	59
3.5.5	Dynamic Stability	60
3.6	Structural Analysis	63
3.6.1	Fuselage	63
3.6.2	Tail Attachment Structure.....	65
3.6.3	Wing Attachment Structure	67
3.6.4	Landing Gear	68
3.6.5	Wing Structure	69
3.6.6	Electronics Payload.....	72
3.7	Predicted Flight Performance.....	73
3.8	Mission Uncertainty	75
4	Detailed Design.....	76
4.1	Summary of Aircraft Parameters.....	76
4.2	Final Sub-System Architectures.....	78
4.2.1	Propulsion System	78
4.2.2	Flight Control System.....	80
4.3	Structure	81
4.4	Aircraft Weight and Balance.....	82
4.5	Final Aircraft Performance.....	84
4.6	Predicted Mission Performance	84
4.7	Drawing Package.....	85

4.8	Ground Test Hardware	1
5	Manufacturing Plan.....	1
5.1	Processes	1
5.1.1	Balsa Construction	2
5.1.2	3D Printing.....	3
5.1.3	Adhesives	3
5.1.4	Hardware.....	4
5.1.5	Metal Component Manufacturing.....	4
5.2	Manufacturing Selection	5
5.2.1	Wing Construction	6
5.2.2	Fuselage Construction.....	7
5.2.3	Landing Gear	8
5.2.4	Tail and Tail Boom	9
5.2.5	Payloads	10
5.2.6	Ground Test Fixture	11
6	Testing Plan	12
6.1	Ground Testing.....	12
6.1.1	Propulsion Test	14
6.1.2	Wind-Tunnel Test	14
6.1.3	Ground Mission Test.....	14
6.1.4	Range Test	15
6.2	Glide Tests.....	15
6.3	Flight Testing	16
6.3.1	Prototype 1 Testing	16
6.3.2	Prototype 2 Testing	16
6.4	Check Lists.....	17
6.5	Testing Schedule	18
7	Performance Results	18
7.1	Ground Testing Results	18
7.1.1	Range Testing Results.....	19
7.1.2	Wind Tunnel Testing Results.....	20
7.2	Flight Testing Results.....	21

7.2.1	Glider Performance – “The Ukraine”	21
7.2.2	Prototype 1 Performance- “The Lizard”	22
7.2.3	Second Prototype Performance – “Flappy Bird”	23
7.2.4	Final Aircraft Performance – “Beluga”	24
8	Conclusion	25
8.1	Summary	25
8.2	Conclusions	26
8.3	Recommendations for Future Work.....	27
8.4	Project Broader Impacts	27
9	References.....	29
10	Appendix.....	30
10.1	Appendix A: Wiring Diagram	30
10.2	Appendix B: Thrust-Drag MATLAB Code.....	31
10.3	Appendix C: Dynamic Stability MATLAB Code	35

1 Introduction

This Worcester Polytechnic Institute Design/Build/Fly (WPIDBF) 2022-23 MQP report documents in detail the conceptualization, design, manufacturing and testing of the *Beluga*, the Flying Goats AIAA DBF team submission to the American Institute of Aeronautics and Astronautics (AIAA) 2023 Design-Build-Fly competition. As specified in the AIAA DBF rules, the aircraft must complete one ground mission and three aerial missions. The purpose of the ground mission is to demonstrate the aircraft's ability to maintain its structural integrity and control surface actuation under a demonstrated load. The first aerial mission, M1, is a staging flight where the empty aircraft is to be flown around the course three times with no payload. M2 is the second aerial mission, where the aircraft must fly the course with an "electronics package" as many times as possible within ten minutes. The final aerial mission, M3, requires the aircraft to complete three laps with a PVC "jamming antenna" attached to one of the wing tips.

Beluga has been designed to meet and exceed all mission requirements while raising the bar on reliability and replication. The aircraft is a conventional taildragger configuration, powered by a single, puller motor, with a tapered, mid-wing configuration. A tapered, mid-wing configuration allows the aircraft to complete the required flight course with minimal drag while maintaining stability. The taildragger configuration allows for a shorter required takeoff distance, less than the required 60-foot limit. The motor drives a two-blade propeller and produces 7.2 lbs of thrust for the aircraft and additional payload.

The aircraft went through many design iterations starting in the preliminary design phase where the aircraft's features began to take shape through propulsive, aerodynamic, and structural design. During the detail design phase, the use of various analysis tools including XFLR5,

SolidWorks, Motocalc8, and MATLAB validated the design choices at the component and aircraft level. The goal of this stage was to further iterate on the aircraft to create a high-performing aircraft capable of completing the missions outlined in the DBF rules.

The final aircraft overall dimensions were set based on shipping box size trade studies, aerodynamic analysis, and aircraft stability studies. Without its payload *Beluga* weighs 5.6 lbs., loaded, the aircraft weighs 7.5 lbs, and generates 9 lbs of lift at cruise. With an aspect ratio of 6.4, the wings span 56.3 inches with a cruise-configuration wing loading of 28 ounces per square foot in the staging flight configuration, and 37 ounces per square foot in mission 2 configuration. The internal fuselage configuration is designed so that the “electronics package” for M2 would not greatly alter the center of gravity. The propulsion system design gives the aircraft a 1.3:1 thrust-to-weight ratio empty and 1:1 thrust-to-weight ratio with payload, racing to a maximum cruise velocity of 58.7 feet per second.

The aircraft is constructed using primarily balsa wood and carbon fiber with the support of aluminum and polylactic acid (PLA) printing material. The tail assembly is comprised of the same materials as the fuselage and wings, which ensured consistency in construction. Each assembly is made using a combination of laser cutting and 3D printing. Each component is precision covered with a heat-reactive shrink wrap to reduce the overall drag force experienced during flight.

Beluga's performance was estimated using simulations and validated using flight tests that have been conducted since January 2023. *Beluga* is a flight proven aircraft that flies consistently well. The aircraft takes off within 48 feet with payload, which is well within the 60 feet mark. At an internal WPI mock DBF competition in mid-February against one other WPI design group, *Beluga* scored the maximum 1 point for M1. The GM, M2, and M3 scores are conservatively

calculated assuming our scores are 80% of eventual max scores at the full competition. In the ground mission 2.2 lbs of added weight was applied without wing failure, yielding a GM score of 0.8. *Beluga* did not complete M2 at the mock competition due to a transmitter communication loss issue, however we estimate that it will complete 7 laps with a 2.4 lb. payload and score 1.6 points. With a 4.5-inch jamming antenna attached, the aircraft completed M3 in 92.7 seconds with an estimated score of 2.6.

In Tucson, *Beluga* placed 44th out of 99 overall. It was able to complete both the ground Mission and Mission 1, however increased altitude and hotter air caused the aircraft to fail to take off within the 60 ft runway. This placing is the best WPI placing at DBF to date.

1.1 Background

Prior to rule release, the team focused primarily on reviewing past DBF documentation including rules and previous reports. Without the 2023 rules, it was difficult to know exactly what to prepare for, so the goal was to look for similarities across previous rulings to help gain a general idea of what our aircraft needed to accomplish. The primary rules we looked at were from 2018, 2019 and 2022. Based on our findings, each year were required to fly the same course and all followed similar general rules on safety such as battery sizing, propulsion systems and radio systems. There were also rules around configuration of aircraft where the aircraft was required to not take the form of a lighter-than-air or rotary wing. The aircraft needed to be prop-driven without the assistance of any external propulsion. When it came to mission requirements, they all changed from year to year. However, a consistent factor when it came to each year's mission requirements is that there was a need to carry some form of payload. Room for payload became an important aspect for our aircraft moving forward.

With the release of the 2023 rules, we began to look more closely at these current years ruling for what was required for our aircraft. We made a list of requirements that were needed for our aircraft to be valid under the 2023 rules. Throughout the project, we would check with this list as well as the rules themselves to make sure we were falling within compliance. In addition to this, over the course of the year the AIAA would release FAQs about the competition and rules that were asked to the director of DBF. These FAQs were useful information in further making sure that our aircraft fell within compliance and that we would be able to pass each mission successfully.

1.2 Project Goals

This MQP aimed to achieve the following goals:

- Design an RC Aircraft to compete and win the 2023 AIAA Design, Build, Fly Competition (DBF). Complete DBF rules can be seen in Appendix X.
 - Design an RC aircraft that when disassembled fits in the allotted 62in. shipping box size, see section X.
 - Maximize Airspeed and Maneuverability
 - Minimize Weight
 - Carry both Payload Requirements, see section X.
 - Successfully Complete all Missions outlined in section X.
- Use the collective student knowledge accrued to apply aeronautical theory in a practical application.
- Explore topics of aerodynamics, controls, propulsion, and structures in a hands-on fashion.

1.3 Project Design Requirements, Constrains, and Other Considerations

The team was formed prior to the AIAA releasing the rules for the 2023 Design, Build, Fly Competition. The AIAA provided the rules to the 2023 DBF competition in September 2022.

Upon release, the team immediately began to consider how the unique requirements of this year’s mission would translate to the aircraft. Some of the general governing rules can be found in Table 1 below:

Table 1: Rule Summary

General Aircraft Parameters
All components of the airplane must fit inside an airline checked baggage compliant shipping box with a maximum length + width + height of 62.00 inches (outside dimensions) and a maximum weight of 50.00 pounds including the shipping box.
Each team must provide two sets of one left and one right wing section. All wing sections must fit inside the shipping box. The left and right wing sections together must make up at least 80% of the total wing span. The wings shall be permanently marked with “L1”, “L2”, “R1” and “R2”
The aircraft assembly and payload installation must be completed in less than 5 minutes.
The aircraft must take-off within 60 feet of the start/finish line. All ground contact points of the aircraft MUST be forward of the start/finish line
The aircraft must always remain in unaided visual control distance of the pilot. The Flight Line Judge may require turns to be made to remain in a safe visual control range at his discretion.
Payload Rules
Electronic Packages will be provided by each team and measure at least 3.00 x 3.00 x 6.00 inches and the weight may be varied to achieve mission objectives with a max weight declared at tech inspection. The minimum weight of the Electronics Package must be equal to or greater than 30% of the gross vehicle weight flown during that mission
Jamming Antennas will be provided by each team. Teams are allowed up to three different length antennas to optimize their mission score. All Jamming Antennas must be carried in the shipping box for all missions. The Jamming Antenna will be securely attached to the wing tip with two fasteners using an adapter of the team’s design; the Jamming Antenna must be capable of attaching to both wing tips without modification.
The Jamming Antenna interface on the wing tips must also be used to attach a ground test fixture using only the two fasteners for attaching the antenna adapter; teams will provide their own ground test fixture; the ground test fixture must be strong enough to support the aircraft during the ground mission and prevent grounding (must not touch anything but the fixture interface) of the airplane during the ground test.

Included with the rules is the scoring rubric for both the design report and the flyoff missions. The flight score is given by the following series of equations:

$$Total\ Mission\ Score = M1 + M2 + M3 + GM$$

Where $M1 = 1$ for a successful completion of Mission 1 and

$$M2 = 1 + \left[\frac{N_-(Payload\ weightht \cdot \# \ laps \ flown)}{Max_-(Payload\ weightht \cdot \# \ laps \ flown)} \right]$$

$$M3 = 2 + \left[\frac{N_-\left(\frac{Antehna\ Length}{Mission\ Time}\right)}{Max_-\left(\frac{Antehna\ Length}{Mission\ Time}\right)} \right]$$

$$GM = \left[\frac{N_-\left(\frac{Total\ Test\ Weight}{Max\ Aircraft\ Weight}\right)}{Max_-\left(\frac{Total\ Test\ Weight}{Max\ Aircraft\ Weight}\right)} \right]$$

From here, the goal is to maximize the score by designing an aircraft that excels most in the areas that have the highest impact on the score. In order to determine which aircraft parameters will affect the score most, a score sensitivity analysis is conducted which shows each characteristic's effect on the score.

1.4 Project Management

The Worcester Polytechnic Institute (WPI) AIAA DBF Student Team was initially comprised of 15 seniors and 8 underclassmen in fall 2022. In addition to the students, the student team had two faculty advisors from WPI's Aerospace Engineering Department. This original

WPI student team was split into two Design Groups 1 and 2 consisting of 7 and 8 WPI seniors, respectively, with the 8 underclassmen supported the efforts of both groups. These two design groups competed in an internal WPI competition including a mock flyoff in mid-February 2023 to select one group's design (Group 2) to represent WPI at the 2023 AIAA DBF Flyoff in Tucson, AZ in April 2023. From this point forward in this report, we only summarize the design work and final aircraft of Design Group 2, hereafter referred to as the WPI Student Team.

The 8 seniors of the WPI Student Team were organized into four sub-groups consisting of Aerodynamics, Propulsion, Structures & Fabrication, and Controls & Stability, as shown in Table 2. The key design and analysis tasks that each sub-group was responsible for are shown along with a 5th column, which lists sub-group interactions. In addition, project advisors and underclassmen members and projects are listed in Table 3.

Table 2: Sub Team Breakdown

Aerodynamics	Propulsion	Structures & Fabrication	Controls and Stability	Sub-Group Interactions
Tyler G. Nick F.	Newton L. Drake H.	Noah C. Dylan G.	Nick P. Joseph S.	ALL
<ul style="list-style-type: none"> - Design airfoil & wing planform shape - Lift & drag analysis - Fuselage shape preliminary designs - Wing and tail locations 	<ul style="list-style-type: none"> - Motor and propeller selection - Thrust calculations - Scoring sensitivity analysis - ESC and servo tuning 	<ul style="list-style-type: none"> - Structural analysis - Internal component configuration - Center of gravity calculation - Internal structures design 	<ul style="list-style-type: none"> - Design control surfaces - Neutral Point calculation - Control surface sizing & actuation - Trim analysis - Servo selection 	<ul style="list-style-type: none"> - Fuselage shape selection - Radio transmission - Fabrication - Rule conformance - Whiteboard design brainstorming

- Wing-tip attachment design			- Dynamic stability analysis	-Design reviews
------------------------------	--	--	------------------------------	-----------------

Table 3: Advisor and Underclass Student Team Member Breakdown

Advisors	Underclass Members - Project
Professor David Olinger	Graham Driscoll-Carignan – Ground Test Fixture Melina Iannacchione – Ground Test Fixture Justin Shen – Testing Assistant Catalina Mudgett – Storage Box Manufacturing

1.5 MQP Objectives, Methods, and Standards

The team used a variety of tools and resources to formulate and iterate the design for the aircraft. The use of a variety of simulation software allowed for changes to be made and implemented in a timely manner, as the team was constrained by the competition deadline. CAD was used to model and manufacture the aircraft. Various simulation software was used to evaluate key parameters such as load capabilities, stability, and aerodynamics to ensure the aircraft would excel at the competition. The tools used are defined further in the following.

1.5.1 MATLAB

MATLAB was used throughout the design process for a variety of tasks ranging in complication. Many of the aerodynamic, control, structural and other components were designed using the aid of MATLAB. Additionally, the graphs produced from select MATLAB codes are presented throughout the report.

1.5.2 XFLR5

XFLR5 is used to simulate airfoils at various airspeeds under user input conditions. This program was used in conjunction with Excel to iterate on different airfoil shapes and ultimately produce the airfoil used on the aircraft.

1.5.3 Fusion 360

Fusion 360 is the driving force of the project. The team uses a CAD driven approach to the project, meaning that any changes are not final until they are reflected in CAD. This allows parts repeatedly manufactured with high consistency, which allows for the ability to comprehensively test and iterate on each component of the aircraft.

1.5.4 MotoCalc8

MotoCalc8 is used to simulate different motor and propeller combinations. This software is used to select the entire powertrain of the aircraft, the motor, propeller, and battery combination. Various combinations are simulated using this software until the optimal configuration is arrived at for this competition.

1.6 MQP Tasks and Timetable

To ensure compliance with all competition deadlines, Table 4 shows planned timing of major tasks was developed to schedule team milestones up through the competition date. The dates included in the chart are categorized into four different categories, Competition Deadlines, Design, Fabrication, and Testing. Most deadlines were kept, except for finalization of design taking longer than anticipated due to flight-testing developments. Completion dates for different tasks from August 2022 - February 2023 are shown. Dates shown after February 2023 are anticipated completion dates.

Table 4: Expected and Actual Completion Dates

Competition Deadlines	Expected Completion Date	Completion Date
Proposal	October 25 th , 2022	October 25 th , 2022
Design Report	February 14 th , 2023	February 14 th , 2023
Sensitivity Analysis	October 15 th , 2022	September 30 th , 2022
Flight Readiness Video	April 1 st , 2023	February 7 th , 2023
Competition Fly-off	February 18 th , 2023	February 18 th , 2023
Design	Expected Completion Date	Completion Date
Mission Leg Analysis	August 31 st – September 15 th , 2022	October 15 th , 2022
Decision Matrix	September 1 st – September 25 th	October 15 th , 2022
Preliminary Design	September 15 th – December 12 th , 2022	October 1 st – December 9 th , 2022
Detailed Design	November 1 st – January 31 st , 2023	November 27 th , 2022 – February 8 th , 2022
Simulations and Analysis	November 1 st – February 24 th , 2023	October 15 th , 2022 - February 14 th , 2023
CAD Model of Aircraft	September 15 th – November 15, 2022	October 1 st , 2022 – February 24 th , 2022
Fabrication	Expected Completion Date	Completion Date
Manufacturing Plan	November 1 st – December 1 st , 2022	November 15 th , 2022
3D Printed Wing Test	November 1 st -December 15 th , 2022	December 9 th , 2022
Glider Construction	December 1 st -December 31 st , 2022	October 30 th – November 5 th , 2022
Manufacturing Prototypes	December 1 st -January 15 th , 2023	November 27 th – January 27 th , 2023
Construction	December 1 st - February 24 th , 2023	November 27 th - February 10 th , 2023
Final Fine-Tuned Design	March 1 st to April 1 st , 2023	February 8 th , 2023
Testing	Expected Completion Date	Completion Date
Scale Wing Testing	November 15 th – December 15 th , 2022	December 9 th , 2022
Glider Testing	December 1 st – December 15 th , 2022	November 5 th – December 1 st , 2022
Flight Testing	December 15 th – March 30 th , 2023	December 5 th , 2022 – February 18 th , 2023
Payload Flight Testing	January 15 th – March 30 th , 2023	February 7 th , 2023
Wing-Tip Flight Testing	January 15 th – March 30 th , 2023	February 9 th , 2023
Ground-Testing	February 1 st – March 30 th , 2023	February 9 th , 2023

1.6.1 Final Aircraft

The completed tasks and timetable resulted in the final design of the Beluga aircraft shown in Figure 1 below. The next chapters in this report outline the design, analysis and testing methods used to develop this aircraft.

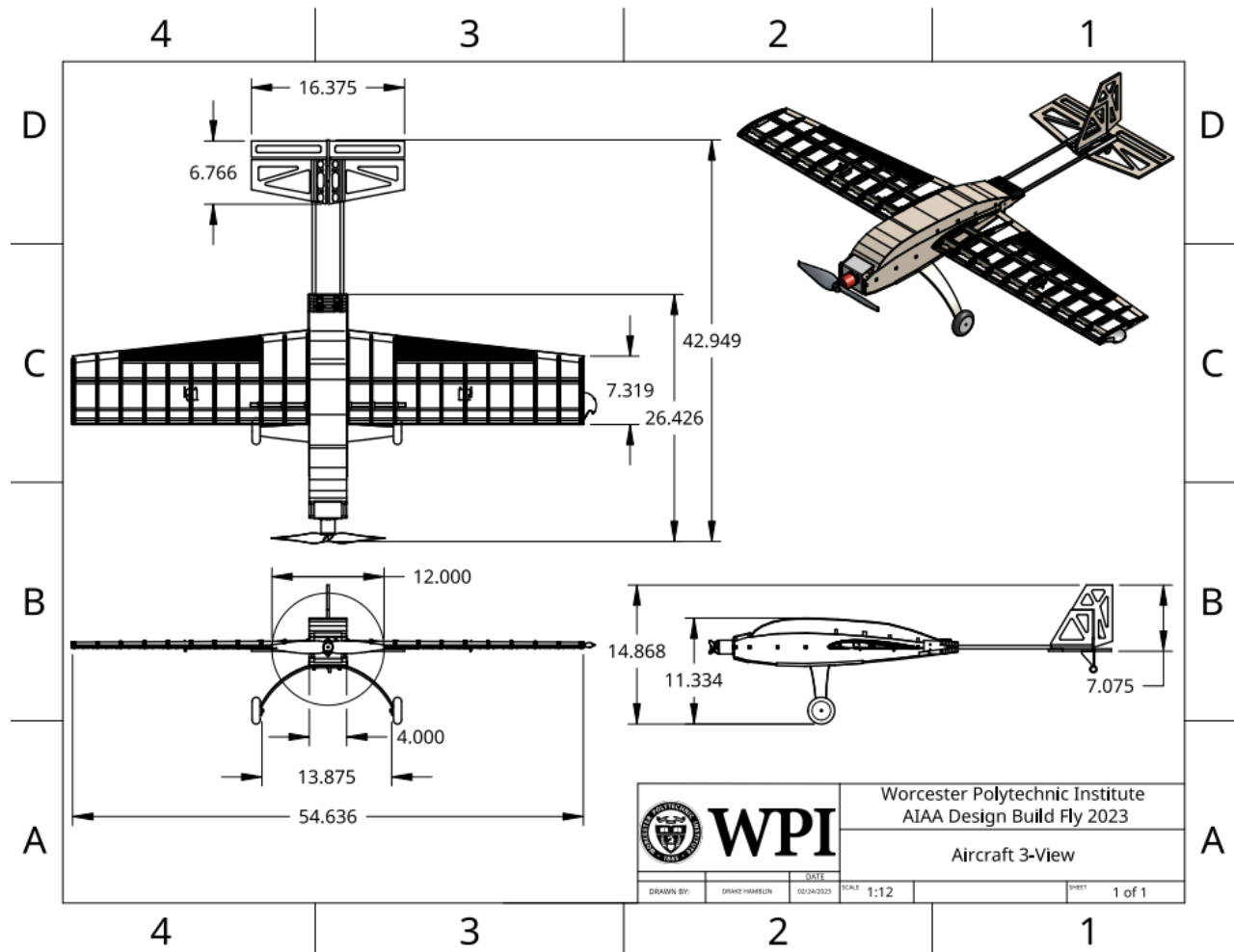


Figure 1: Beluga Final Iteration

2 Conceptual Design Approach

2.1 Mission Requirements

The Electronic Warfare mission for the 2023 AIAA Design/Build/Fly Competition consists of 3 aerial missions accompanied by one ground mission. In the staging flight, the aircraft is required to perform 3 laps to ensure flyability and controllability. In the surveillance flight, a team-designed payload must be flown, allotted to 30 percent of the mission weight of the aircraft. For the jamming flight, a jamming antenna must be attached to a single wing tip for flight. With a fixed runway length of 60 feet, the team is required to stage and deploy the aircraft within 5 minutes. Then, the aircraft must complete the course and associated maneuvers as specified in the 2023 AIAA DBF Rules [1]. The overall competition score will be calculated using the below function of the design report score:

$$Score = Design\ Report\ Score \cdot Total\ Mission\ Score + P \quad (Eq.2.1)$$

Where the value of P is determined using Table 5:

Table 5: Participation Point Chart from AIAA

P Value	Extent of Participation
1	Attending the Fly-off
2	Completing Tech Inspection
3	Attempting a Flight Mission

And the Total Mission Score is given as:

$$Total\ Mission\ Score = M1 + M2 + M3 + GM \quad (Eq. 2.2)$$

Although three aerial missions are required to be completed in order, the ground mission can be completed at any time. A desirable A detailed breakdown of specific mission requirements is as follows.

The Course:

The flight path is in the shape of a stadium with its parallel sections spanning 1000 feet each. Simultaneously, the runway was limited to 60 feet for all takeoff and landing involved. A map of the course can be seen in Figure 2.

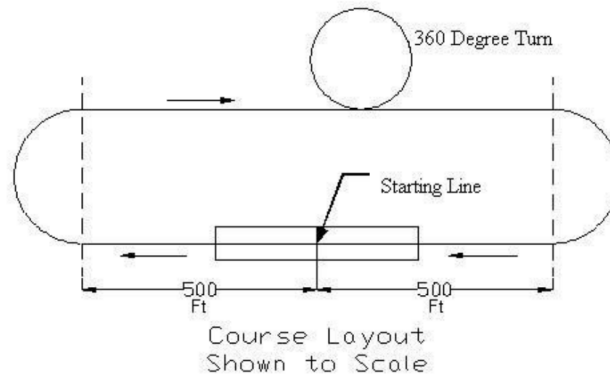


Figure 2: Nominal Flight Course Layout

Mission 1, Staging Flight

Mission 1 is the staging flight mission, where the empty aircraft is to be flown around the course with no payload. The aircraft must complete 3 laps around the course within a 5-minute window, however landing time is not included in these 5 minutes. The score for this mission is based solely on completion with $M1 = 1$ for a successful mission.

Mission 2, Surveillance Flight

This mission requires the team to carry an "electronics package" around the course. The goal is to complete as many laps as possible within the 10-minute window. Payload, as defined as an "electronics package" which, created by the team, was required to be at least 3"x3"x6", and account for at least 30% of the gross aircraft weight (including the payload). Additionally, no parts of the package could be carried outside of the aircraft. The surveillance flight mission lasts for 10 minutes and requires the competitors to complete as many laps as possible within the time limit. The

scoring for this mission relied on payload weight and laps completed, represented by the equation below:

$$M2 = 1 + \left[\frac{N_{-}(\text{Payload weight} \cdot \# \text{ laps flown})}{\text{Max}_{-}(\text{Payload weight} \cdot \# \text{ laps flown})} \right] \quad (\text{Eq. 2.3})$$

Mission 3, Jamming Antenna Flight

The payload for this mission is a PVC “jamming antenna” that is attached to the end of one wing. For this mission, the team is also allowed to add a wing tip to the opposite wing to counteract the drag effects of the jamming antenna. The goal of the final mission is to complete 3 laps within 5 minutes while minimizing completion time and simultaneously maximizing antenna length, shown in the following equation:

$$M3 = 2 + \left[\frac{N_{-} \left(\frac{\text{Antenna Length}}{\text{Mission Time}} \right)}{\text{Max}_{-} \left(\frac{\text{Antenna Length}}{\text{Mission Time}} \right)} \right] \quad (\text{Eq. 2.4})$$

Ground Mission

For this mission, a ground test fixture will be attached to each wing tip, and the aircraft will be loaded to its maximum payload. Next, a series of test weights will be applied to test the limit of the aircraft. The more test weight is applied, the more points the team garners from this mission.

$$GM = \left[\frac{N_{-} \left(\frac{\text{Total Test Weight}}{\text{Max Aircraft Weight}} \right)}{\text{Max}_{-} \left(\frac{\text{Total Test Weight}}{\text{Max Aircraft Weight}} \right)} \right] \quad (\text{Eq. 2.5})$$

2.2 Sub-System Requirements

From the specific aircraft requirements outlined in the rules, a compliance chart was formulated to ensure the aircraft is constructed in accordance with the rules. Each requirement was assigned to a sub-group as outlined in section 2.1. The requirements were validated through one of two methods, analysis (to be described in section 4.1) or tests (see section 7). As each

requirement was validated, compliance was denoted by A (Analysis) or T (Tests) respectively in Table 6. Mission scoring was outlined to exemplify needs of the aircraft dynamically. The team also developed a mission scoring breakdown seen in Table 7 which highlights important characteristics to consider during the design. The chart was later used to develop a decision matrix to select the general design characteristics that would best suit the aircraft.

Table 6: Aircraft Requirements Chart [1]

Requirement	Sub-Group/Method	Pass/fail
There must be two sets of left- and right-wing sections provided.	Aerodynamics, Visual	Pass, T
Wing sections must make up 80 percent of the total wing span.	Aerodynamics, CAD	Pass, A
All components of the airplane must fit inside a box of 62 in. (l+w+h) with weight under 50 lbs [1].	Aircraft, Tape Measure & Scale	Pass, T
Aircraft must not be lighter than air or rotary wing based.	Aircraft, CAD	Pass, A
Aircraft must be powered by on-board propulsion battery packs.	Aircraft, Visual	Pass, T
Take of gross weight must be less than 55 lb.	Aircraft, Scale	Pass, T
Team must submit proof that the exact aircraft being presented had been flown prior to contest date.	Aircraft, See Video Submission	Pass, A
The aircraft must be the same as documented in the report.	Aircraft, Comparison	Pass, A
Aircraft must have an externally accessible switch to turn on the radio control system.	Aircraft, Visual	Pass, T
Aircraft must have a mechanical motor arming fuse separate from the radio switch.	Aircraft, Visual	Pass, T
Aircraft radios must have fail safe mode that commands the following: Throttle closed, Full up elevator, Full right rudder, Full right aileron, Full Flaps down	Controls, Radio Transmitter	Pass, A
Must be propeller driven and electrically powered.	Propulsion, Visual	Pass, T

Must utilize an over-the-counter model electric motor.	Propulsion, Source	Pass, A
Each aircraft must use commercially available propellers and blades.	Propulsion, Source	Pass, A
The aircraft must connect a single battery to the propulsion system. Where the propulsion system is outlined as one battery, one externally accessible arming fuse, one or more ESCs, and one of more motors.	Propulsion, Visual	Pass, T
Battery packs must be identical and independently connected to its own propulsion system.	Propulsion, Visual	Pass, T
Each battery must have its own arming fuse.	Propulsion, Visual	Pass, T
Propulsion total stored energy cannot exceed 100 Watt-hours.	Propulsion, Source	Pass, A
Maximum rating of arming fuse must not exceed the maximum continuous discharge of the LiPo battery pack (up to 100 A).	Propulsion, Visual	Pass, T
There must be a means to safe the propulsion system.	Propulsion, Visual	Pass, T
Aircraft must be able to complete a 2.5 g load at the wing tip.	Structures, Load Test	Pass, T
Empty and loaded cg locations must be labeled on the aircraft.	Structures, Visual	Pass, T

Table 7: Mission Scoring Breakdown

Mission	Scoring Equation	Synopsis of Mission	Emphasized Characteristics
M1	$M1 = 1.0 \text{ for successful mission}$	Field assembly of aircraft. No payload. Take off within 60ft. Complete 3 laps within 5 minutes. Land on runway.	Easy Assembly. Stability unaffected when flying without payload. Able to land softly.
M2	$M2 = 1 + \left[\frac{N_{-}(\text{Payload weight} \cdot \# \text{ laps flown})}{\text{Max}_{-}(\text{Payload weight} \cdot \# \text{ laps flown})} \right]$	Payload is “electronics” package. Must be at least 3x3x6 inches. Complete as many laps as possible within 10 minutes.	Payload must not adversely affect stability of aircraft. Ability to carry over 30% of the plane’s gross weight as payload. High flight speed to maximize laps completed.
M3	$M3 = 2 + \left[\frac{N_{-} \left(\frac{\text{Antenna Length}}{\text{Mission Time}} \right)}{\text{Max}_{-} \left(\frac{\text{Antenna Length}}{\text{Mission Time}} \right)} \right]$	Payload is jamming antenna. Must complete 3 laps within 5-minute window. Antenna must be easily attached.	Wing tip counterweight. Ability to carry a large antenna. Aircraft must remain stable during flight while carrying antenna.
GM	$GM = \left[\frac{N_{-} \left(\frac{\text{Total Test Weight}}{\text{Max Aircraft Weight}} \right)}{\text{Max}_{-} \left(\frac{\text{Total Test Weight}}{\text{Max Aircraft Weight}} \right)} \right]$	Loading of heaviest payload. Structural test of aircraft wings. Actuation of control surfaces under load.	Structural stiff wings to increase carrying capacity. Minimize aircraft weight, maximize carrying capacity. Design ground fixture that meets test requirements.

2.3 Scoring Sensitivity Analysis

To evaluate the importance of the above outlined characteristics, the team conducted a sensitivity analysis consisting of twosteps. The first was an analysis of each mission’s parameters and the second was of each independent variable impacting all missions. To predict the scores for each mission, a standard distribution model based on the standard deviation of scores from the 2021-2022 Design Build Fly competition was created. The mean is derived from the score of assumed parameter values. With the mean and standard deviation, a coefficient of variation was

used to predict the distribution of scores based on the assumed mean score. The coefficient of variation (CV) is a statistical measure of the relative variability, or dispersion, of a dataset, expressed as a percentage of the mean. It is calculated as the ratio of the standard deviation (SD) to the mean, multiplied by 100.

$$CV = \frac{\sigma}{Mean} * 100\% \quad (Eq. 2.6)$$

It was found that airspeed is the most important factor in scoring. This is due to the positive impact it has on both the scores of Missions 2 and 3. While the payload weight and antenna length have similar impacts on score, an increase in payload weight slightly reduces the Ground Mission score, making antenna length the second most important score. Finally, the least important independent variables are the empty_plane weight and Ground Mission added weight. This is due to their effect being reduced by the maximum gross lift-off weight.

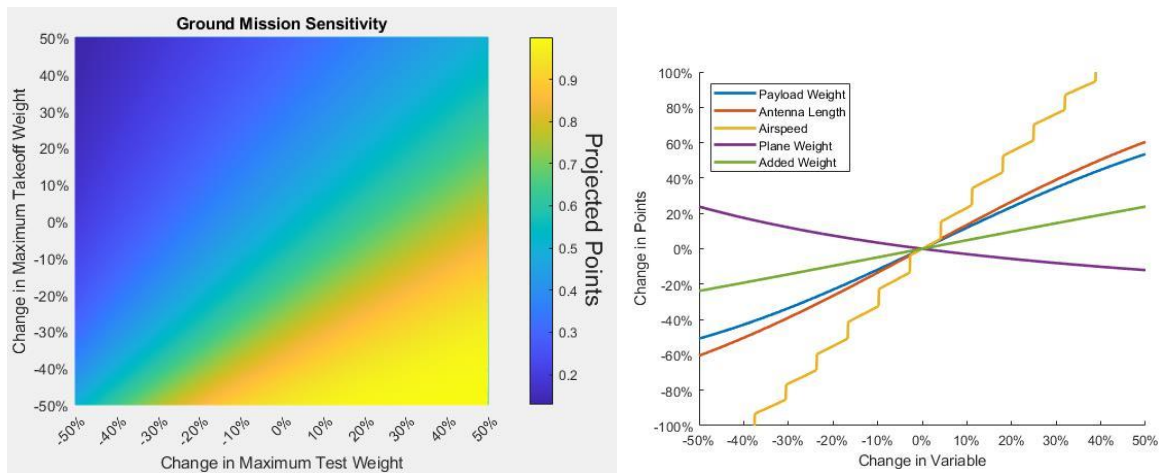


Figure 3: The scoring sensitivity charts. The left chart displays the percent change of the takeoff weight over the percent change in the ground mission test weight. The graph to the right displays all the missions and their relation to their respective percent change of points in the overall mission score.

2.4 Design Configurations Considered

Once the scoring analysis was complete, the team was able to see which parameters had the biggest impact on the score obtained. To compare multiple designs for different parts of the aircraft, the team generated a decision matrix based on the following categories.

Table 8: Effects of Aircraft Design Decisions

Category	Effects
Wing Planform Shape	Different wing planform shapes can affect aircraft lift-to-drag ratio, aircraft stability, and wing fabrication times. Good stability/maneuverability characteristics and relatively simple manufacturing processes were desired.
Wing Vertical Position	Wing location affects overall maneuverability and stability of the aircraft. Additionally, how and where wings are attached greatly affects the possible configurations of internal components, specifically the electronics package payload.
Fuselage Shape	Overall fuselage shape directly affects maximum payload size and limits the number of possible configurations for weight distribution. Fuselage shape also has a large effect on the overall drag and lift values of aircraft.
Number of Tail Booms	Type and configuration of tail boom(s) can greatly affect structural rigidity while also having a large effect on CG location. One tail boom is typical for most aircraft but is a clear potential torsion point and allows for more aggressive flutter during flight. Two or more tail booms reduces the potential for structural deflection or failures but does move the center of gravity towards the back of the aircraft, thus reducing stability.
Tail Design	The team determined that controllability and dynamic properties are nuanced and very similar across different tail designs, therefore ease of manufacturing and control system design was a major deciding factor.
Motor Configuration	While looking at motor configurations, it was determined that a pusher configuration has little overall benefit over a puller configuration but does raise considerable controllability and manufacturing concerns.
Number of Motors	Multiple motors results in increased thrust and therefore a higher flight speed. However, more motors would add weight and power requirements negating the benefits of the extra thrust gained.
Landing Gear	Location and configuration of the landing gear has a great effect on the complexity of the fuselage, with marginal changes in takeoff performance and controllability. Therefore, manufacturability and simplicity were desired characteristics.

To select an aircraft configuration, different design options for each of the categories in Table 8 above were considered with respect to the defined design variables of Manufacturability,

Dynamic Properties, Aircraft Controllability, Simplicity, Payload Capacity/Access, and Cost. The design options and variables are listed in the rows and columns, respectively, of the following scoring tables. Scores from 1 (low) to 5 (high) were assigned to weight each design option and aid the selection process. Manufacturability considered the component’s ability to be manufactured within the scope of resources and skills readily available. Dynamic properties focused on the components ability to perform high performance maneuvers, whereas Controllability considered the ease of controlling the aircraft through various maneuvers. Simplicity explored overall design simplicity from structures to control surface actuation. Payload Capacity/Access considered how each component would negatively affect the capacity or ability to access the payload. Each category is explored more in depth below.

2.4.1 Wing Planform Shape

The team considered six different wing combinations before ultimately deciding on one. Several configurations were quickly out ruled due to the velocity the aircraft will be flying at and controllability/structural issues. Additionally, as the team needed to be able to manufacture at least two sets of wings for competition, manufacturability was a major concern and further guided the team's end decision. However, as with the rest of the selections processes, a low drag component was also high priority as shown by the scoring sensitivity analysis.

Table 9: Wing Planform Shape Decision Matrix

Wing Type	Dynamic			Payload Capacity/			Score
	Manufacturability	Properties	Controllability	Simplicity	Access	Cost	
Rectangular	5	3.5	3	5	5	4	25.5
Elliptical	2	5	5	3	5	3	23
Tapered	4	5	5	4	5	3	26
Delta	2	1	3.5	1	5	3	15.5
Swept Back	3.5	3	4	1	5	3	19.5
Swept Forward	3	0.5	2	1	5	3	14.5

The total scores in Table 9 led to choose of a tapered wing design for the final aircraft.

2.4.2 Wing Vertical Position

Four different configurations were considered for the wing placement for low-speed aircraft. A high wing design is common in RC plane design, primarily because it tends to be the most stable design. This is because the high wing causes the fuselage of the plane to act as a pendulum when in the air which provides natural dynamic stability at the expense of rapid maneuverability. Additionally, a high wing provides sufficient ground clearance for takeoff. A low wing design excels in the categories that a high wing lacks, it provides a lower overall drag profile of the aircraft and makes rolling maneuvers easier, while sacrificing stability. A mid wing design reaps benefits of both the high wing and the low wing, providing more stability than the low wing, while not entirely sacrificing the performance of the low wing. A major disadvantage of the mid wing design is that the wing attachment often significantly interferes with payload capacity. The team also explored an oblique wing design; however, these have only been used in experimental applications and would not be feasible to design or manufacture within the given time frame.

Table 10: Wing Vertical Position Decision Matrix

Wing Location	Dynamic				Payload Capacity/		Score
	Manufacturability	Properties	Controlability	Simplicity	Access	Cost	
High Wing	5	3.5	4	4	3.5	4	24
Mid Wing	4	5	5	3.5	3	4	24.5
Low Wing	5	4	3	4	3.5	4	23.5
Oblique Wing	1	3.5	1.5	1	3	2	12

From the scores developed in Table 10, a Mid-wing design was selected.

2.4.3 Fuselage Shape

For the fuselage shape, the team considered four different designs. It was considered important to select a variety of options for the fuselage design as the team figured most overall shapes would be feasible for our team to design/manufacture. The shape of the fuselage, due to the size of it compared to the rest of the aircraft, was assumed to have a large impact on overall dynamic properties of the plane. Although some shapes received varying scores in the manufacturability column, dynamic properties and payload capacity were the main concern when selecting the shape for this component of the aircraft. Going down the list, manufacturability, controllability, and payload capacity were some of the most major factors influencing the final decision. Utilizing a rectangular body would made modular arrangements of payloads and systems very easy within the fuselage, but the dynamic properties, namely the aerodynamics of this component were called into question early. The airfoil shape was a favorite from the beginning of design discussions, having strong aerodynamic properties. A non-teardrop form would allow for the planform to appear as a rectangle from the top view, while supporting aerodynamic qualities of the aircraft. The cylindrical and tear-drop options were considered for their typical use in aviation, but both were less than ideal in the area of manufacturability and payload arrangements. Since the airfoil shape remained consistent in each category, and above average in 3/6 categories, it was chosen as the most desirable geometry for the fuselage.

Table 11: Fuselage Shape Decision Matrix

Shape	Dynamic			Payload Capacity/		Score	
	Manufacturability	Properties	Controllability	Simplicity	Access		Cost
Rectangular	3	3	5	3	3.5	2	19.5
Airfoil	3.5	3.5	5	3.5	4	4	23.5
Cylindrical	5	3	3	5	3	3	22
Tear-drop	3	2.5	4	1	3.5	3	17

An airfoil shape was selected based on the data developed in Table 11.

2.4.4 Tail Boom

The team considered two different options, either one or two tail booms. One would reduce weight in the back of the aircraft, thus increasing the static stability. However, the “twist factor” is a major concern for this configuration. Two increases the manufacturing time as well as weight, although the extra rigidity of the system would also most likely increase stability.

Table 12: Tail Boom Decision Matrix

Boom Configuration	Dynamic				Payload Capacity/		Score
	Manufacturability	Properties	Controllability	Simplicity	Access	Cost	
Two	4	4	5	4	4.5	3	24.5
Single	5	4	5	5	4.5	4	27.5

From the data in Table 12, a single boom was initially selected to attach the tail.

2.4.5 Tail Configuration

With a wide variety of tail configurations to choose from, the team developed a list of 7 of the most common. The lessened manufacturability and increased complexity of options with multiple stabilizers ruled out the more exotic dual, twin, Y, V, and inverted variants. This leaves a decision between a conventional tail, T-tail, and cruciform. A conventional tail design, although slightly more susceptible to lack of control due to motor and wing wash, was chosen thanks to its ease of manufacturing and design simplicity.

Table 13: Tail Configuration Decision Matrix

Tail Configuration	Dynamic				Payload Capacity/		Score
	Manufacturability	Properties	Controllability	Simplicity	Access	Cost	
Conventional	5	4	4	5	4	3	25
T-tail	4	4	5	4	4	3.5	24.5
Cruciform	3	4	5	4	4	3	23
Dual/Triple	3	4	3	3	4	2	19
Twin	3.5	3	3	3	4	4	20.5
Inverted Y	1	2	5	1	4	3.5	16.5
V/Inverted V	1	1	3	1	4	4	14

Based on the data from Table 13, a conventional tail configuration was employed.

2.4.6 Motor Configuration

Propeller aircraft can be configured as either a pusher or puller configuration. When comparing the two, the greatest concern was the structural conflict with the motor and tail boom. With a pusher aircraft, the motor must be mounted to the back of the fuselage, which would mean the motor and tail boom would conflict with each other. Either the tail boom would have to be moved to make clearance for the propeller, or the motor would have to be mounted higher or lower on the fuselage. This conflict would complicate the design since the alignment of the motor, wing, and tail would not be the same anymore.

The team also compared the benefits of a single motor versus a twin motor setup. Due to the empty plane weight being a driving factor for a higher score, having a second motor increases the weight of the plane considerably. Also, manufacturing a twin motor aircraft would be complex since the motors would need to be mounted on the wings of the aircraft.

Table 14: Motor Configuration Decision Matrix

Type of Motor Config.	Dynamic				Payload Capacity/		Score
	Manufacturability	Properties	Controllability	Simplicity	Access	Cost	
Pusher	4	4	5	3.5	2	5	23.5
Puller	4	5	5	4	5	4	27
Single Motor	5	4	4	5	4	5	27
Twin motor	3	4.5	5	3	5	3	23.5

The scores provided in Table 14 caused the selection of a single motor in a pusher configuration.

2.4.7 Landing Gear

There are three configurations the team considered for the aircraft's landing gear. Due to a lack of simplicity, and concern over sub-par dynamic properties, a tandem wheel design was easily ruled out. The decision to pursue a tail wheel design is down to its ease of manufacturability, and its ability to be adjustable to accommodate different take-off angle of attacks. In addition, the tail wheel design, is a lighter alternative to the tricycle requiring only two main struts compared to three for the tricycle.

Table 15: Landing Gear Decision Matrix

Landing Gear	Dynamic				Payload Capacity/		Score
	Manufacturability	Properties	Controllability	Simplicity	Access	Cost	
Tail Wheel	5	4	4	5	3	4	25
Tandem Wheel	2	2	2	1	3	3	13
Tricycle	4	3	3	5	3	4	22

From the scores outlined in Table 15, the tail wheel configuration was selected for the landing gear.

2.5 Resulting Aircraft Configuration

Combining the decisions from the above scoring tables, the resulting aircraft configuration has a tapered wing planform with a mid-position, an airfoil shaped fuselage, a conventional tail with a single tail boom, powered by a single puller motor, with a tail wheel landing gear configuration. Figure 4 depicts the first prototype developed using the configurations above.

As a result of the tests outlined in the following sections, some design configurations were modified in effort to produce the optimal aircraft for the mission. The wing vertical location and planform shape remain the same, as well as the landing gear and the conventional tail setup. The number of tail booms was changed to two, and the fuselage partially abandoned the airfoil shape. The justification for doing so is outlined in the subsequent sections. A final configuration drawing is shown in Figure 4.

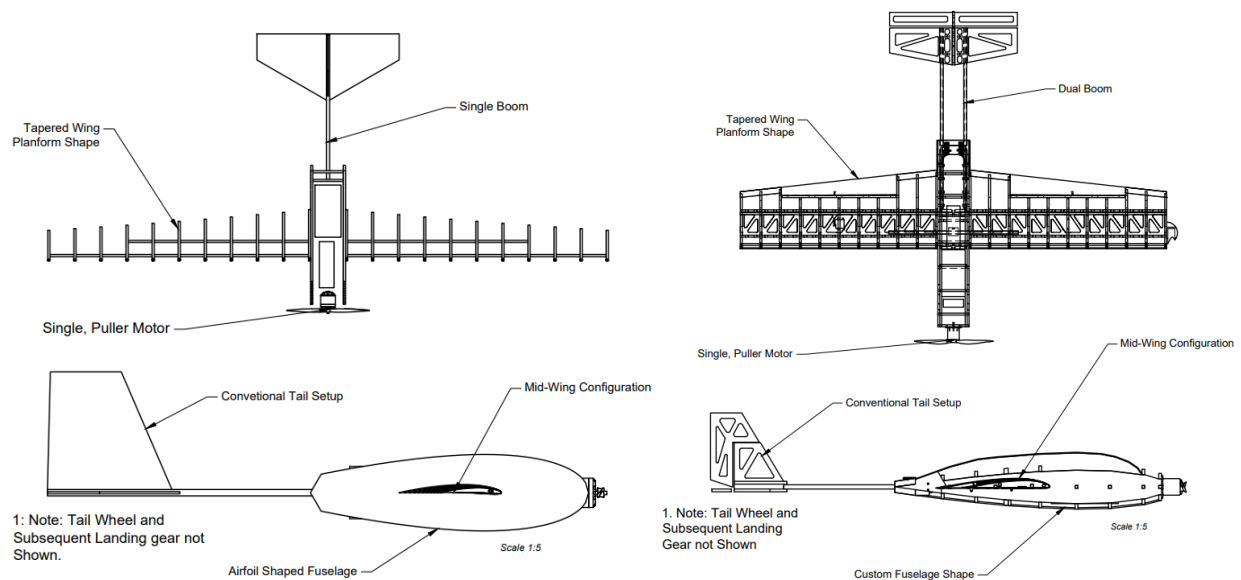


Figure 4: Initial (left) and Final (right) Conceptual Design Summary Drawing Comparison

3 Preliminary Design

3.1 Design and Analysis Methodology

Once all conceptual decisions were made, each sub-group was responsible for formulating the individual design components. To do so, the conceptual decisions were then used in conjunction with various methods to develop specific details for each component. The approach is summarized in Figure 5.

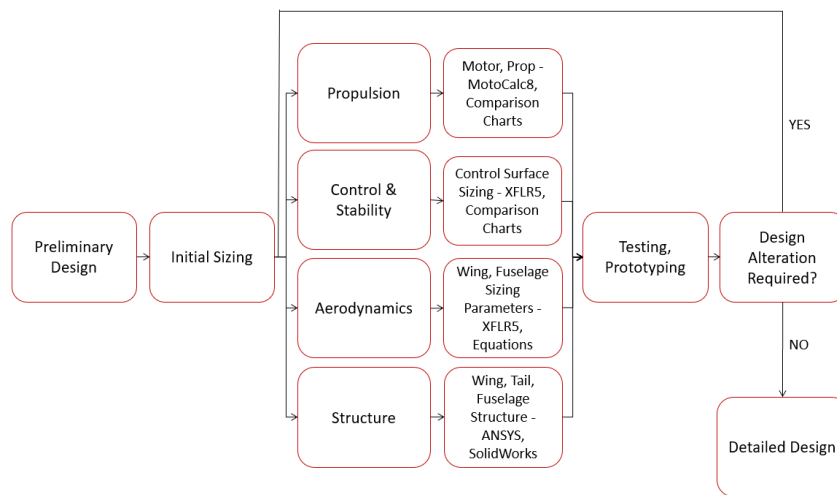


Figure 5: Preliminary Design Process Flowchart

Various methods of testing and comparison were used for each key area of the aircraft as summarized in Table 16. For the motors, comparison charts were used to directly compare key attributes. Aerodynamic analysis consisted of in-depth lift-drag analysis using aircraft design equations and ANSYS simulations. Lastly, structural decisions were made based on CAD simulations and physical durability tests of model wings. The goal of these decisions was to create a durable and maneuverable aircraft.

Table 16: Design and Analysis Methodology

Design and Analysis Methodology	
Initial Aircraft Sizing	Equations, Historical Data
Electric Motor Selection	MotoCalc8
Battery Selection	MotoCalc8, Comparison Charts
Center of Gravity	Solidworks, NDT
Stability	MATLAB
Airfoil Selection	XFLR5
Wing Area Sizing	Equations, XFLR5
Aspect Ratio	Equations
Drag Analysis	XFLR5, Equations
Wing-Tip Fixture Analysis	XFLR5, MATLAB
Flight Dynamics	Equations
Structural Simulations	Solidworks, ANSYS
Control Surface Sizing	MATLAB, Equations
Empennage Sizing	MATLAB, Equations

3.2 Initial Aircraft Sizing

The primary focus of early aircraft design was the design of a shipping box, capable of containing our aircraft and all tools used to assemble the aircraft at competition. Aspect ratios of previously built aircraft for WPI major qualifying projects were used to determine an initial sizing for the containment box. A primary goal was to allow a large wingspan and chord, while maximizing space for the fuselage and empennage attachments. Preliminary calculations with respect to wing root chord, C_r , span, b , and aspect ratio, AR , are shown below: The desired shipping box has a length that is around 75 percent of the wingspan of the aircraft, to allow space for each half-wing, with extra room for structural attachments.

$$l = (0.75 * b) \quad (Eq. 3.1) \quad AR = 6.5 = \frac{b^2}{S} \quad (Eq. 3.2) \quad S = b((0.7 C_r + C_r)/2) \quad (Eq. 3.1)$$

Solving for the root chord (which is essentially the desired box width), a function of span can be found from the aspect ratio of the aircraft. Root chord was calculated as “average chord” of

the tapered wing since extra space was desired for other components. From Fahad [6], the vertical stabilizer area was found to be around 10 percent of the aircraft wing area using the second equation below. This created a function of the aircraft height, which would be needed to define the minimum height of the aircraft box. This creates a function of the wingspan, meaning that the box could be defined based upon any given wingspan.

$$C_r = \frac{b}{5.525} = w \quad (\text{Eq. 3.2})$$

$$A_{vert} = S * 0.0495 \quad (\text{Eq. 3.3})$$

$$l + w + h = 62 = (0.75b) + \frac{b}{5.525} + 0.1 * \left(\frac{1}{6.5}\right) b^2 \quad (\text{Eq. 3.4})$$

Shown in Figure 6 is first-iteration aircraft sizing based upon a calculated box l, w, h, of 31 inches, 20.5 inches, and 10.5 inches respectively.

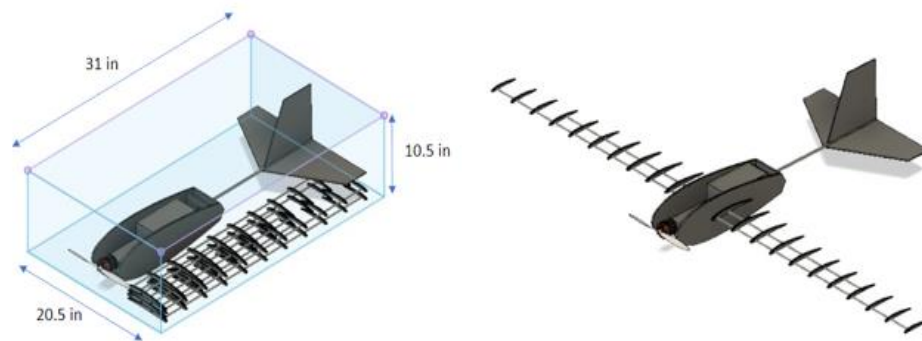


Figure 6: Initial aircraft configuration and Internal box dimensions

Assembling a sized conceptual sketch of the aircraft in this box, a few observations were made. Firstly, the wing loading, given the chord of the aircraft to be around 7 inches, was found to be greater than 20 oz/ft², a large figure for such an aircraft size. It was also observed that this box size would not allow space for the electric motor mounted to the front of the aircraft. With these issues known, the mean chord of the aircraft was increased to 10 inches, slightly increasing

the aspect ratio of the aircraft to 6.6. This resulted in a box that fit wings extremely well in a facedown configuration.

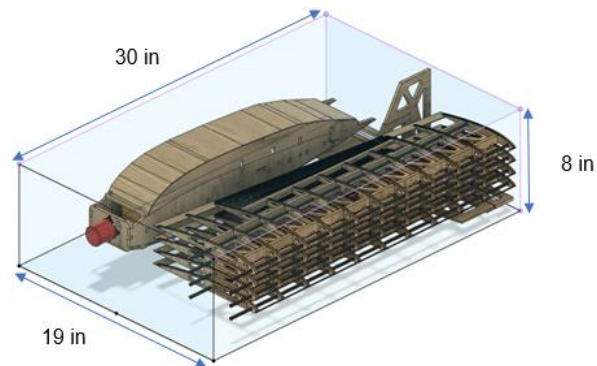


Figure 7: The arrangement of the aircraft in final box with interior dimensions

It should be noted that the dimensions shown in Figure 6 and Figure 7 are the required internal dimensions of the box. This would have made it impossible to manufacture the first iteration of the box and stay under 62 inches for the $L+W+H$. To decrease the required internal dimensions of the box, the arrangement of the aircraft within the box was changed. As seen in Figure 6, the tail was made removable so it can be stored on the bottom of the box allowing for room for the motor and for the body of the aircraft to be placed on top of the horizontal tail and the wings, being treated as flat rectangles in the configuration, to be stacked on top of each other next to the body with the vertical tail between them. With the new arrangement, the internal dimensions add up to 57 inches. As the plan was to manufacture the box using $\frac{1}{2}$ inch ply, the dimensions were expanded to account for the thickness and room as safety. Once assembled, the length would be 31 inches, the width 19.5 inches, and the height being 9.5 inches.

$$L + W + H = (30 + 1) + (19 + 0.5) + (8 + 1.5) = 61 \text{ in} \quad (\text{Eq. 3.5})$$

Based upon previously built aircraft for the design, build, fly competition, the general goal was to have an aircraft capable of flying at 45 miles per hour. Using this speed, and the general dimensions of the aircraft containment box, an analysis could be formulated to decide on wing

aerodynamic properties. Knowing that the box enables 8 inches of height-wise space, and 30 inches of lengthwise space, a general layout of the aircraft's dimensions could be deduced. With the payload requiring a minimum of 3 inches of space within the fuselage, it was determined that the fuselage should allow 0.5 inches of wall space for bulkheads in the fuselage, meaning there would be a fuselage width of 4 inches. The premise of this aircraft is to have dual-removable wings from each side for easy storage in the box. As discussed, this enables a chord of around 8 inches, and a one-side span of 30 inches. Of those 30 inches, 2 inches are allotted to the fuselage when looking at the assembled aircraft, as well as 2 inches allotted on the wingtips for antenna and ground-test fixture attachment.

3.3 Propulsion System

The following paragraphs describe the selection process for the aircraft's motor, propeller, battery, and receiver. Technical evaluations of motor properties and thrust performance data of different motors from MotoCalc8. By comparing the thrust properties on a thrust curve, as well as other properties such as weight, the best motor can be chosen.

3.3.1 Electric Motor Selection

The aircraft weight was estimated at 2.7 lbs, with a safety factor of 2 added to account for payload weight and potential increases, resulting in a total weight of 5.4 lbs. Using MotoCalc8 software with inputs of a 10-minute flight time, 5.4 lbs weight, and 40 mph airspeed, four motors were recommended (see Table 17) and their performance compared using the thrust curves in Figure 8.

Table 17: Motor Properties from MotoCalc8 software.

Motor	Scorpion SII-3014-1220	Sunnysky X3120-950Kv	Sunnysky X2820-1100Kv	A40-10L V4 8-Pole kv1100
RPM per Volt (Kv)	1220	950	1100	1100
Weight (oz)	4.55	5.3	5.1	9.7
Recommended Propeller	12 x 11	10 x 7	9 x 6	12 x 11

Based on the analyzed data from the motor properties table and thrust curves figure, the best motor was the Sunnysky X3120-950Kv. The A40-10L V4 8-Pole 1100Kv motor had a significantly higher mass and lower thrust performance, thus it was eliminated from consideration. The Scorpion SII motor exhibited superior performance at speeds exceeding 40 mph, however, the Sunnysky X3120-950Kv displayed greater thrust capability in the 0-40 mph range, which was deemed essential for successful completion of all three competition missions. The Sunnysky X2820-1100Kv motor demonstrated the lowest performance among the evaluated options and was accordingly excluded from consideration.

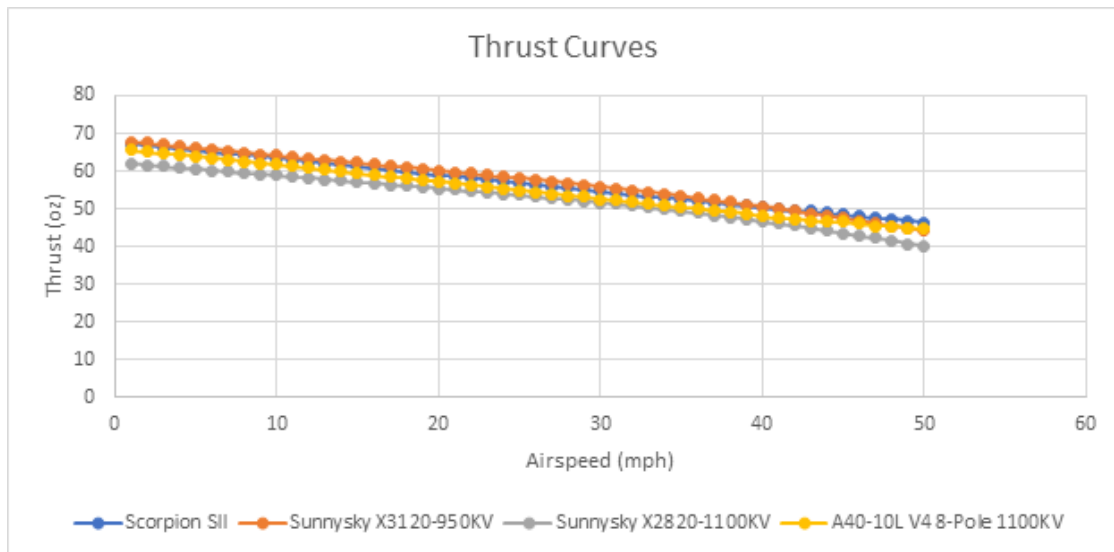


Figure 8: Thrust Curve Data of Motor Candidates from MotoCalc8 software

3.3.2 Battery

The competition rules limited the size and capacity of a battery to one battery pack, not exceeding the FAA limits of 100 watt-hours. The rules allow use of either LiPo (Lithium Polymer) or NiMH (Nickel-Metal-Hydride) batteries. LiPo batteries, which we chose to use, offer a higher energy density, power to weight ratio, discharge rate, efficiency, and reliability. After analyzing the motor selection data, as well as determining a maximum 10-minute flight time, a minimum battery capacity requirement of 100 watt-hrs was found which was lower than the limit allowed. TheMotoCalc8 test data recommended 4 cell battery, with 3200 mAh capacity, and 30C discharge rate to accommodate the selected motor. Taking into consideration a safety factor to account for higher capacity and discharge rate, as well as battery availability, the chosen battery was the Liperior Li-Poly battery that is 4s, 5000 mAh, and 35C. The battery chosen will sit below the 100 Wh limit at 74 Wh and provide a continuous current of 175 amps.

3.4 Aerodynamics

Aerodynamic sizing and design depended largely on the desired flight envelope of the aircraft. Analysis was based upon velocity, maximum payload weight, flight altitude, and thrust available to the aircraft. Desired specifications influencing aircraft design are shown below, with dimensions of wing components being driven by the design of the aircraft containment box.

With general sizing and speed parameters set, a study of the aircraft Reynolds number was conducted. The Reynolds number determined for the desired aircraft velocity of 45 mph (66 ft/s) was around 300,000 to 350,000 using an air density of 0.07765 lb/ft³ and kinematic viscosity of 3.7845e-7 lb-s/ft². The study was conducted for velocities of 40, 50, 60, and 70 ft/s, with chord-length representing the characteristic length when calculating Reynolds number.

$$Re = \frac{\rho V c}{\mu} \quad (Eq. 3.6)$$

Table 18: Target aircraft design parameters

Aircraft Purpose	Carry antenna payload and reserve lift for weighted payload
Desired Flight Speed @ cruise (mph)	45 mph
Cruise Altitude (ft)	300 ft
Max. Cargo Weight (lb)	0.3*(M2 Weight)
Range (# laps)	15 laps in 10 minutes
Ground Roll Distance Max. (ft)	60 ft
Total Aircraft Weight Estimate	7 lbs
Aircraft Wing Root Chord	10 inches
Aircraft Wing Aspect Ratio	6.43

3.4.1 Required Coefficient of Lift

Airfoil selection was made based upon the estimate of the desired aircraft weight. An aircraft weight of 7 lbs at maximum payload capacity was desired. With the first mission's goal being to complete 3 laps, excess lift due to the lesser weight of the aircraft will be ignored. A 7 lb weight with payload indicates an aircraft base weight of 4.9 lbs, with a minimum payload of 2.1 lbs. Given this desired weight, the required lift coefficient of the aircraft could be found by defining a function of the density at the competition site, the desired flight velocity, and the estimated aircraft planform area. The desired lift coefficient assumes steady level flight, where lift must be equal to weight.

$$C_{l_{required}} = \frac{W_{desired}}{\frac{1}{2}\rho V^2 S_w} \left(1 + \frac{2}{AR}\right) \quad (Eq. 3.7)$$

Assuming flight in Tucson, AZ, where the altitude is around 2300 ft above sea level, the air density is 0.07078 lb/ft³. Finding the planform area. A proposed chord of 10 inches and aspect ratio of 6.43, and an estimated wingspan of 60 inches based upon storage box dimensions. The lift

coefficient required for these flight characteristics was found to be 0.3509 given the input parameters. Since this was a non-dimensionalized approach, the lift coefficient of the aircraft was adjusted for the testing environment in Worcester, Massachusetts, where the lift coefficient is required to be lower, as 0.3257 because of its closer proximity to sea level. Since lift coefficient will not change, airfoil selection will attempt to replicate the lift coefficient required for the lower density atmosphere in Tucson.


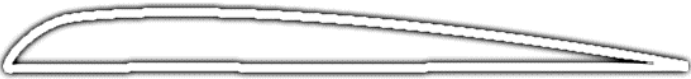


Table 19: Comparison of test location and competition location

Worcester, MA	Tucson, AZ
Altitude = 419 ft	Altitude = 2389 ft
$C_{l_{required}} = 0.3257$	$C_{l_{required}} = 0.3509$
$\rho_0 = 0.0762 \frac{lb}{ft^3}$	$\rho_{2500} = 0.0707 \frac{lb}{ft^3}$

3.4.2 Wing Aerodynamics

The aircraft wings required a high-lift airfoil while being structurally rigid and easy to manufacture. A study was conducted on various airfoils designed for the Reynolds number range of 250,000 to 300,000 appropriate for the estimated aircraft flight speed and wing dimensions discussed above. The kinematic viscosity was set using average air temperatures in Worcester, MA, our initial test location. Since this test location has a density that is only 7 percent larger than in Tucson, AZ, it could be assumed that the aircraft will perform similarly, and within the same Reynolds number range. Airfoil thickness was studied as an output variable since it was desired to have a thickness exceeding twice the thickness of the desired carbon fiber rods (1/4 inch) to be used as major structural elements of the wing. Several different airfoils were compared using XFLR5 software, as detailed in Table 20.

Table 20: Airfoil Selection Criteria

Airfoil Selection				
Airfoil	Max Thickness	Max Lift Coefficient (C _L)	Cruise (0 degree) Lift Coefficient	Max L/D
Clark Y	28.03%	1.44	0.4068	84.8
				
NACA 4108 Mod	29.03%	1.39	0.3901	51.3
				
NACA 4208 Mod	29.03%	1.39	0.3908	78.7
				
NACA 4308 Mod	29.03%	1.31	0.3971	86.0
				

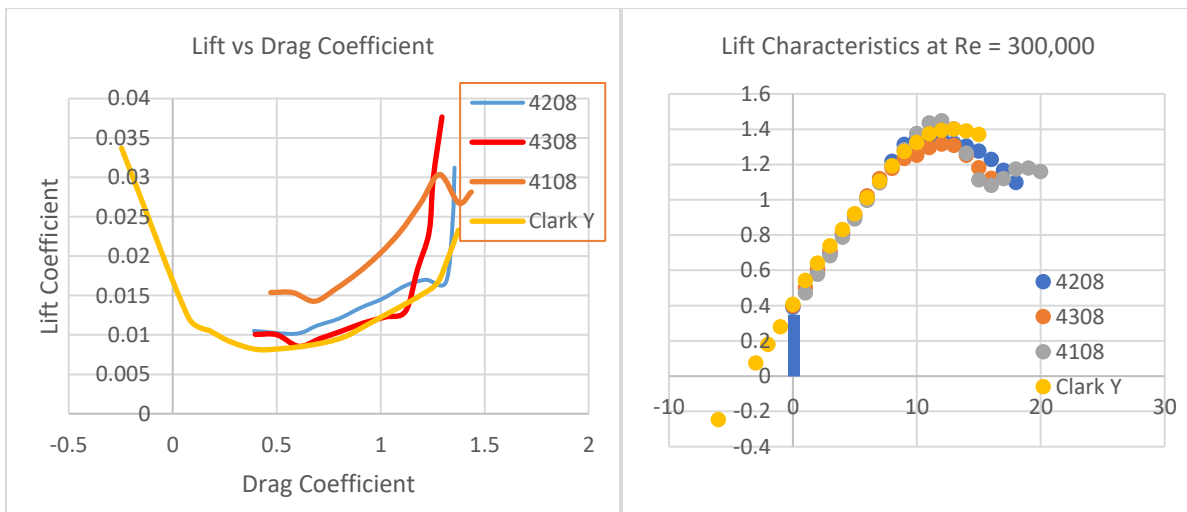


Figure 9: Airfoil selection plots from XFLR5

As seen in Table 20, the airfoils chosen for analysis all had very similar properties, but a few stood out as unique options. NACA 4108, 4208, and 4308 airfoils modified with a flatter lower surface were used and compared to the Clark Y airfoil, a well-known choice for RC aircraft. The modified airfoils were expected to be easier to manufacture while also streamlining their shape to a smaller airfoil thickness. This was expected to benefit the drag characteristics since the base airfoils in the NACA 4108, 4208, and 4308 are typically used for higher Reynolds number-flight. Another key factor considered was that each of these airfoils are relatively thin, meaning that they will have a very low drag profile. Since the competition emphasizes a fast aircraft, this was desirable.

The modified NACA 4308 airfoil was chosen due to its similar lift-curve to the Clark Y airfoil, as they share a similar lift-curve slope, at the cost of a slightly lower max lift coefficient. The greatest improvement between the two airfoils was in their maximum lift to drag ratios. The required lift coefficient at our estimated cruise angle of attack of zero degrees was 0.3971, which is a 1.13 factor of safety over the earlier calculated value in the Table. Stall characteristics of the airfoil in Figure 9 lift curve to be desirable up to 12 degrees angle of attack. The wing exhibits very minimal flow separation, which is shown by the relatively small amount of drag produced in the XFLR5 simulation.

$$V_{stall} = \sqrt{\frac{2\frac{W}{S}}{\rho C_{Lmax}}} \quad (Eq. 3.8)$$

The stall velocity of the aircraft is a critical parameter. It is the minimum speed at which an aircraft can maintain level flight, and any speed below this value will result in the loss of lift, causing the plane to drop. The equation used to calculate the stall velocity considers several factors,

including the weight of the aircraft, the surface area of the wing, the density of the air, and the maximum lift coefficient. The calculated stall velocity of the aircraft with the NACA 4308 airfoil is 6.581 ft/s.

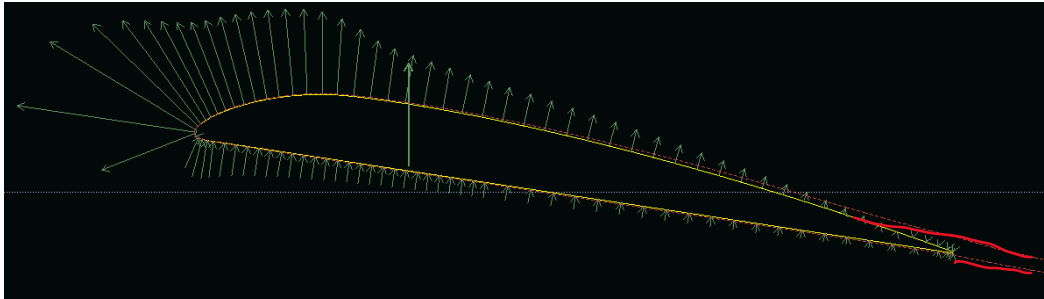


Figure 10: Flow separation of modified NACA 4308 airfoil as shown in XFLR5

As noted, before, the half-wing span is $b_{1/2} = 26$ inches. To allow for some extra space in the shipping box, this final dimension was chosen to be $b_{1/2} = 25.3$ inches, and the wing mean aerodynamic chord was set at $c = 8.65$ inches. With a 4 inch fuselage width, the full tip-tip wingspan is $b = 54.6$ in. A tapered wing planform shape with taper ratio = 0.73 (root chord = 10 in, tip chord = 7.32 in) was selected in order to approximate an elliptic wing lift-distribution and geometry. Taper of the wing also meant that the mounting fixture of the wing-tip antenna could be more easily incorporated into the geometry of the wingtip. The choice to taper only the wing trailing edge was made so that a “D-tube” structural element at the wing leading edge could be used to strengthen the wing structure, thereby stiffening the wing.

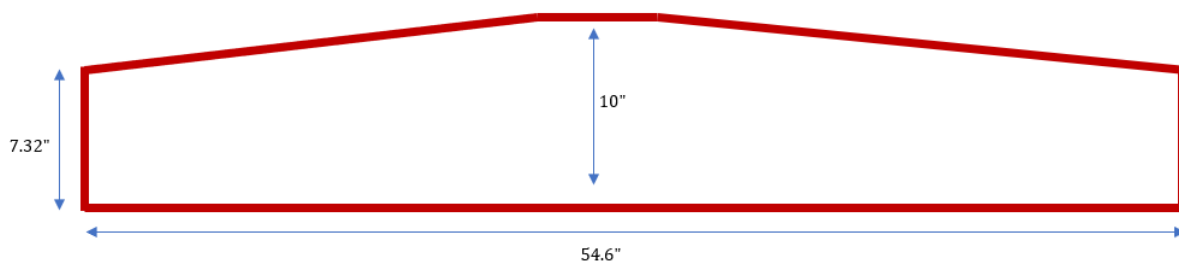


Figure 11: The Beluga's wing planform shape. The straight wing leading edge (bottom) and tapered trailing edge (top) are shown.

An analysis of the three-dimensional airfoil and planform shape was conducted using XFLR5 software in wing analysis mode, and the lift coefficient was found to be 0.4489 which includes the lift contributed by the airfoil-shaped fuselage. The full-wing simulations were run based upon the density of air in Tucson, to replicate competition conditions most closely. At a cruise speed of $V = 45$ mph, the lift generated is calculated to be around $L = 7.74$ lbf, which is larger than the initial estimated aircraft weight $W = 4.43$ lbf by 74.8%. Lift on the wing was found by correcting the 2D data for lift coefficient found in XFLR5 with the following equation, which inputs the wing aspect ratio, as well as the lift curve slope deduced from the airfoil:

$$C_{La} = \frac{C_{la}}{1 + \frac{C_{la}}{\pi AR}} \quad (\text{Eq. 3.9})$$

This yielded a corrected lift curve slope of 0.0589 lbf/degree, which is slightly less than that for the airfoil, by about 10 percent. This lift—curve slope was used to find the lift during cruise and takeoff and allowed for dynamic analysis of aircraft maneuvers. Lift from the fuselage was neglected as the span of the fuselage is small in comparison to the size of the wing planform span.

3.4.3 Tail Aerodynamics

As the tail of the aircraft is relatively small, to minimize time spent on analysis of various components, a flat plate airfoil was chosen for both the vertical and horizontal stabilizers. From thin airfoil theory it is known that the lift-curve slope of a flat plate is assumed to be around 2π in rad^{-1} . The main area of concern for the tail was angle of incidence. It was decided that the tail would have a zero-degree angle of incidence to remain colinear with the aircraft thrust line and provide positive decalage between the wing and horizontal tail.

3.4.4 Drag Analysis

An in-depth drag analysis was carried out to ensure that drag on all aircraft components was estimated. The curve from Figure 9 from section 3.4.2 shows the relation between lift and drag for the modified NACA 4308 airfoil. A curve fit, in terms of the coefficient of lift was determined to fit the parasitic, induced, and viscous drag. To determine a corrected form of this drag equation in 2D, the parameter k had to be determined by setting the following equation equal to the actual curve of coefficient of lift and drag outputted from XFLR5.

$$C_D = C_{d0} + k(C_L - C_{l_0})^2 = 0.0309C_L^2 - 0.04C_L + 0.0222 \quad (\text{Eq. 3.10})$$

Using the C_{d0} and C_{L0} of 0.6 and 0.0096 determined from Figure 9 in the 2D airfoil analysis, k was determined to be 0.0340. This enabled the calculation of the 3D drag equation, which adds drag due to lift (wingspan) to the above equation of drag. The first term in the following equation represents the parasitic drag, the second term, induced drag due to wing tip vortices, and the third term pressure drag due to lift, all respectively applied to only the wing.

$$C_D = C_{d0} + k(C_L - 0.6)^2 + \frac{C_L^2}{\pi(AR)(e0)} \quad (\text{Eq. 3.11})$$

$$C_D = 0.0096 + 0.034(C_L - 0.6)^2 + \frac{C_L^2}{\pi(6.43)(0.8)} \quad (\text{Eq. 3.12})$$

To determine inputs for the C_L in this function, the whole-aircraft lift coefficient was determined based upon the lift-curve slopes of both the lifting fuselage and the aircraft wings. The max lift coefficient was determined to be around 1.2 (12 degrees) accounting for the effects of the 3D wing, as discussed above. The values of lift were deduced based upon the flight-phase for each analysis, with differing lift coefficients for each. Drag calculations were continued by using the component build-up method from Raymer's aircraft design textbook [3].

Table 21: Aircraft Drag Analysis Data

Drag Analysis			
Component	Area (in ²)	Wetted Area (in ²)	C _{d0}
Wing	464.44	942.26	0.0071
Body	114.32	234.40	0.0015
Horz. Tail	89.27	180.59	0.0015
Vert. Tail	27.84	143.31	0.0014
Total C_{D0}: 0.0215			

Using the previous equation and replacing the parasitic drag term with the new value in cruise this means that the aircraft experiences 0.6343 lbf of drag when the free-stream velocity is 45 miles per hour (66 ft/s). Comparing this to the lift of the aircraft at cruise, 8.946 lbf, a lift-drag ratio of 14.1 is calculated. The new equation for the full aircraft drag in terms of the coefficient of lift, can be found below.

$$C_D = 0.0215 + 0.034(C_L - 0.6)^2 + \frac{C_L^2}{\pi(6.43)(0.8)} \quad (Eq. 3.13)$$

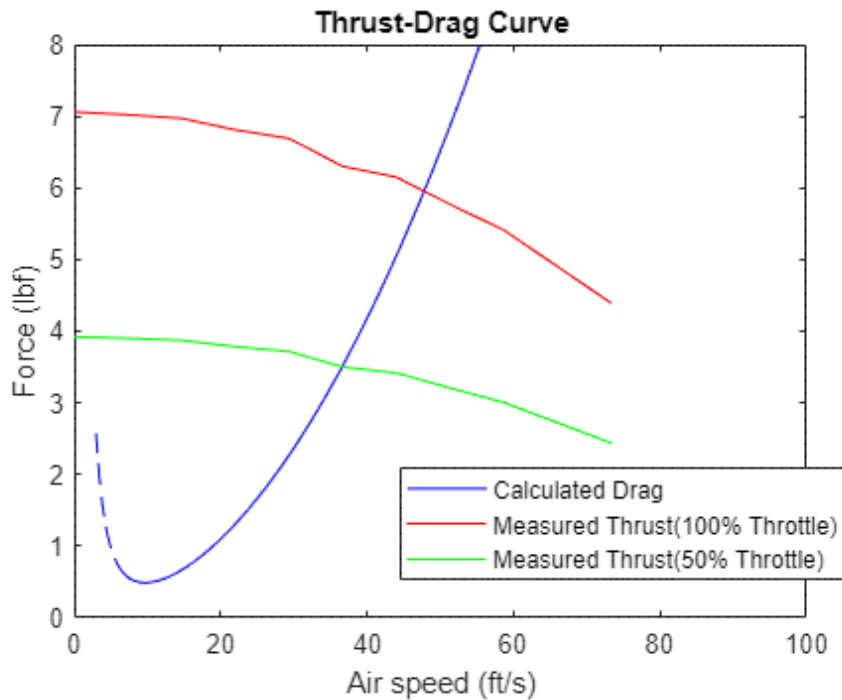


Figure 12: Thrust and Drag forces plotted over the airspeed. V^* is the intersection of the thrust and drag curves which intersect at ~48 ft/s. The dotted lines on the blue curve indicate the calculated drag values below the stall velocity.

Using the cruise velocity of 58.67 ft/s and weight of 7lbs (aircraft w/ payload), the recommended thrust is 8.92 lbf. This follows close to the general rule of thumb of a 1:1 thrust-weight ratio in RC aircraft [4]. By plotting both the drag and thrust, the intersection of the curves determines if the thrust is reasonable. Shown in Figure 12, the thrust curve of the measured motor is less than the recommended thrust of 8.92 lbf. The target airspeed is 58.6 ft/s, indicating that the motor may be underpowered for the missions.

3.4.5 Wing-tip Antenna

Along with the drag analysis on the aircraft configurations for missions 1 and 2 above, a drag analysis was also conducted on the wing-tip antenna. It was apparent that adding pipe with a diameter and length approaching one wing chord length scale to the tip of the wing would increase the pressure drag of the aircraft, creating a yawing moment around the aircraft center of gravity. The solution examined is a scooped “windvane” attachment on the wing tip opposite the antenna that aims to equalize the drag on the opposite wing tip so that the aircraft is still controllable. The expected length of the PVC pipe was 2 to 5 inches depending on flight conditions. The goal was to create a component that would generate drag in an internal scoop, while creating drag on the outside of the fixture using golf-ball like dimples, which increase drag on streamlined bodies by creating turbulence.

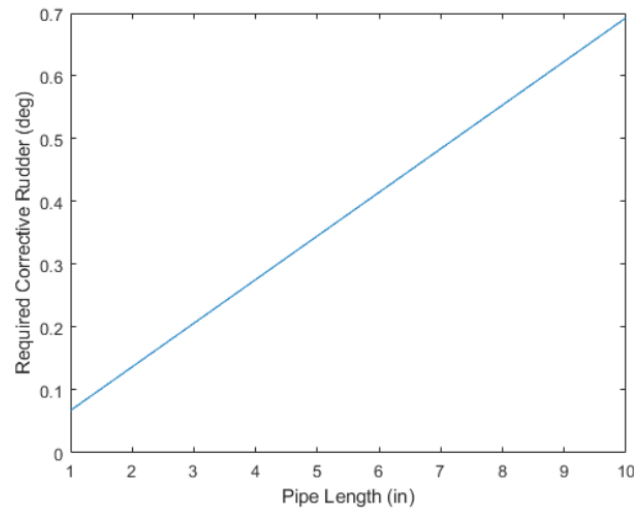


Figure 13: Required rudder deflection for various pipe lengths

Drag on the scoop was determined to be around 1/3 of that of the pipe and holder fixture when a 5-inch pipe is used, as shown in Figure 13. This means that the moment of the antenna drag force about the CG would be entirely balanced by the scoop for a 5/3-inch length pipe without any required rudder deflection. For a 5-inch-long pipe, it was determined that the rudder would need to be deflected by 0.0247 degrees to correct for the antenna drag moment. This deflection is small compared to the achievable deflection of the rudder.

Figure 13 shows results for the same analysis for required rudder deflection angle to offset antenna drag at different antenna lengths. The results show that the required deflection never exceeds 0.7 degrees even with a much larger than planned pipe of 10 inches length. This analysis examined the moment created by the free-stream flow on each of the wing-tip components. The goal was to make a static system, where the sum of moments about the center of gravity were zero. First, the moment balance was set to zero, and the known moments on the center of gravity were inputted. The force that was unknown, was the side-force generated by the rudder. This was deduced by using flat plate airfoil theory, and the size of the rudder. This enabled an equation in terms of deflection angle to be formulated. Rudder size was inputted as 16.8 square inches, with a

pipe length varied from 1 in to 10 inches. Below, d_p half the span of the wing (pipe location), d_s is half the span in the opposite direction (scoop location), and d_r is the rudder location. CFD simulations at cruise velocity were used to determine pipe and scoop drag coefficients.

$$\Sigma M = 0 = F_p(d_p) - F_s(d_s) - L_r(d_r) \quad (\text{Eq. 3.14})$$

$$C_l = 2\pi\alpha \quad (\text{Eq. 3.15})$$

$$L = \frac{32.2C_l\rho V^2 S}{2} \quad (\text{Eq. 3.16})$$

$$\alpha = \frac{\left(\frac{b}{2}\right)(C_{D_{cyl}}S_{cyl} - C_{D_{scoop}}S_{scoop})}{2\pi S_{rud}d_r} \quad (\text{Eq. 3.17})$$

Since the rules state that both the “counterweight” and the antenna holder must be of the same size, this enables the dual purpose of balancing drag and weight. It is thought that with further testing, drag can be increased, especially once weights are placed on the outside of the fixture, in the form of brass inserts.

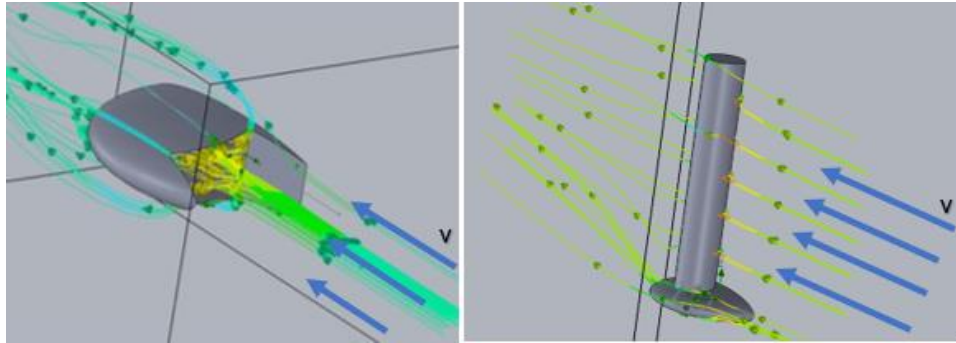


Figure 14: CFD Simulation of Wing-tip antenna payload and opposite wing-tip scoop fixture.

Table 22: Scoop and Pipe Drag

Component	Drag
Pipe Assembly	0.472 lbf
Scoop	0.138 lbf

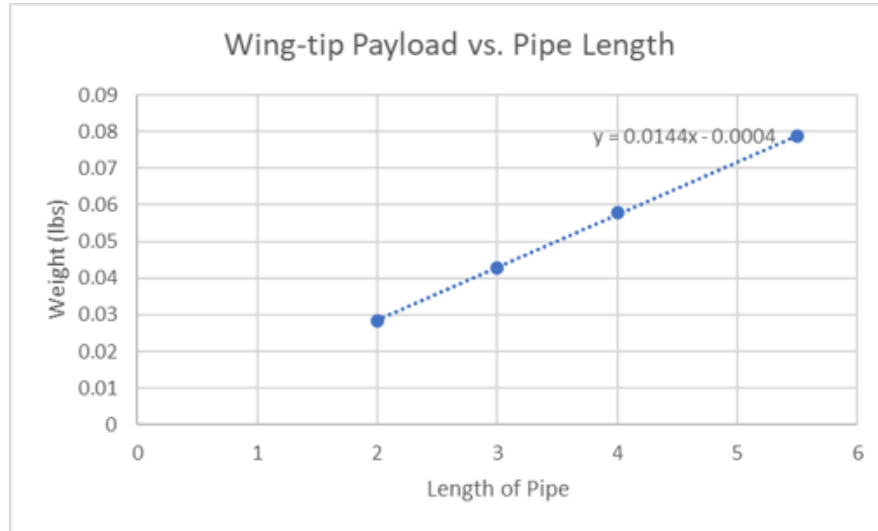


Figure 15: Wing tip payload weight versus payload

Balancing drag was only one component of the antenna payload’s problem. A significant amount of weight would also be added to the wingtip when the wing-tip fixture has been mounted. A linear curve was created to determine how much ballasting weight would be required on the opposing wingtip to counteract the rolling moment caused by the greater weight of the antenna payload. For a given pipe length, the balancing counterweight is then known.

3.4.6 Predicted Take-Off Distance

Based upon the given aircraft aerodynamics parameters deduced above, the takeoff distance was estimated. Since the competition allows 60 feet for takeoff, the goal was to produce as much lift as possible at takeoff. As discussed previously, the maximum lift coefficient with a safety factor (preventing stall) occurs at 10 degrees angle of attack with a lift coefficient of 1.11. Assuming that the weight of the aircraft was around 5 lbs, the takeoff distance of the aircraft could be determined from the lift, drag, and max thrust characteristics. At a 10-degree angle of attack, 6.73 lbf of lift are generated when at the proposed takeoff velocity of 32.32 ft/s. The corresponding

drag is 0.6484 lbf. Using the simple dynamic equation shown below, the takeoff distance could be confirmed to be less than 60 feet, coming in at around 43 feet.

$$a_{ground} = \frac{32.2}{W}((T - D) - 0.015(W - L)) \quad (Eq. 3.18)$$

$$S_{groundroll} = \frac{v^2}{2a} \quad (Eq. 3.19)$$

Since this takeoff distance was determined to be smaller than the allowed 60 feet, especially with the consideration that thrust during take-off is much greater than the needed amount for the aircraft. Excess thrust would enable the aircraft to not only climb faster, but takeoff in shorter distances as well. Takeoff distance was predicted using models from Raymer's aircraft design textbook [3].

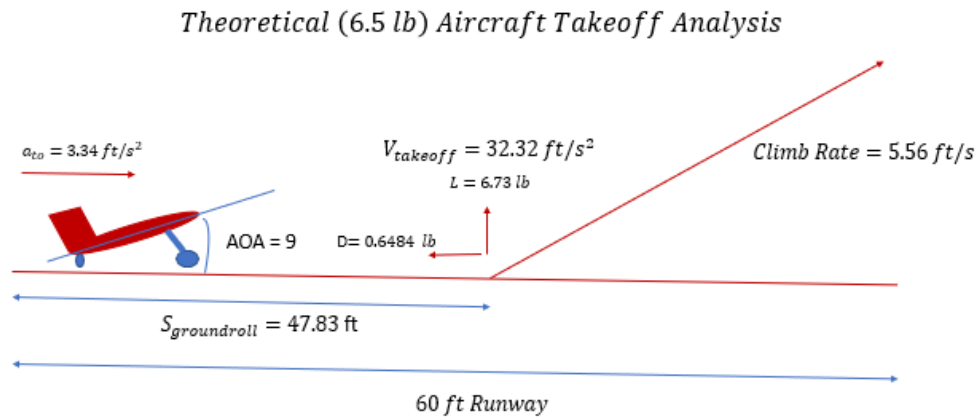


Figure 16: Theoretical takeoff analysis diagram

3.5 Stability and Controls

3.5.2 Flight Controllers

As per the competition regulations, utilization of autopilot or aircraft axis stabilization systems was prohibited, necessitating the exclusion of flight controllers with gyroscopic functionality from procurement. To mitigate expenses and optimize budget allocation, a radio transmitter equipped with FrSky ACCESS protocol was repurposed, leading to the selection of

FrSky RX6R receiver in conjunction with a FrSky XM+ redundancy receiver. A Futaba receiver and transmitter were also considered since the Central Mass Radio Control Modelers offered to give equipment.

3.5.2 Actuators

The servo motors play a critical role in the actuation of the aircraft's control surfaces, making their selection a significant factor in ensuring mission success. The servo motors must exhibit robust functionality under high loads and thermal exposure to effectively perform throughout the competition. To determine the optimal servo, a comparative analysis was performed and presented in Table 23.

Table 23: Servo Comparison Chart

Assume 6v battery	Hitec HS-65MG	Hitec HS-311	Hitec HS-5055MG	Futaba S3115	TowerPro MG946R	Hextronik HXT12K
Torque: (oz-in)	31	49	22	39 (4.8v)	180.54	208
Speed: (sec/60deg)	0.11	0.15	0.17	0.15	0.17	0.13
Weight: (oz)	0.42	1.51	0.33	0.6	1.94	1.69
Length: (in)	0.92	1.57	0.89	1.1	1.6	1.56
Width: (in)	0.45	0.78	0.45	0.51	0.78	0.79
Height: (in)	0.94	1.43	0.94	1.18	1.69	1.5
Gear Type:	Metal	Plastic	Metal	Plastic	Metal	Metal
Cost: (\$)	30	10	17	23	19	12

Table 23 displays the evaluated servo models and their relevant specifications [7]. The desired servo characteristics, including compact size, adequate torque, and utilization of metal gears to prevent gear stripping, were listed in the left column of the chart. After conducting research and seeking input from experienced RC airplane pilots, the Hitec HS-65MG servo was

determined to be the optimal choice for the aircraft due to its alignment with the desired characteristics.

3.5.3 Static Stability

A further analysis conducted using the aerodynamic parameters set forth here was the static stability analysis of the aircraft. This analysis determines the stability of the aircraft when it is subject to a disturbance. In general, a negative moment slope indicated that the aircraft is statically stable. In XFLR5, the aircraft geometry was inputted to determine if this was the case. A study was conducted at 66 ft/s (45 miles per hour), to determine how the aircraft would respond. The results are shown in Figure 17.

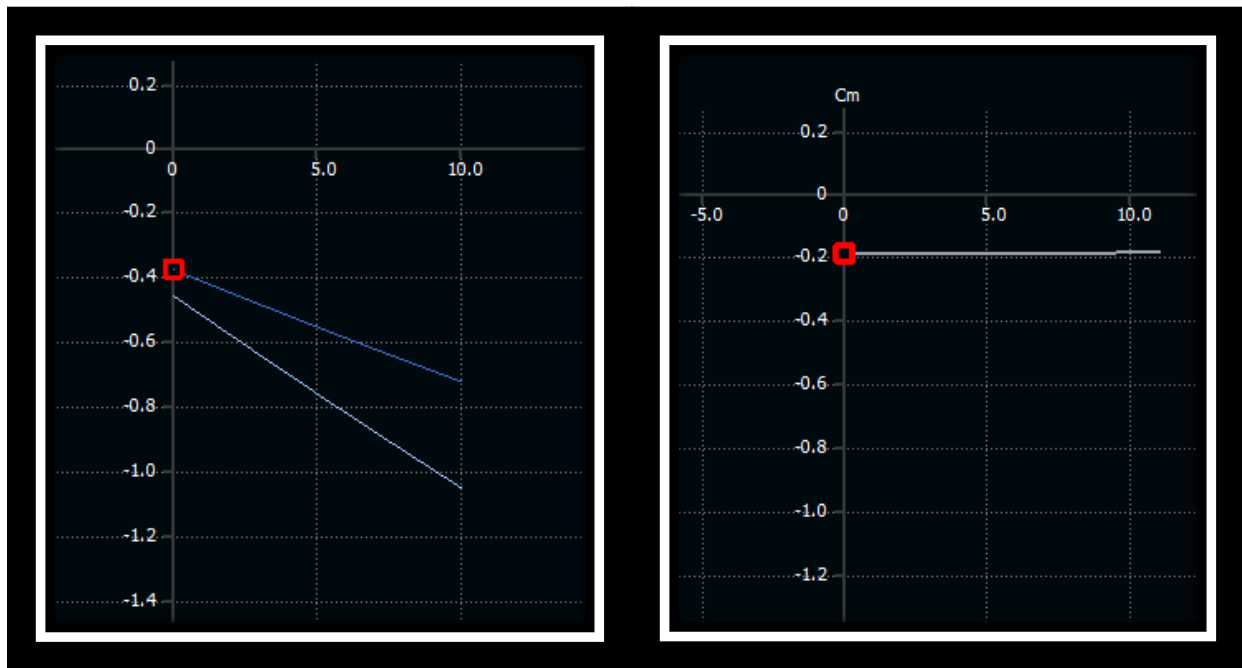


Figure 17: Static Stability Analysis of moment for calculation of neutral point

Shown in Figure 17, this analysis was also used to determine the aerodynamic neutral point of the aircraft. This was done by repeatedly setting the CG of the aircraft in different locations to determine where the moment slope would be zero. At this point, the CG and the neutral point are

equal, meaning that the neutral point occurs at that inputted CG. Neutral Point (or aerodynamic center) was found to be 4.5 inches from the leading edge of the wing.

3.5.4 Center of Gravity and Neutral Point Comparison

It is essential to find the center of gravity (CG) location of the aircraft. Ideal CG on an aircraft sits directly centered through the fuselage horizontally and as close to the thickest part of the wing's airfoil as possible. The leading edge of the aircraft's wing sits roughly 12.1" from the front of the fuselage. With the motor and battery being the heaviest components of the aircraft, the placement of both will affect the location of the CG the most. The motor being in a fixed location on the front face of the fuselage will mean for a more rear located battery placement. A zeroed alignment of the motor, wing and tail elevator will assist in centering the CG vertically, as well as also increasing maneuverability. Mission 2 will implement the payload, thus altering the location of the CG. It will be crucial to plan the location of the payload as central to the CG and airfoil of wing as possible. During this mission, movement of the battery can assist in countering the change due to the payload.

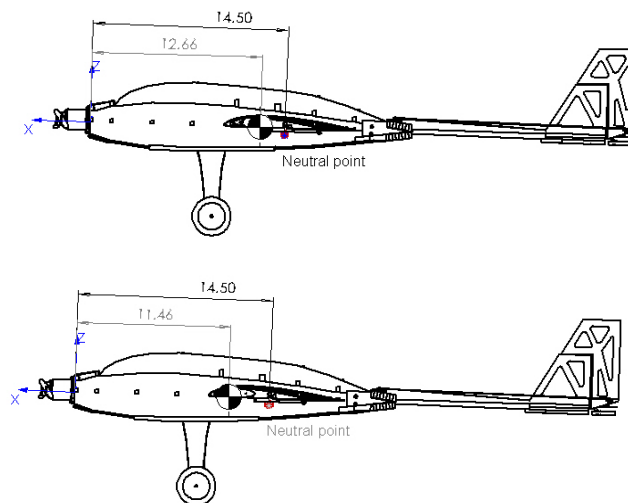


Figure 18: Location of center of gravity in relation to the neutral point. (Top) The CG location for the non-payload configuration. (Bottom) The CG location for the payload configuration

Comparing this predicted center of gravity to the neutral point calculated from the aircraft XFLR5 model from section 3.5.3, the static margin of the aircraft can be deduced. A desirable static margin for the aircraft is from 0 to about 15 percent, which is where the aircraft can be assumed to be stable in pitch with good maneuverability characteristics [5]. Static margin was calculated (shown below) by subtracting the center of gravity location from the neutral point and normalizing the result using the mean aerodynamic chord of the wing.

$$SM = (x_{NP} - x_{CG})/MAC \quad (Eq. 3.20)$$

The result from the above equation is a static margin of 0.212 for the non-payload case, and 0.351 for the payload case. Both static margins are positive, indicating stability, however they are out of the ideal range of $0 < SM < 0.15$. Results greater than 0.15 indicate that the aircraft will need more elevator authority, decreasing the overall maneuverability of the aircraft, such as the turning radius. The addition of epoxy to the aft portions of the aircraft were expected to bring this static margin within the recommended range, or very close to it. Minor adjustments to the aircraft during assembly allowed for the aircraft CG to move farther back towards the neutral point, as discussion in the performance results section (Section 7).

3.5.5 Dynamic Stability

A dynamic stability analysis was conducted aimed at modeling the aircraft's response over time to external disturbances. The section presents a detailed analysis of an aircraft's longitudinal pitch stability, focusing on its behavior when experiencing disturbances in the pitching axis. Using general control theory, the aircraft with the payload can be modeled with the following state equation and state vector:

$$\dot{x} = Ax + Bu \quad (Eq. 3.21)$$

$$x = \begin{bmatrix} u \\ w \\ q \\ \theta \end{bmatrix} \begin{array}{l} \text{linear velocity in } x \\ \text{linear velocity in } z \\ \text{rotational velocity in } y \\ \text{pitch angle} \end{array}$$

Since the free response of the system is the objective of the analysis, the input response and the B matrix were ignored; therefore, the A matrix is modeled as:

$$\mathbf{A} = \begin{pmatrix} X_u & X_w & 0 & -g_0 \cos \Theta_0 \\ \frac{Z_u}{1-Z_{\dot{w}}} & \frac{Z_w}{1-Z_{\dot{w}}} & \frac{u_0+Z_q}{1-Z_{\dot{w}}} & \frac{-g_0 \sin \Theta_0}{1-Z_{\dot{w}}} \\ M_u + \frac{M_{\dot{w}}Z_u}{1-Z_{\dot{w}}} & M_w + \frac{M_{\dot{w}}Z_w}{1-Z_{\dot{w}}} & M_q + \frac{(u_0+Z_q)M_{\dot{w}}}{1-Z_{\dot{w}}} & \frac{-M_{\dot{w}}g_0 \sin \Theta_0}{1-Z_{\dot{w}}} \\ 0 & 0 & 1 & 0 \end{pmatrix}$$

Where each of the values in the A matrix are stability derivatives that are determined by the aircraft's properties as shown in Table 24 below.

Table 24: Coefficients to calculate the dynamic stability of the aircraft

Dynamic Stability Coefficients			
b	54.64	wingspan	inches
c	8.685	wing chord	inches
S	439.8084	wing area	in ²
S_t	94.4	horizontal tail area	in ²
AR_W	5.83074266	Aspect ratio of wing	ratio
AR_T	2.842207627	Aspect Ratio of tail	ratio
W	7	Weight of aircraft w payload	lbs
h	0.22	location of center of gravity as a fraction of chord length	%
h_{ac}	0.643638457	location of aerodynamic center as fraction of chord length	%
I_t	20.7	dist. Between aerodynamic centers of wing and horizontal tail	in
e_0	0.951	Oswald efficiency factor	
I_y	514.6	y-direction moment of inertia	lb* in ²
Cd_0	0.0192	Induced coefficient of drag	
M	0.052551	Mach number for cruise cond.	Mach
Λ	0	wing sweep angle	deg
ρ	4.60767E-05	air density at sea level	lb/ in ³
u_0	704.04	velocity	in/sec
n_h	0.414270463	dynamic pres. Ratio	
V_h	0.588187254	horizontal tail volume ratio	
a_t	6.283185307	lift curve slope of tail	
a_w	0.059	lift curve slope of wing	

By taking the eigenvalues of the A matrix, the phugoid response, the long-period oscillation controlled by the elevator, and the short-period, the fast oscillation controlled by both the elevator and stabilizer, are modelled.

$$\lambda = \begin{matrix} -1.066 \pm 10.405 & \text{short period} \\ -0.137 \pm 0.476 & \text{phugoid} \end{matrix} \quad (\text{Eq. 3.22})$$

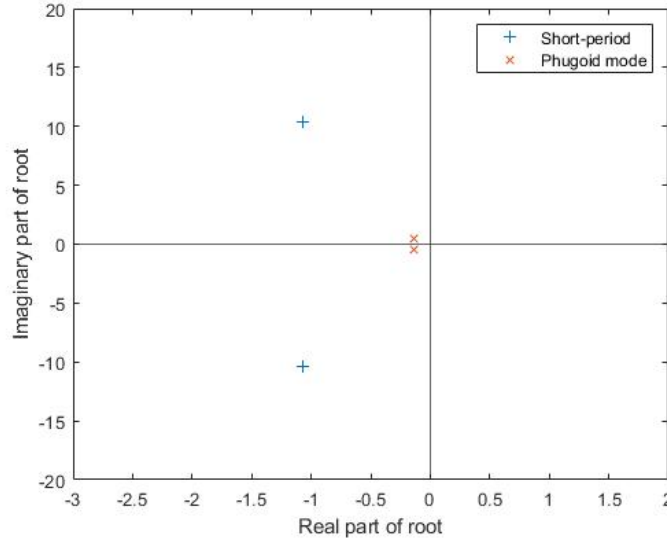


Figure 19: Phugoid and Short-period mode roots plotted. Both modes are conjugates with negative real roots which show that the aircraft is dynamically stable

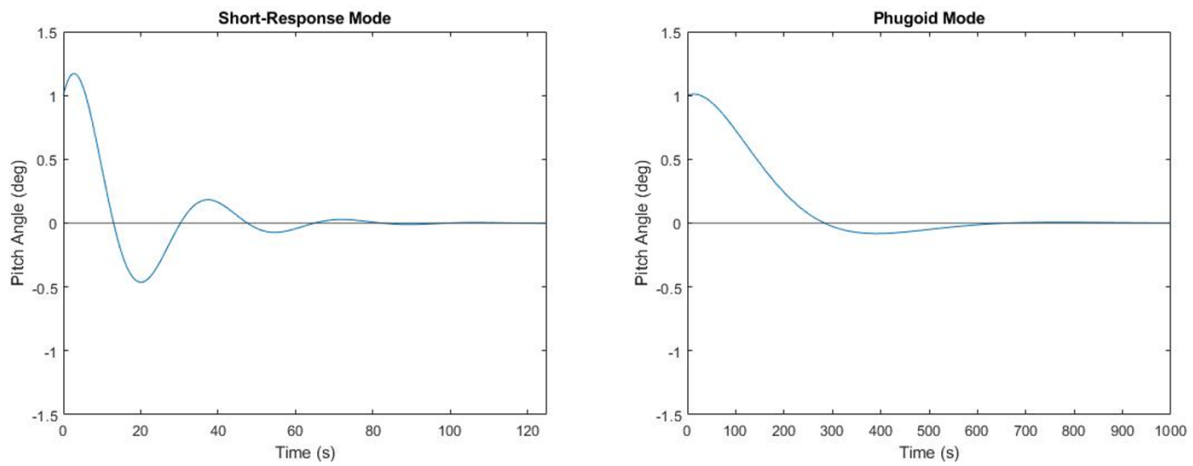


Figure 20: The short-period (left) and the phugoid (right) response of the aircraft, both plots showing the stability of the aircraft over time.

According to Figure 19 and Figure 20, the aircraft along the longitudinal axis is stable which is important because longitudinal stability helps ensure that the aircraft remains in a safe and controllable flight regime. This allows the aircraft to maintain a constant angle of attack and airspeed with minimal control inputs from the pilot increasing the overall efficiency.

3.6 Structural Analysis

The structural analysis of the aircraft consisted of mainly numerical modelling within ANSYS structural. Designs were formulated using prior knowledge of aerospace structures, with a goal of creating lightweight, stiff assemblies. Main components of these assemblies were formed into box-beams, spars, and formers to improve structural performance. Focus was placed on connecting major structural components to ensure point-to-point rigidity in the design.

Analysis was conducted on almost all major structural components of the aircraft to determine the best method of design, these being the fuselage-tail attachment, wings, wing-clamps, and landing-gear assemblies. Each of these components were analyzed using simulated mechanical forces that would be sustained in competition to best inform design decisions. These components are brought together for analysis in Section 4 of this report.

3.6.1 Fuselage

There are four major requirements of the fuselage that were deemed critical for development. These requirements were: sufficient volume to allow proper placement of the Mission 2 payload, battery, electronics, and the mid-wing attachment structure. The volume allowed for the mission 2 payload and the battery were especially important. When Mission 2 payload is installed, it and the battery are the two heaviest elements in the aircraft. In addition, depending on the size of the payload, the overall size of the fuselage affects the center of gravity

of the whole aircraft. As seen in Figure 21, the payload is placed as far forward as possible and takes up most of the room in the bulkhead. The ESC is placed in the bulkhead with the payload. The more sensitive electronics, such as the receiver and its antennae, are placed securely in the middle of the aircraft between the mid wing attachment points. The transmitter is secured with high density foam to prevent any unwanted movement or interference. The antenna also rests in small plastic tubes, facing 90 degrees from each other, secured down with tape. To quickly install and remove the wings, the mid-wing attachment points are made of 3D printed parts. The carbon fiber wing supports slide into these attachment points. The attachments points are fastened with bolts and screws preinstalled in the 3D printed fixture to further secure the wings. Above the mid-wing attachment rests the battery. The goal of having the battery located right above the wings is to help keep the center of gravity near the quarter-chord point of the wing. Enough slack is left in the wires in the fuselage so the ESC can move unimpeded when the payload is loaded into the aircraft and to access fuselage components when needed.

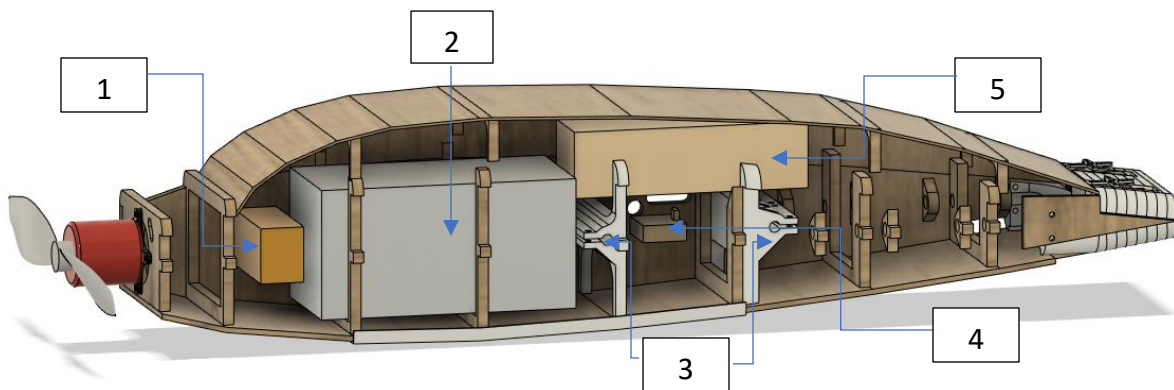


Figure 21: Fuselage configuration. 1) ECU 2) Mission 2 payload 3) Mid-wing attachment points 4) Telemetry components 5) Battery

Next, we discuss the overall structural shape of fuselage. The top and bottom have an airfoil profile, and the sides are rectangular sections as shown in Figure 21. The airfoil shape of the fuselage allows it to act as a lifting body. A series of formers are placed internally providing

strength and rigidity. In addition to these formers, two 3D printed wing attachments provide extra rigidity in the center of the fuselage. The nose cap, which the motor is mounted to, is reinforced with 1/16 in aluminum sheeting, which then runs to the bottom of the fuselage and coupled to a plywood floor. The combination of the plywood floor, aluminum reinforcements, and internal formers, provides the required load carrying capabilities. This allows for the top of the fuselage to be non-load bearing. The top contains a large access door with minimal structural requirements allowing for ease of access to the electronics and payload.

3.6.2 Tail Attachment Structure

Because the fuselage was designed around all the necessary internals for the aircraft, the decision with how to attach the tail was based largely on what would be the lightest solution with the simplest process to attach and detach the tail during assembly. A single carbon fiber tail boom is a commonly used technique for this and was the first attachment strategy explored. For ease of assembly at competition, it was decided that the control servos for the elevator and rudder should be attached to the tail all in one piece to remove the need for control surface tuning during the assembly process. The cleanest solution presented was to 3D print a tail attachment piece that would have slots for both servos, a hole to attach the tail boom and cutouts that allow the fuselage to interface with the attachment piece for increased strength. It was decided that 3D printing was the best solution for this piece due to the relatively complicated geometries involved. It would have been very difficult to design a single component that served all these purposes while maintaining minimal fabrication time and an aerodynamic shape. This is easily attached with two bolts to the fuselage in such a way that much of the support would come from the interfacing with the main plates of the fuselage, thus distributing any force experienced across the 0.25" balsawood side panels instead of just the two bolts used for attachment.

After reviewing footage from the first test flight (single boom design), it was determined that there were two major problems with the design. First: the single tail boom flexed considerably more than expected causing a severe lack of controllability. Second: upon landing, the tail experienced enough force to shear through the 0.25” balsawood side panels. To address both issues, properties described using the parallel axis theorem were utilized:

$$\text{Moment of Inertia} = \text{Moment About Object Center} + \text{Mass} \cdot Z^2 \quad (\text{Eq. 3.23})$$

Increasing the moment of the tail boom or adding mass to increase the moment of inertia of the system would move the center of the mass of the plane backwards, decreasing aircraft stability. The Z component was identified as the best way to increase the moment (and rigidity) of this structure. By incorporating two smaller tail booms, the moment of the system would increase exponentially the further the distance between the two booms. Additionally, small pieces of 0.125” plywood were attached to the point where the 0.25” balsawood had initially sheared. By adding both more mass and thickening the shear point, the strength of the entire tail assembly in relation to the fuselage was increased considerably. Finally, the booms were extended into the fuselage to provide a rigid attachment for the tail, while also adding an easy point to disassemble the aircraft for fitting into the box dimensions.

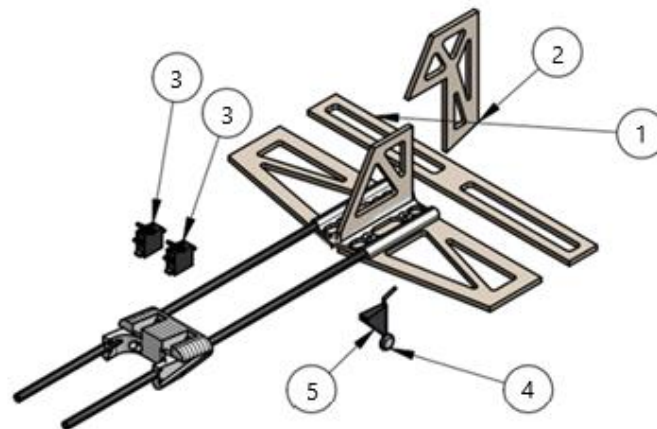


Figure 22: Tail Attachment Structure: 1) Elevator, 2) Rudder, 3) Servos, 4) Tail Wheel, 5) Tail Wheel Support

The final design of the tail attachment system features two tail booms to increase rigidity as explained above, as well as extending the booms far into the fuselage to more evenly distribute forces and increase moment of inertia, as also described by the parallel axis theorem.

3.6.3 Wing Attachment Structure

As per competition rules, wings must be detachable from the aircraft to meet the five-minute assembly time requirement. This led to the decision to use a clamping mechanism in the form of a 3D printed PLA part which is shown in Figure 24. The part shown utilizes threaded heat set inserts in the bottom portion of the clamp with bolts that can be quickly tightened to hold the wings in place using only friction as shown in Figure 23. Due to no little to no axial force being applied during flight to pull the wings out, the friction fit was deemed sufficient for the maneuvers required of the aircraft during the missions. The wing attachment structures were each printed in two parts in order to give extra strength to each part in the direction that they would endure the most stress. This greatly reduced the possibility of layer separation during the process of quickly tightening bolts during the assembly process.

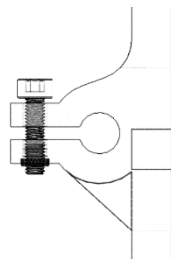


Figure 23: Wire Frame View of Heat Set Insert Clamping Mechanism

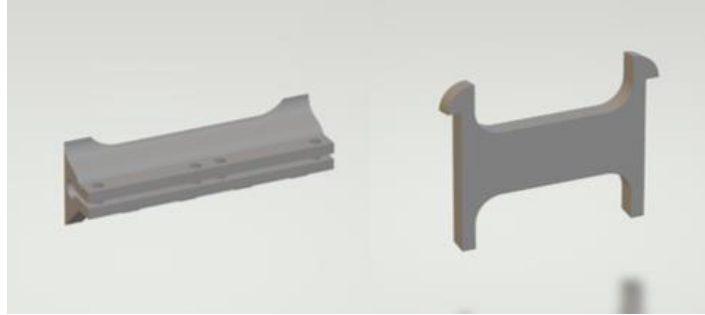


Figure 24: CAD Depiction of Wing Clamping mechanism

3.6.4 Landing Gear

A tail dragger design was chosen for the aircraft. A tail dragger can be customized to adjust the angle of attack and gear location to allow for ease of tail rotation at take-off. In addition, the

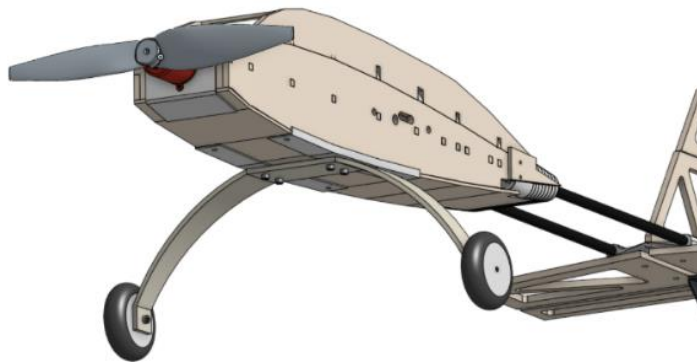


Figure 25: Landing gear location and size

tail dragger design is deemed superior in taxi performance and ground controllability compared to other conventional designs. A Du-Bro, main gear and tail wheel were used due to convenience, and minimal manufacturing required compared to an in-house fabrication.

Before procurement, measurements of the plane were taken to determine the required height and location of both the main landing gear, and the tail wheel. The tail wheel sits directly underneath the interface between the vertical stabilizer and rudder. It attaches a rod to the rudder

so that the tail wheel's movement is coupled to the rudder. This allows for a large degree of ground control at a minimal cost to aerodynamics and weight. The main landing gear features a single piece design constructed out of nylon. The location of the main gear's wheels are one inch in front of the wing leading edge, and the angle of attack of the wing is 10 degrees during take-off roll. This allows the aircraft to easily rotate upon takeoff, without jeopardizing ground stability. The attachment point to the fuselage is reinforced with 1/16" thick aluminum.

3.6.5 Wing Structure

The wings represent a crucial structural component of the aircraft, as they are providing sufficient lift to maximize payload capacity, which in turn impacts the overall score. Analysis using ANSYS simulation tools determined that the use of carbon fiber rods would be the ideal material for the main wing spars, based on the desired structural characteristics and performance criteria. Initially, the maximum deformation results of the wing were quite alarming. As further testing was completed, the carbon fiber spars were added to structurally stiffen the wing along with the addition of a wing leading edge D-tube and a third structural member. Maximum experienced stress of these rods was not a concern, due to the relatively low experienced stress compared to the 230 GPa failure stresses of the rods.

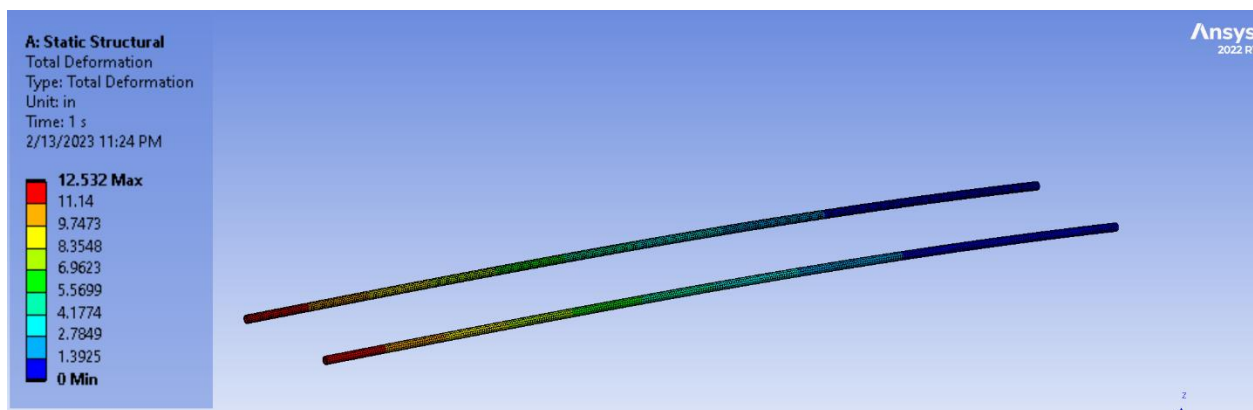


Figure 26: Wing tip deflection of carbon fiber spars from ANSYS simulation for 2.5 g load (wing root)

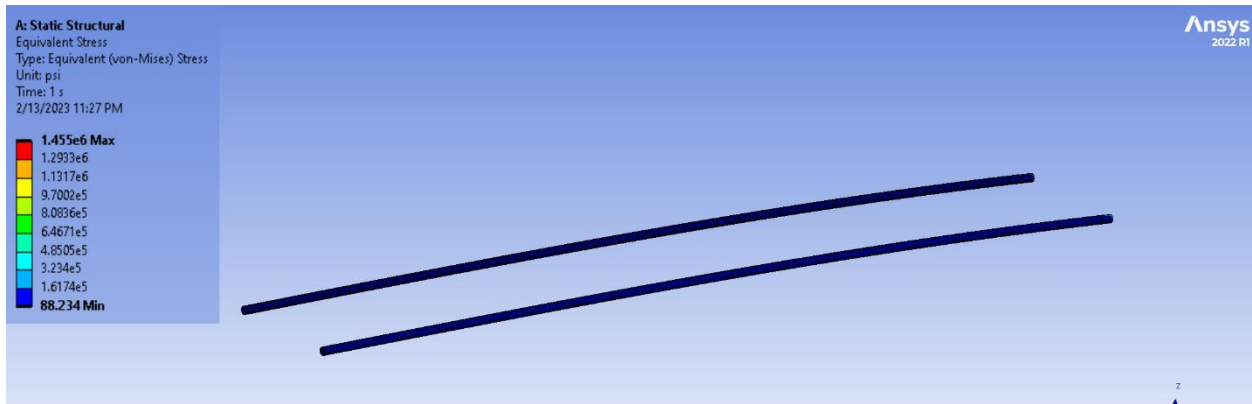


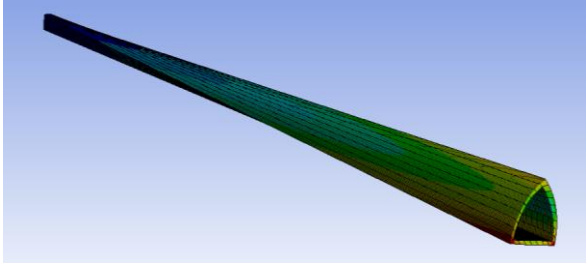
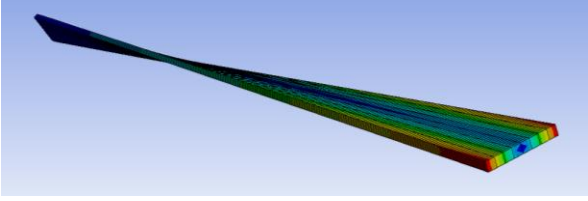
Figure 27: Equivalent Stress ANSYS Carbon Fiber stress for a 2.5g load (Wingtip)

Table 25: Stress at wing root from ANSYS simulation for 2.5 g load

Carbon Fiber Rod (2.5 g load test)		
Maximum Stress	1455000 psi	Location: Rear Face of Rod
Maximum Deformation	12.523 in	Location: Rear Face of Rod

To reinforce the wing's rigidity and maintain its structural integrity, a leading-edge D Tube wing structure, made of balsa, was employed. The D Tube reduces the wing flex and ensures reliable performance under increased payload loads. Rigidity is a crucial aspect of aircraft design, as it impacts both ground mission scoring and maneuverability. Wing flex during flight can result in reduced controllability and increase the likelihood of aircraft failure. To mitigate this risk, the design team placed a strong emphasis on ensuring the structural rigidity of the aircraft's wings. This reasoning for a D tube style structure is validated by the ANSYS simulations below. The generic balsa wood structure, with applied 10 lbf-in load to the tip of the specimen exhibits 20 times less deformation than the rectangular balsa spar. This improved torque response shows a distinct justification for the D-tube structural member as part of the main wing structure.

Table 26: Comparison of D-tube beam and plate beam in ANSYS

Component	Deformation from 10 lbf-in load	Analysis Visual (ANSYS)
Balsa D-tube	0.01256 in	
Balsa Rectangular Spar	0.2556 in	

With deflection of the carbon fiber rods being much larger than desired, coming in at 12 inches, controllability via ailerons would be a difficult task. Stiffening the wings with other structural members was imperative to preserving the geometry of the wings. As shown above, the D-tube would help to improve the torsional load of the wing. The goal was to create a wing structure that would allow for the incorporation of both carbon fiber rods and a D-tube section at

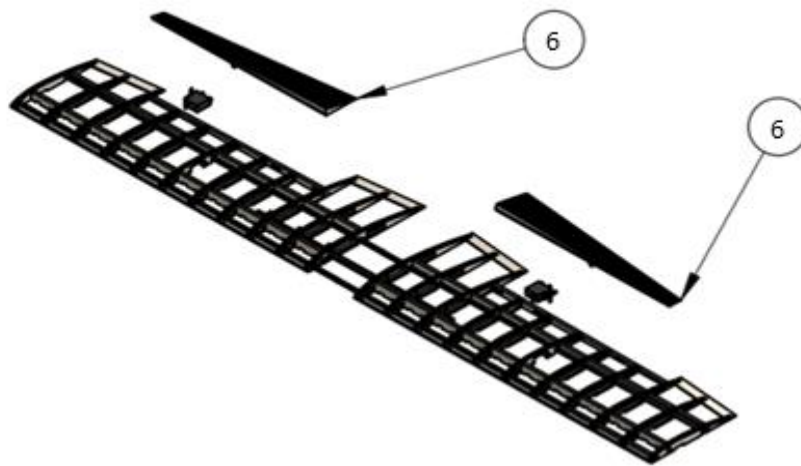


Figure 28: Final Wing prototype, incorporating previously discussed elements, 6) Ailerons

the leading edge of the wing. Spars along the wing, defining the wing's aerodynamic shape, were set along the carbon fiber rods and to connect the aforementioned D-tube to the front of the wing. This resulted in a first-generation wing which had rigidity, but still struggled in torsion about the wing-axis. Stiffening the wing beyond this was achieved using box beam construction. Two main spars were added alongside the carbon fiber rods to add torsional rigidity. With wing deflection occurring in an upwards direction in all loading scenarios, including the ground test, 2.5 g wing tip test, and flight of the aircraft, it was decided to add a component tying the tip and root ribs together, while also connecting the front and back spars. By doing this, a box-beam structure was created, with two spars acting as flanges, and ribs acting as stiffeners. The bottom plate connects each of these structural members to reduce deflection.

With a mid-wing design, the left- and right-wing sections are only tied together by the wing-attachment clamps described in the previous sections. Another supporting member, through the fuselage, and 1/3 of the way into each wing was added to stiffen the main attachment point. This was in the form of a 3/8-inch carbon fiber tube. Being a unidirectional-weave composite, this beam was a strong candidate to create a connection between wing-sections, as it exhibits almost no deflection in 2.5g load testing and absorbs most of the maximum stresses during bending. This is further explored in the ANSYS simulations in section 4.3.

3.6.6 Electronics Payload

A point of concern when adding the electronics payload was the effect it would have on the center of gravity. Any major shift in the center of gravity would cause the flight characteristic to drastically change. While a shift in the center of gravity is difficult to fully negate, a goal was to have the center of gravity with the payload to be as close to the original center of gravity as

possible. To accomplish this, it was decided that the payload weight position within the payload box needed to be adjustable. Using spacers made of foam within the payload box allowed for this while adding negligible weight. A requirement of the electronics payload is that it weighs a minimum of 30% of the total weight of the aircraft during the Mission 2 flight. The equation below is used to calculate said weight of the payload.

$$\frac{W_p}{W_e + W_p} = \frac{3}{10} \frac{W_p}{W_e + W_p} = 0.3 \quad (\text{Eq. 3.24})$$

Where $W_e = 71.2$ oz is the empty weight of the aircraft, and W_p is the mass of the electronics payload. Below is the estimated calculation of the payload weight.

$$W_p = \frac{3}{7} * 71.2 = 30.5 \quad (\text{Eq. 3.25})$$

3.7 Predicted Flight Performance

A maneuverability analysis was done with the current weights and configurations of the aircraft. A minimum turning radius at constant altitude and velocity is calculated assuming a maximum g-loading of 2.5 as shown in Figure 29. In addition, the maximum climb rate is analyzed from the maximum continuous thrust calculated in section 4.2.1 and the weight from Table 31. All calculations are done at cruise velocity of 58 ft/s and the staging flight aircraft configuration.

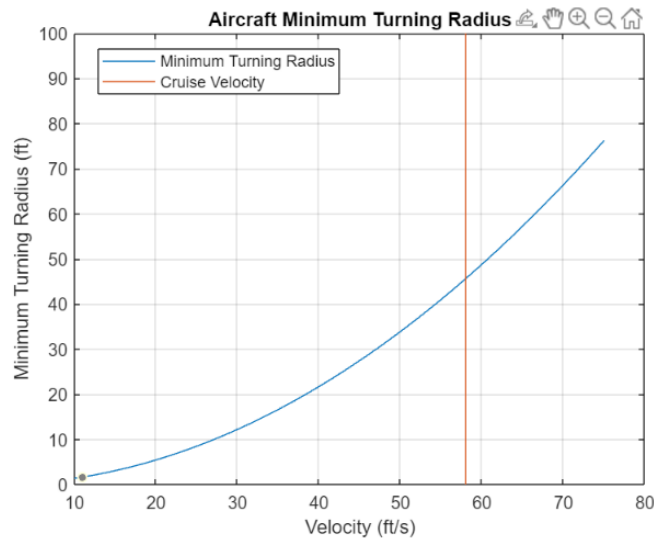
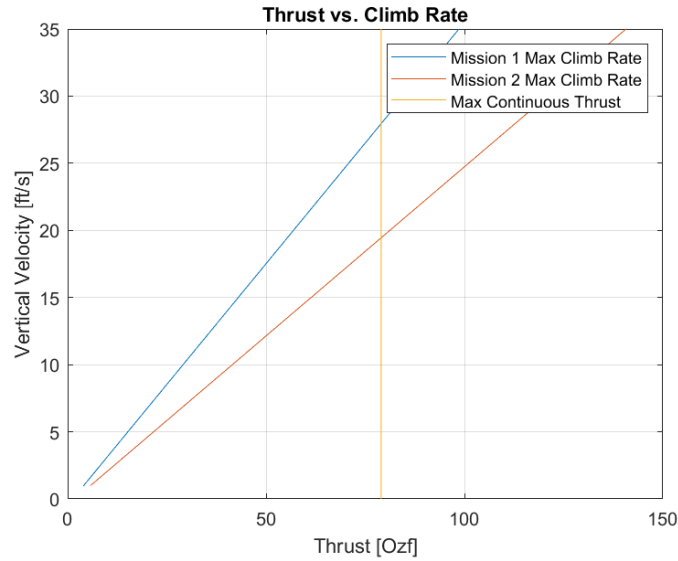


Figure 29: Thrust vs. Rate of Climb

The level turn analysis is critical in defining the flight envelope and predicted mission performance of the aircraft. It is crucial that the level turn required in the AIAA flight pattern can be completed as quick as possible, which enhances the aircrafts ability to complete laps. Further, the climb rate analysis verifies the theoretical take off distance calculations done in section 3.4.6. The estimated aircraft performance is shown in Table 27 below.

Table 27: Estimated Aircraft Performance

Aircraft	M1	M2	M3
All-Up Weight [Oz]	71	103	75
Payload Weight [Oz]	N/A	31	4
Wing Loading [oz/sq.ft]	22.3	31.9	23.2
Cruise Throttle	0.65	0.8	0.7
Static Thrust [ozf]	70	86.5	75.5
Turn Load Factor	2.5	2.5	2.5
Ground Roll [ft]	17.5	38.5	19
Cruise Velocity [ft/s]	58	55	58
Number of Laps	3	8	3
Lap Time [s]	45	55	48
Mission Time [s]	135	440	144

Throttle position at cruise is estimated based on thrust to weight ratio assumptions. In addition, an estimated number of laps and mission time are calculated to formulate initial mission score performance.

3.8 Mission Uncertainty

Though the design methodology was done using proven methods and widely used software, some assumptions had to be made during calculations which lead to a small degree of uncertainty within each measurement. In order to mitigate uncertainty, a factor of safety was implemented where necessary.

When designing the aerodynamic properties of the aircraft, it was necessary to first assume the flight characteristics at cruise altitude. Assumptions included density of air, aircraft weight,

wingspan, and chord length. And, once the required lift coefficient was calculated, a 1.13 factor of safety was added to the required lift. Because of the assumptions and included factor of safety, the calculated values for lift and drag are expected to differ slightly from the actual observed values. However, the factor of safety ensures that the lift and drag produced by the aircraft is conducive to flight.

Using MotoCalc8 to perform motor analysis allowed unification of uncertainty, at a value of around 10%. MotoCalc8 contains a database of different electric motors, which was used to measure performance metrics of all motors to be studied. Since each motor was analyzed in the same program, it was assumed that uncertainty would be uniform from motor to motor and thus would be negligible.

4 Detailed Design

The preliminary design of the aircraft allowed for the development of various systems to be incorporated into the aircraft. The detailed design phase allowed the use of various analysis tools in order to validate the design choices at the component and aircraft level. In this section the final dimensions, structural characteristics and capabilities, sub-system components and weight and balance of the aircraft are documented.

4.1 Summary of Aircraft Parameters

A comprehensive table was developed summarizing the main dimensions of each of the aircraft's components. Additionally, it specifies mounting parameters for the landing gear.

Table 28: Aircraft Parameter Summary

Aircraft Parameters			
Wing Geometry		Tail Geometry	
Wing Span, b_w	54.6 in	Horizontal Tail Span, b_H	16.125 in
Wing Chord, c_w	8.65 in	MAC Horz	CH _T Tip
		5.75 in	5.0 in
Wing Aspect Ratio, AR_w	6.42	Horizontal Tail AR/Taper	6.34/0.77
		Vertical Tail Span, b_v	8.2 in (each)
Wing Planform Area (Actual), S_w	464.44 in ²	MAC Vert	C _{VT} Tip
Wing Planform Area (Calculated), S_w	1016 in ²	4.68 in	2.8 in
		C _{VT} Root	6.5 in
Mounting Parameters		Wheel Geometry	
Fuselage length, l_f	24 in	Front Wheel Diameter, d_{wheel}	2.5 in
Fuselage Diameter, d_f	4 in	Rear Wheel Diameter, $d_{wheel, rear}$	1 in
Wing Location	10.0 in (LE)		
Front Wheel Location	8.5 in (LE)	Landing Gear Height	6.1 in
Back Wheel Location	38.5 in (LE)		
Vertical Tail Location	36.5 in (LE)		
Weights and Sizing			
Aircraft Weight, W_0	5.6 lbs	Battery Sizing	5.5 in by 11.69 in by 1.54 in
M2 Total Weight, W_{M2}	7.5 lbs	Battery Weight	1.1 lbs
M3 Total Weight, W_{M3}	5.74 lbs		
Aircraft Aerodynamics and Stability			
Takeoff Airfoil	NACA 4308-Mod	Tail Airfoil	Flat Plate
Coefficient of Lift, Takeoff, $C_{L_{Takeoff}}$	1.11	Coefficient of Lift, Cruise, $C_{L_{Cruise}}$	0.3971
Drag Coefficient, Takeoff	0.1	Drag Coefficient	0.0827
Lift Slope, Tail	2π	Lift Slope, Wing	5.71
Tail Angle of Attack	0 deg	Wing AOA	0 deg
Aerodynamic Center	12.1 in	Center of Gravity	14.5 in
Power and Thrust			
Engine Thrust and Power	SunnySky X-3120, 750 W	Motor Thrust	7.2 lbf

4.2 Final Sub-System Architectures

In the final assembly of each subsystem, analytical comparisons were taken from the collected simulation and experimental datasets. This allowed for each sub-system to be improved incrementally, from propeller and motor configurations, to wing structure designs. This analysis, for example, allowed for an increase in wing stiffness upon redesign, and a change in battery to allow for considerably longer flight time. Other lesser changes include aluminum hardware for final assembly, and material changes from balsa wood to plywood in certain high-stress areas.

4.2.1 Propulsion System

The motor selected was the SunnySky X3120 950Kv. The above table shows the plotted data gathered from thrust stand testing completed with the physical motor vs the MotoCalc8 simulated data from the prior estimation. In this testing, the motor was found to provide sufficient thrust compared to the projected velocity of travel during flight. The motor, along with all wiring included, weighs roughly 7.25 ounces. It was found that using a 12x6 propeller in tandem with the motor selected would provide the most efficient thrust to watt ratio desired as shown in Table 29. From endurance testing for the motor and battery, the estimated flight time is 9.3 minutes at 70% throttle, which satisfies the 10 minutes flight window for Mission 2.

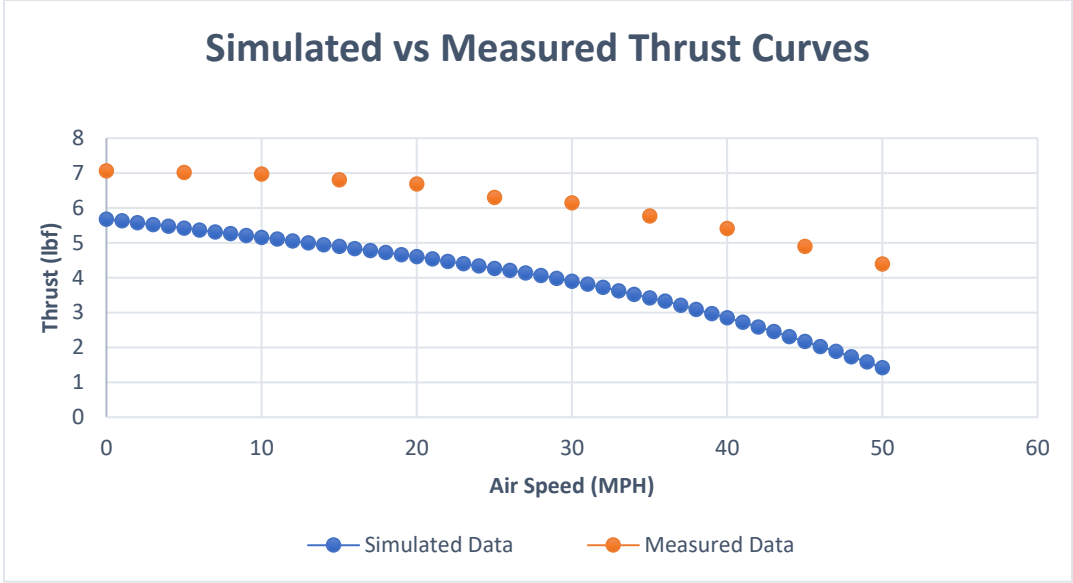


Figure 30: Dynamic thrust stand data and MotoCalc8 simulated data.

Table 29: Propeller performances with a SunnySky X3120 950Kv motor

Propeller	Thrust (lbf)	Current draw (A)	Battery Voltage	Power (W)
12x6	6.3	52	13.9	750
10x7	3.9	41	14	580
11x8	6.15	47	14	700
12x8	5.2	60	13.8	900
12x8	5.2	56	13.8	750
13x8	6.3	60	13.5	900

4.2.2 Flight Control System

The mission course consists of a single oval with a 360 degree turn integrated into the non-runway side straightaway. A main component of each mission is taking off in no more than 60 feet. A takeoff greater than 60 feet will result in disqualification.

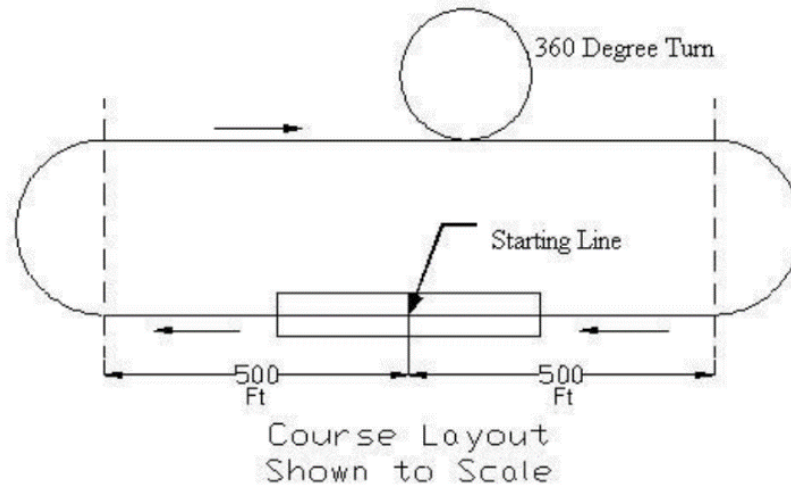


Figure 31: Nominal flight course

In Figure 31, the mission course has a length of at least 1000ft. Assuming the aircraft is flown at an altitude based on the FAA legal altitude limit of 400ft [2], the maximum range between the radio/receiver is estimated to be 640ft if the pilot stands at the starting line. To account for a factor of safety, the team aimed for a minimum RSSI value of 55 at 1280ft to ensure a reliable connection and prevent loss of signal (LOS) according to FrSky's Taranis X9D Access Manual. The Received Signal Strength Indicator (RSSI) is a metric used to quantify the power level of a received radio signal in wireless communications. The wiring setup of the system is showcased in Appendix A.

4.3 Structure

The overall design of the aircraft began from an aerodynamic standpoint in which overall dimensions of large components like wing shape, fuselage, and tailplane dimensions. Following overall shape, basic CAD models and prototypes were created for the various components to test their structural properties. The rigidity of the overall structure was considered incredibly important and was accomplished through various techniques. While brainstorming designs for structural components, a rule of thumb that was followed was that two plates attached at 90 degrees to each other is more rigid in every direction than just one plate on its own. This can be seen in the fuselage design as the bottom and two side plates attach in such a way that they reduce bending and twisting along its length. This design choice can also be seen in the box created internally on the airfoil spacing members on the wings along with the D shaped tube of thin balsa wood attached along the leading edges. In addition to attaching laser cut plates to each other to maximize rigidity and strength, carbon fiber tubes were also used to obtain rigidity along longer sections of the aircraft such as the wings and tail attachment.

Finite element analysis was performed on the final wing design shown in Figure 32 and Figure 33. With three major load bearing carbon fiber rods, and a balsa wood construction, 2.34 inches of wing deflection was measured. All testing was at an expected maximum load of 2.5g, which is equivalent to a 17.5 lbf load for a 7 lb aircraft. In all cases (I.e. full wing and main load bearing carbon fiber rod) static structural simulations were run. This force was applied to the tip of the carbon-fiber supporting rods, directed immediately downwards, in the negative z-direction.

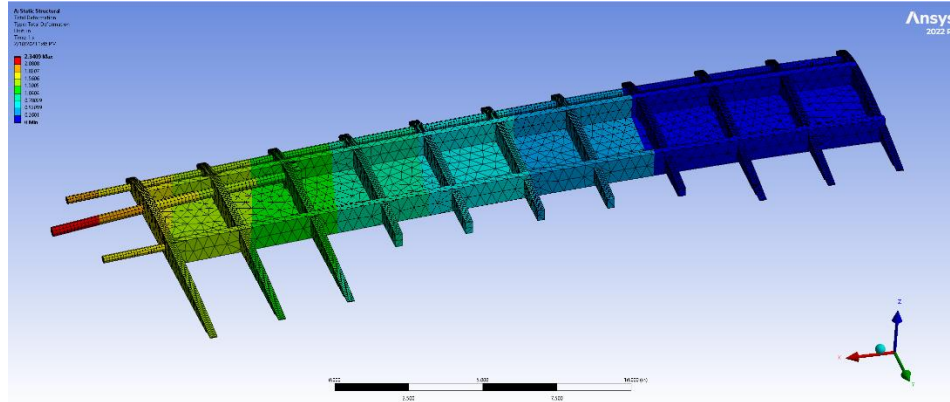


Figure 32: Wing Deflection Simulation of 2.5g load

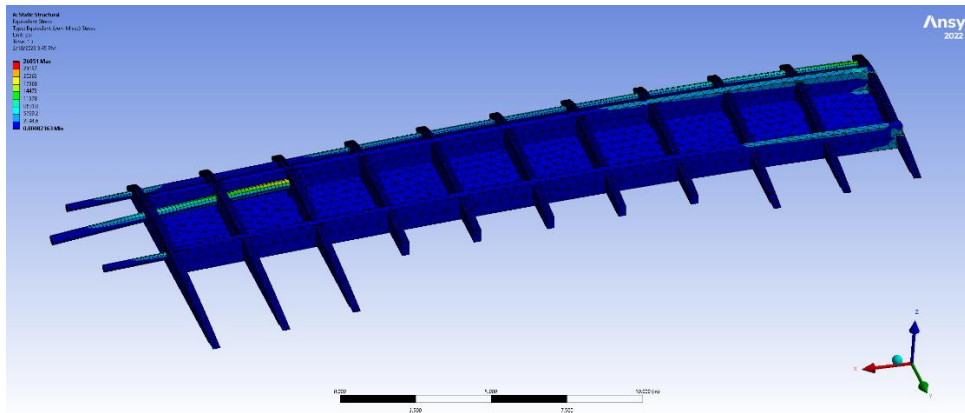


Figure 33: Wing Stress Simulation of 2.5g load

Table 30: Stress and Deformation results from ANSYS simulation

Wing Simulation Results (2.5 g load test on wing-tip)		
Maximum Stress	26,851 psi	Location: 3/8" Carbon Fiber Structural Rod
Maximum Deformation	2.34 in	Location: Wing Attachment to Fuselage

4.4 Aircraft Weight and Balance

The final aircraft weights shown in Table 31 were determined using an aircraft component build-up and from weight measurements using a digital scale or manufacturer data. The Cg measurements in Table 32 are indexed from the leading edge of the wing, negative in front and

positive behind. A 5% factor of safety to the total weight is added to ensure payload compliance. The CG remains constant throughout all missions due to minor adjustments in payload and battery locations.

Table 31: Weight Table

Mission 1 Weight		Mission 2 Weight		Mission 3 Weight	
Component	Weight (oz)	Component	Weight (oz)	Component	Weight (oz)
Fuselage	16.5	Fuselage	16.5	Fuselage	16.5
Landing Gear	9	Landing Gear	9	Landing Gear	9
Motor/Propeller	7.25	Motor/Propeller	7.25	Motor/Propeller	7.25
Right Wing	7.8	Right Wing	7.8	Right Wing	7.8
Left Wing	7.8	Left Wing	7.8	Left Wing	7.8
Battery	17.6	Battery	17.6	Battery	17.6
Electronics	7	Electronics	7	Electronics	7
Tail Assembly	12	Tail Assembly	12	Tail Assembly	12
Payload	N/A	Payload	38	Payload	2.6
5% Safety Factor	4.25	5% Safety Factor	4.25	5% Safety Factor	4.25
Total	89.2	Total	127.2	Total	91.8

Table 32: Aircraft Balance Table

Mission 1 CG			Mission 2 CG			Mission 3 CG		
Component	X [in]	% Chord	Component	X [in]	% Chord	Component	X [in]	% Chord
Fuselage	-0.5	-5	Fuselage	-0.5	-5	Fuselage	-0.5	-5
Landing Gear	-1.25	-12.5	Landing Gear	-1.25	-12.5	Landing Gear	-1.25	-12.5
Motor/Propeller	-11	-110	Motor/Propeller	-11	-110	Motor/Propeller	-11	-110
Right Wing	3.25	32.5	Right Wing	3.25	32.5	Right Wing	3.25	32.5
Left Wing	3.25	32.5	Left Wing	3.25	32.5	Left Wing	3.25	32.5
Battery	3	30	Battery	4.5	45	Battery	3	30
Electronics	-7	-70	Electronics	-7	-70	Electronics	-7	-70
Tail Assembly	21.25	212.5	Tail Assembly	21.25	212.5	Tail Assembly	21.25	212.5
Payload	N/A	N/A	Payload	-1	-10	Payload	2	20
Full Aircraft	2	20	Full Aircraft	2	20	Full Aircraft	2	20

4.5 Final Aircraft Performance

Final aircraft performance is updated with final build up weights and further analysis of subsystems. The extracted performance estimates are shown in Table 33 below.

Table 33: Estimated Aircraft Performance

Aircraft	M1	M2	M3
All-Up Weight [Oz]	89.2	127.2	91.8
Payload Weight [Oz]	N/A	38	2.6
Wing Loading [oz/sq.ft]	27.6	39.44	28.46
Cruise Throttle	0.5	0.65	0.5
Static Thrust [ozf]	39	50.7	39
Turn Load Factor	2.5	2.5	2.5
Ground Roll [ft]	18.9	40.2	20.18
Cruise Velocity [ft/s]	58	55	58
Number of Laps	3	8	3
Lap Time [s]	45	55	48
Mission Time [s]	135	440	144

4.6 Predicted Mission Performance

The final mission performance is estimated based upon the final configurations and parameters of the final flight performance. The best performing team score is calculated by assuming that the Beluga aircraft performs at 80% of the maximum for each mission segment. Table 34 below displays the calculated mission performance of the final design. Throughout the design process it is noted that an emphasis on flight speed was placed to improve scores in M2 and M3 respectively.

Table 34: Mission Performance of Final Design

Aircraft	GM		M1	M2		M3	
	Aircraft Weight [Oz]	Test Weight [Oz]		Payload Weight [Oz]	Laps Flown	Antenna Length [in]	Mission Time [s]
Flying Goat	127	205	1	38	7	5	156
Assumed Best	150	300	1	48	10	6.25	125
Personal Mission Score	0.8		1	1.55		2.64	
Total Score	5.99						

4.7 Drawing Package

The following pages illustrate CAD drawings of the mid wing aircraft. The first page, showing a three-view drawing of the aircraft with all relevant dimensions labeled. The second page is the Structural Arrangements drawings showing an exploded view of the aircraft with a ‘Bill of Materials’ table included. Each key part is labeled with bubble numbers corresponding to the table. The third page is the Systems Layout and Location drawings which includes detailed views of each joint attachment point, motor, and motor mount, as well as a view of the landing gear and its attachments.

4

3

2

1

D

D

C

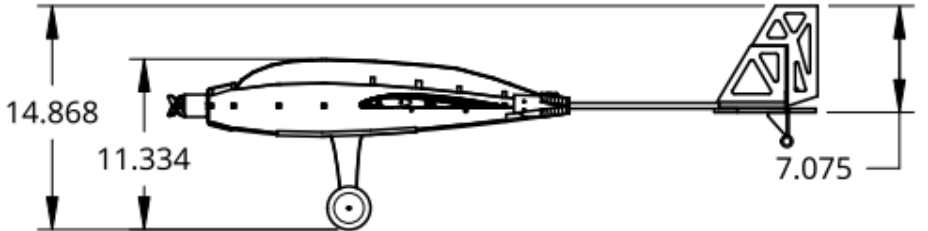
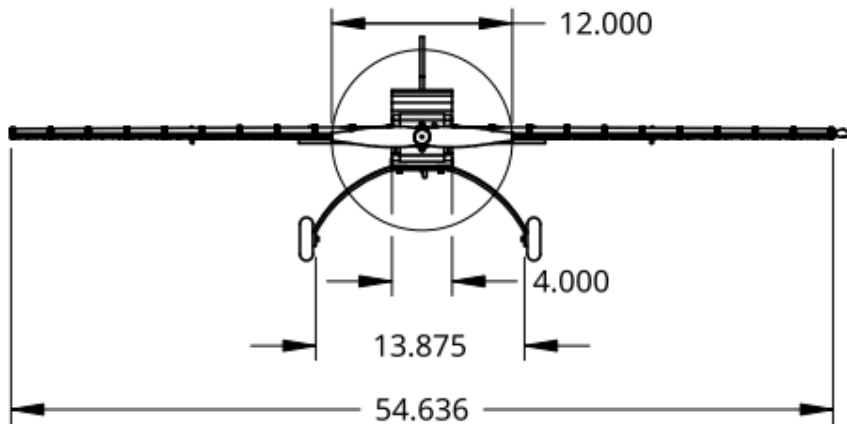
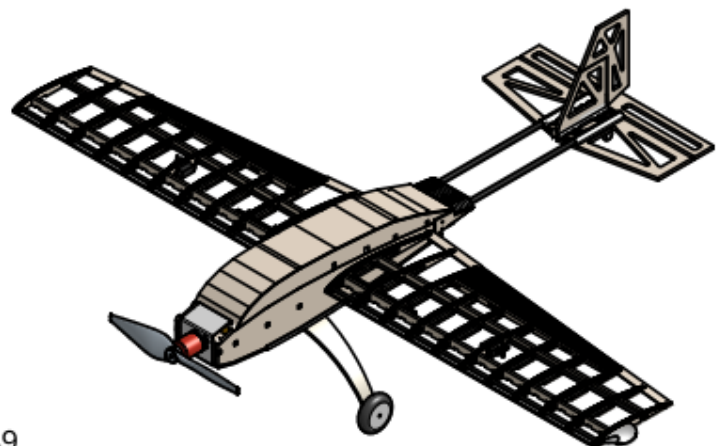
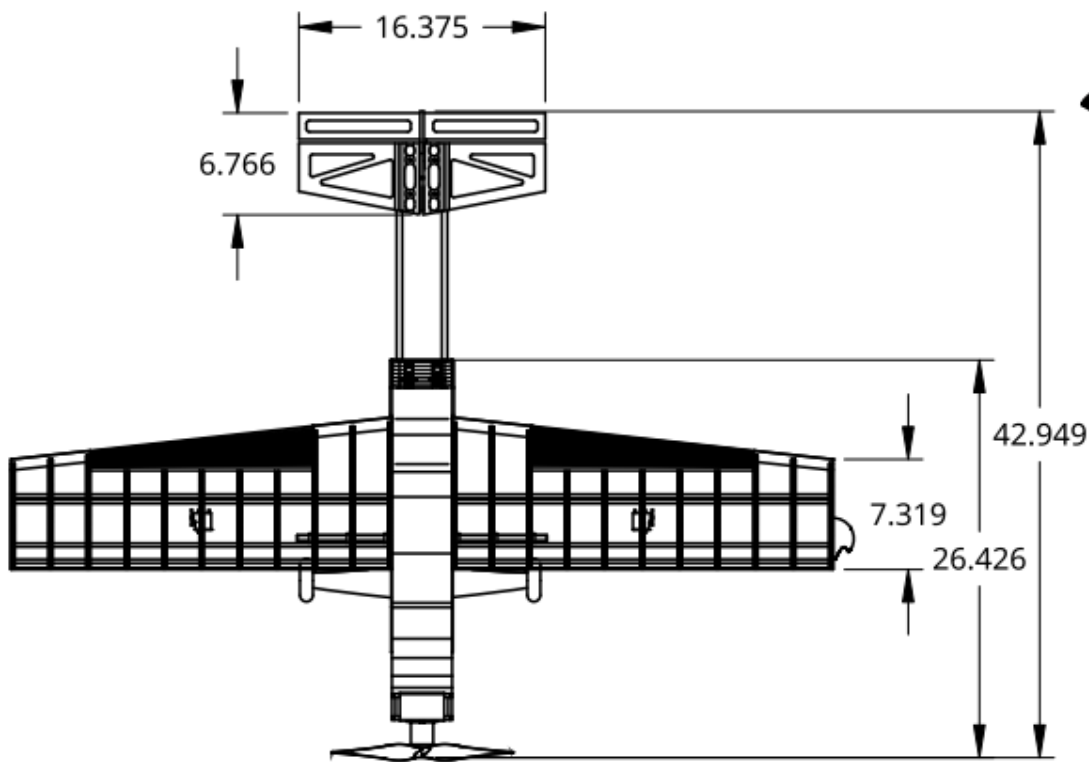
C


B

B

A

A



 WPI		Worcester Polytechnic Institute	
		AIAA Design Build Fly 2023	
Aircraft 3-View			
DRAWN BY:	DATE	SCALE	SHEET
DRAKE HAMLIN	02/06/2023	1:12	1 of 3

4

3

2

1

4

3

2

1

D

D

C

C

B

B

A

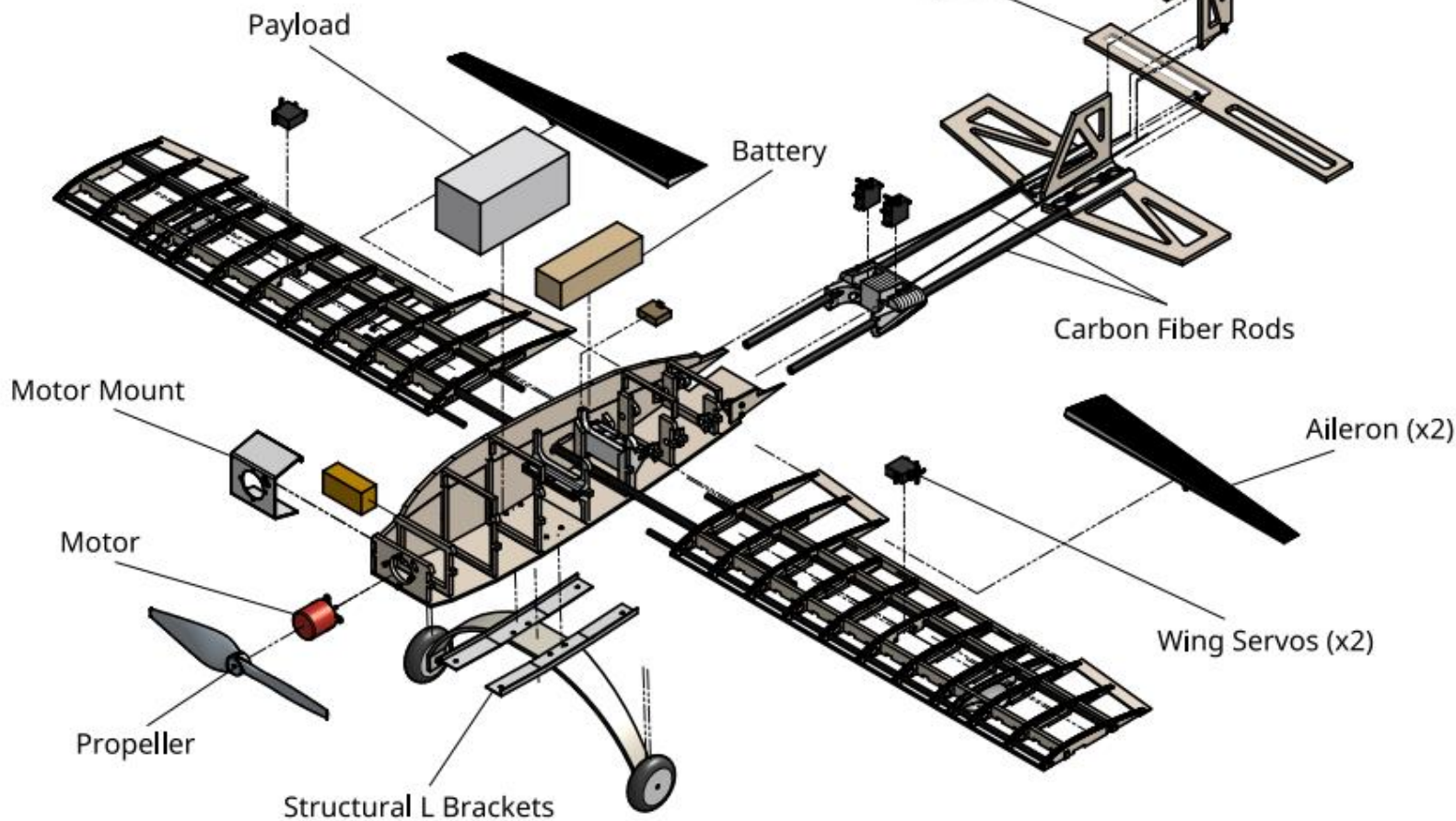
A


4

3

2

1



 WPI	Worcester Polytechnic Institute AIAA Design Build Fly 2023	
	Structural Arrangement View	
DRAWN BY: DRAKE HAMBLIN	DATE: 02/06/2023	SCALE: 1:8
		SHEET: 2 of 4

4

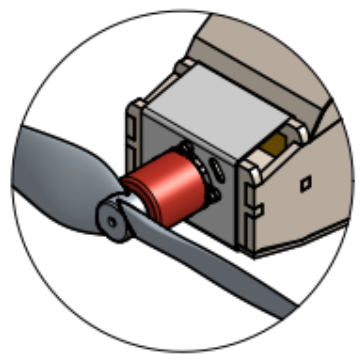
3

2

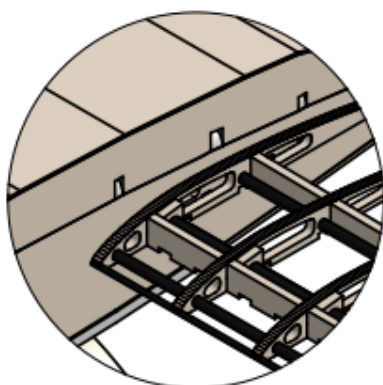
1

D

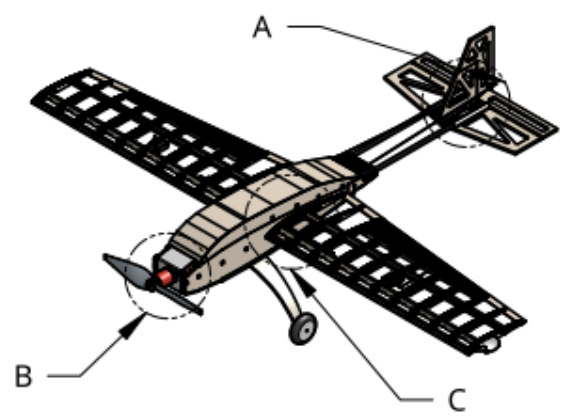
D



DETAIL B
Motor Mount Attachment
SCALE 1:4

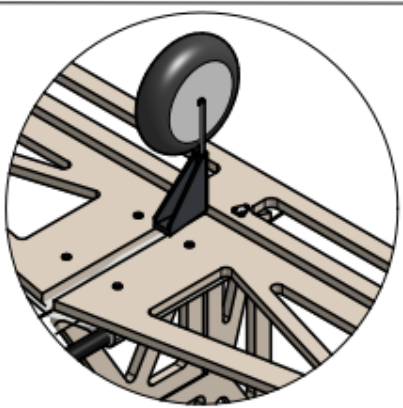


DETAIL C
Wing Fuselage Connection
SCALE 1:4

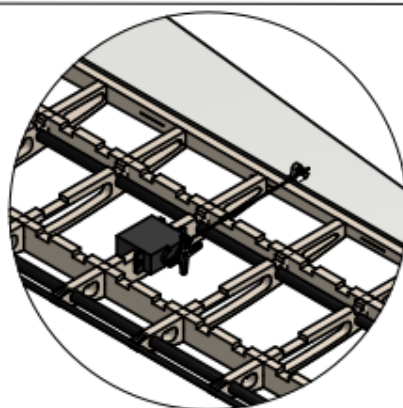


C

C



DETAIL D
Tail Wheel Connection
SCALE 1:4



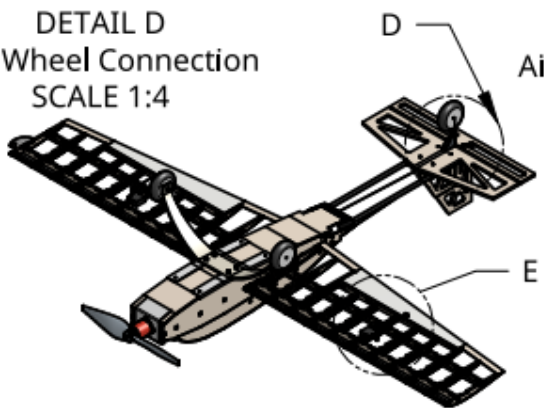
DETAIL E
Aileron Connection
SCALE 1:4



DETAIL A
Tail Control Surface Connections
SCALE 1:4

B

B



A

A



WPI

Worcester Polytechnic Institute
AIAA Design Build Fly 2023

Systems Layout Location View

DRAWN BY:	DATE	SCALE	SHEET
DRAKE HAMBLIN	02/06/2023	1:16	3 of 4

4

3

2

1

4

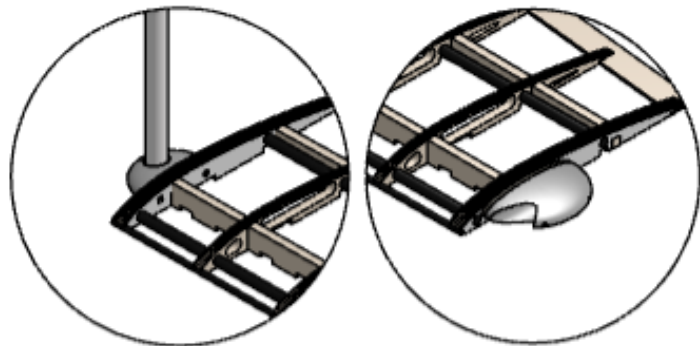
3

2

1

D

D



DETAIL F
PVC w/ Attachment Holder
SCALE 1:4

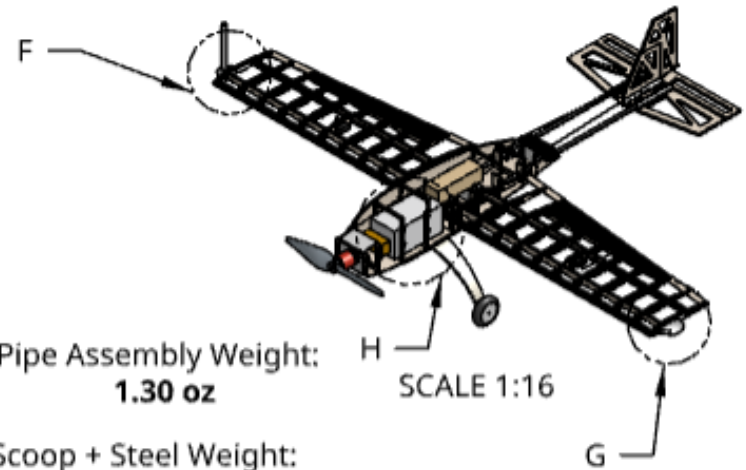
DETAIL G
Scoop Attachment
SCALE 1:4

Pipe Assembly Drag:
0.472 lbf

Pipe Assembly Weight:
1.30 oz

Scoop Attachment Drag:
0.138 lb

Scoop + Steel Weight:
1.30 oz

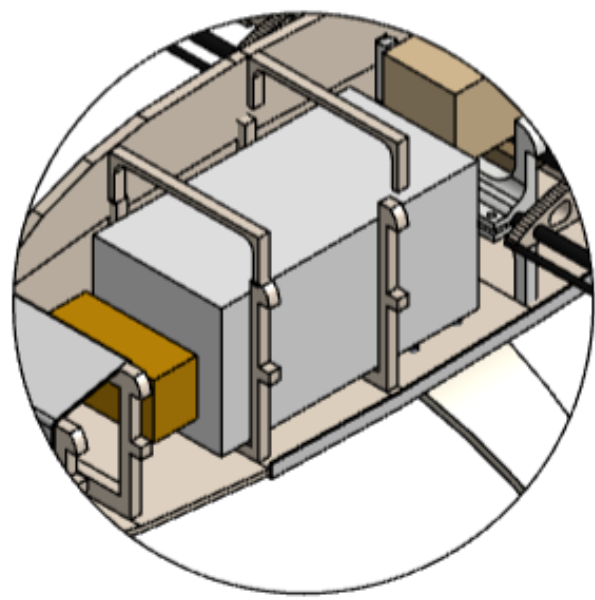


H
SCALE 1:16

G

C

C



DETAIL H
Payload Location
SCALE 1:3

*Grey Box - Payload
Loaded with custom solder
disks and square steel plates to
provide the 1/3 required
weight.
Total Aircraft Weight - 89.2 oz
Payload Weight - 38.0 oz


Scoop Attachment Designed to
increase drag opposite PVC
attachment. Total drag created by
scoop acting as 'counterweight',
providing roughly 1/3 the amount
of drag.

B

B

A

A

 WPI		Worcester Polytechnic Institute	
		AIAA Design Build Fly 2023	
		Aircraft Payload Accommodation	
DRAWN BY:	DAVID HASBUN	DATE:	02/09/2023
		SCALE:	1:12
		PAGE:	
		4 of 4	

4

3

2

1

4.8 Ground Test Hardware

The final iteration of the ground test fixture (GTF) is 20 inches high from ground to wingtip to allow for the aircraft landing gear wheels to not touch the ground, and strong enough to support the aircraft while additional weight is added during ground testing. Two holes with a diameter of 0.1693 inches were drilled 1.42 inches apart into the wing tips to attach the antenna adapter, and since these holes would also be used to secure the aircraft to the GTF, two holes of the same diameter and distance apart were included into the GTF design on its interface.

5 Manufacturing Plan

5.1 Processes

Before beginning any sort of design deeper than a general overall shape, the team spent time looking into the most common strategies used by hobbyists for fixed wing RC competitions. It was found that many of these strategies, while delivering a competitive final product, were incredibly time-consuming, tedious, and made iterative design approaches more difficult for a group that had never constructed a model aircraft before. The strategy developed by the team to get a best of both worlds' scenario was to utilize a traditional balsa-wood construction for a lightweight and strong structure, but to utilize the tools available to the group to cut back on manufacturing time as much as possible. This was accomplished by spending more time on the CAD model in order to ensure that as many components as possible of the aircraft could be either laser cut or 3D printed. This cuts down on both manufacturing time for simple and complicated components, as well as almost eliminating room for human error in all components. In addition to designing components in such a way that they could be mass manufactured, it was also determined that as many parts as possible should lock together. The interlocking of components served two

main purposes: reducing room for human error during assembly by giving each piece exactly one position and orientation it could be placed at, and greatly increasing the strength of each joint. By following the goal of having each component precision cut by a machine and ensuring that all piece's lock together in a clear manner, a structurally sound aircraft could be quickly manufactured, assembled, and iterated upon.

5.1.1 Balsa Construction

Balsawood, as it is lightweight compared to the other materials readily available to the team, (balsa wood, plywood, aluminum, insulation foam) made up the bulk of the aircraft's construction. Most portions of the aircraft were made either out of 0.25" or 0.125" thick pieces of laser-cut balsa wood. For larger load bearing components that needed extra strength in one specific direction, laser-cut 0.25" balsa wood was used with grain direction being strategically chosen to more support the direction of the largest load. For applications where less strength was needed, but a large surface area of material was necessary (payload hatch, bottom plates in wings), 0.125" balsa wood was used. For parts where strength in multiple directions was needed, but where heavy plywood would have been excessive, two pieces of 0.125" balsa wood were glued together with grain directions 90 degrees to each other. This allowed for an incredibly lightweight but uniformly strong component to be made. This technique was used for all ribs along the length of the fuselage. In order to minimize room for human error and ensure the strongest bond between balsa wood pieces, as many components were designed to lock together as possible. This not only added strength because of the extra surface area for super glue to adhere to, but also in many cases would require balsa to break against the grain direction in order to separate two interlocking components.

5.1.2 3D Printing

3D Printing was used for the wing attachment points, tail boom attachment piece and tail support piece shown in our detailed drawing since they required strength and more complicated 3D geometries that would have been difficult to replicate either by hand or by a series of interlocking laser-cut pieces. The clamps that hold the wings in place, the tail attachment/servo mounting piece, and the component used to attach the empennage all have complex 3D geometries that would make them difficult to make any way except for additive manufacturing. In addition, these parts all require more strength than just balsa wood would allow, also making them excellent candidates for being a 3D printed component.

5.1.3 Adhesives

Cyanoacrylate (CA) glue is a fast setting, thin layer adhesive, commonly used in woodworking applications. CA is fast bonding allowing it to dry incredibly quickly upon activation, making it an ideal glue to be used in RC building applications. Usually laying very thin, it is available in many various viscosities to better penetrate wood and form a strong bond. As well as being an excellent glue used with wood, CA glue is also capable of sealing or bonding metal and other materials. The use of CA glue in this project was crucial in most fittings and bonding of parts together.

Epoxy was used to bond more permanent fixtures, as it sets like a plastic. This allowed the use of epoxy to affix components such as the tail booms, which should be extremely rigid during flight. JB Weld, 5 minute quick-set, 2-part epoxy was mainly used. This product is made specifically for hobby and wood applications, as well as soft metal adhesion.

5.1.4 Hardware

During the prototyping phase, most of the hardware used was miscellaneous. Once the design was finalized, standardization of hardware was introduced. Table 35 lists the type of hardware used as well as the material. To save weight, most of the hardware was switched from steel to aluminum.

Table 35: Hardware List

Hardware List:		
Wing clamps	M4x16 mm	Aluminum
Tail Fixture	M4x14 mm, 4 mm nylon lock nut	Steel, Aluminum
Tail Attachment	M3x16 mm	Aluminum
Tail Wheel	M2x12	Steel
Landing gear	M4x20 mm, 4mm nylon lock nut	Steel, Aluminum
Motor mount	M3x16 mm, 3 mm nylon lock nuts	Aluminum
All	#6 Flat washer	Aluminum

5.1.5 Metal Component Manufacturing

The weights used in the mission 2 payload were created from steel alloy stock and solder. The primary weights were created from steel stock. Using a bandsaw, the 0.125-inch-thick stock was cut down to be 2.7 by 1.5 inches. Each of these cut pieces of stock weigh about 2.3 oz. The solder was melted using a in a steel can on a small camping propane stove. It was then poured in

a muffin pan that was lined with aluminum foil. The raw pucks were then sanded and cut down to make them even to each other. The pucks are about 2 inches in diameter and weigh about 2.5 oz.



Figure 34: The formed solder pucks and the uncut steel stock

A motor mount was made to wrap the front end of the fuselage. Made from 1/16" aluminum, it was water jet cut to run the length of one section of the fuselage on the top and bottom. Holes were also cut to precisely align the motor and its mounting bolts. The mount was cut to 2.95" x 11.00". The motor mount itself weighs 1.875 ounces in total. The water jet and 1/16" aluminum was also used to cut aluminum spars that match the dimensions and fit the last spar on each wing.

5.2 Manufacturing Selection

Material choice for each section of the aircraft was carefully selected such that strength, overall structure profile, and weight fit the needs for that portion of the aircraft. Balsa wood was used for many components as it is incredibly light, strong, and easy to cut into accurate shapes with a laser cutter. In addition, when pieces are arranged with grain direction being strategically planned and constructed in a box shape, it was found that overall rigidity and strength increased significantly. This application was used heavily for portions of the aircraft where a larger profile was considered acceptable. Carbon fiber tubes were used for structures that needed both strong

and lightweight structural members while maintaining a minimal profile. These were utilized throughout the aircraft, but only in places it was deemed especially necessary due to increased cost of carbon fiber. In places where complicated 3D geometry was necessary and where more strength than balsa wood would allow was needed, 3D printed components were implemented. Infill percentage and layer direction were both tools used to ensure that all 3D printed parts were optimized for their location on the aircraft and for the load capacities necessary. Finally, aluminum was used for components that would endure large strains and were in locations where weight also needed to be strategically placed. When combined, all these materials created a strong yet light structure.

5.2.1 Wing Construction

A combination of competition grade balsa wood and carbon fiber rods comprise the primary structural components of the aircraft's wings. As seen before, two primary manufacturing methods were considered: laser cutting and 3D printing. Balsa wood was selected as the primary material in the wing due to its low density, strength, and ease of workability via a laser cutter. Because everything was modeled in CAD before construction, this reduced the time to cut all pieces for a wing to less than a fifteen-minute process.



Figure 35: Initial laser cut wing.

Each part was laser cut using a DXF file exported from Fusion 360 in conjunction with Inkscape and Retina Engrave to arrange and export files to the laser cutter. The time of cut generally depends on the size of the part, however the low density of balsa wood allows for the laser to run on maximum speed, greatly reducing cut time for these applications. The CAD driven approach used allows

replicated parts to be easily produced and iterated upon, as the laser cutter has a tight tolerance on each cut. Figure 35 is an example of the first wing cut. These wings were easily duplicated which allowed for further iteration.

Physical tests were conducted on the early wing prototypes. These wings were used for glide tests, torsion tests, deflection tests, as well as giving the team experience in assembling wing pieces in the best order of operation possible. As different wing designs are iterated upon, they are simultaneously updated in the CAD model. This allows the subsequent versions of the wings to be produced quickly. Overall, this creates an efficient iteration process. This process will cycle for three to five iterations at which time the final iteration will be arrived at.

5.2.2 Fuselage Construction

The fuselage is assembled with a combination of laser cut and 3D printed components. Two large side profiles of the fuselage airfoil are the main load bearing members and are attached together by thin ribs each made of pieces of balsa wood with grains in opposing directions. In addition to the balsa wood ribs, two 3D printed wing clamps also act as major structural members to prevent the side plates from moving in relation to each other. Thin plywood is bent around the bottom of the fuselage and epoxied along its length to provide more structural integrity and to act as a rigid attachment point for the landing gear.

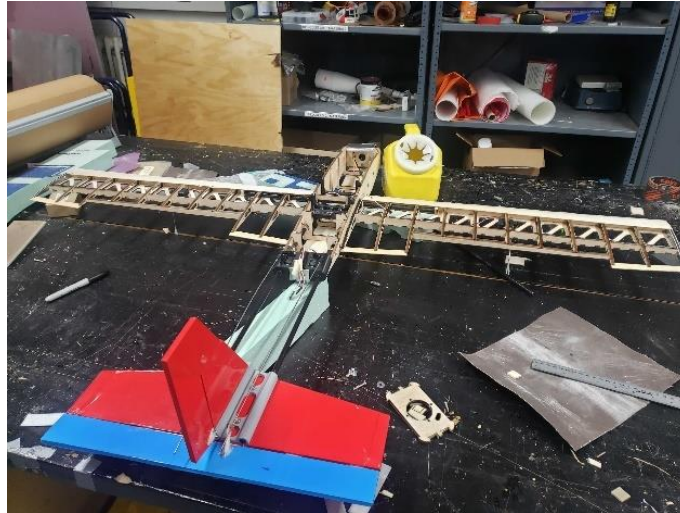


Figure 36: The aircraft assembled before Monokote is applied to wings and body

5.2.3 Landing Gear

The landing gear the team elected to use is comprised of a main structure made of nylon, a mix of foam and rubber wheels, and aluminum belly pan reinforcements. The primary components of the landing gear are off the shelf components from Du-Bro. The tail wheel is attached to the underside of the horizontal stabilizer and is attached to the rudder in such a way that both move together, allowing for steering while taxiing without adding an extra channel or servo. Two



Figure 37: Landing gear bottom attachment point

foam/rubber wheels with an axle diameter of $5/32$ " are fixed to the landing gear with a $5/32$ " steel axel shaft and two nickel plated wheel collars. The fuselage reinforcements connecting the landing gear to the fuselage are constructed out of $1/20$ " aluminum L metal.

As seen in Figure 37, the L metal runs along the outside edge of the fuselage and connects 3.5" in front and 4" behind the landing gear respectively. The reinforcements connect through the fuselage and across four internal bulkheads to provide the strength and rigidity required upon landing.

5.2.4 Tail and Tail Boom

The tail planes, tail booms, and mounting for tail control servos are all constructed as one assembly for ease of attachment during the five-minute assembly time. The team opted to use a conventional tail configuration for both ease of maneuver calculations and to radio channel mixing. Two smaller tail booms were used instead of one larger one to reduce twist of the empennage in relation to the rest of the aircraft. Control servos were placed in the 3D printed tail attachment fixture rather than on the empennage to reduce the exposed profile that would increase drag as well as moving the center of mass forward to increase static stability of the aircraft.

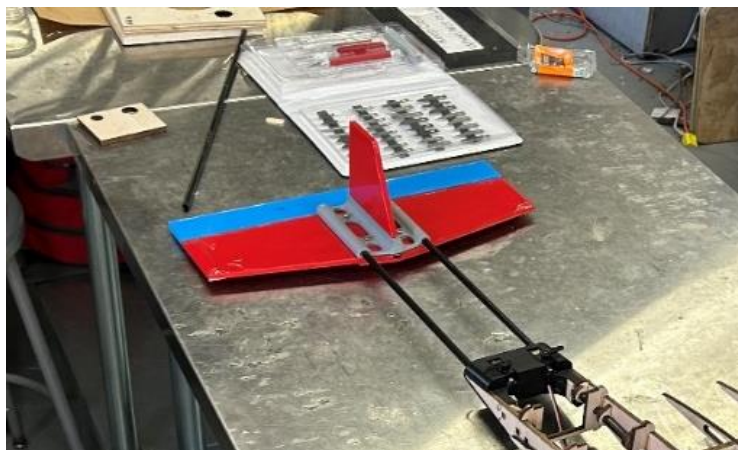


Figure 38: Tail attachment piece during manufacturing

5.2.5 Payloads

As specified in the mission requirements, the electronics package must be entirely contained in the aircraft. Using CAD, a box was modeled with the outer dimensions meeting the minimum dimensions of 6x3x3 inches when the lid is on. The internal dimensions of the box are 5.8x2.8x2.8in. This model is then 3D printed.



Figure 39: Mission 2 Payload with weights and spacers

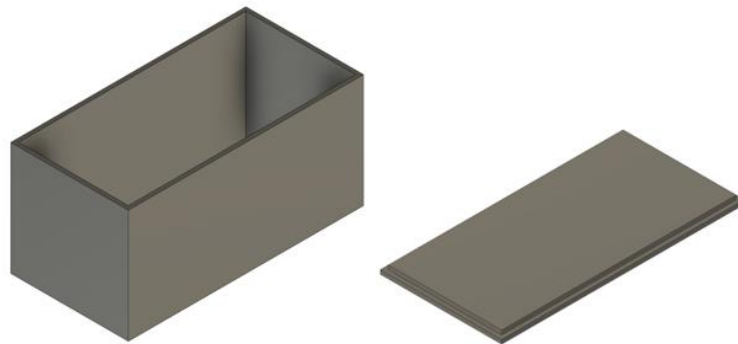


Figure 40: Payload box CAD model

Within the box are foam spacers and weights formed from steal stock and solder pucks. The stock is 0.125 inches thick and cut to 2.7 by 1.5 inches. Each piece of cut stock weighs 2.3 oz. Each solder puck is about 2 inches in diameter and weighs around 2.5 oz. 9 pieces of stock and 5 pucks were added to the box. Foam spacers allow for the internal weight in the payload to be shifted forward or backward to adjust the aircraft center of gravity. The foam spacers also prevent the weights from shifting in flight. In total, the weight of the payload was 34.4 oz, slightly exceeding minimum weight, 30.5 oz, calculated in section 4.4.

Wing-tip fixtures are constructed using 3D printers, and PLA filament. This allows for quick and accurate manufacturing of the wing tip fixtures. Wing-tip fixtures are mounted to the final rib using M3 2-inch bolts and connecting to solder-welded nuts secured on the inside of the final rib. This attachment method will allow for the fixtures to be held secure on the side of the wing, with the 2-bolt attachment preventing spinning or drooping of the attachments.

5.2.6 Ground Test Fixture

CAD models were created of the ground test fixture using SolidWorks for the early iterations. The first design was a solid 3D block to model the general shape of the fixture before deciding on the method of manufacturing. Possibilities that were considered for manufacturing included 3D printing and CNC, before settling on laser cutting due to the ability to manufacture large structures while being efficient with the number of materials needed. The solid 3D model was redesigned to be 8 separate pieces that could be laser cut and interlocked into a hollow yet strong structure. 0.25-inch plywood was decided as the material because of its rigidity. Onshape was used for the final model, and when the pieces were laser cut, the edges were sanded to ensure

a smooth surface for the faces to fit together. CA glue was used to secure the faces of the fixture together.

6 Testing Plan

The testing plan for the aircraft was imperative to developing our design from the ground up. Different tests were used to verify the aerodynamic design of the aircraft, and to confirm aircraft stability in a fully assembled state. Testing was primarily meant to show systems working in combination to ensure that the designs set forth by each sub-team were compatible on the full-aircraft scale. Three prototypes and a glider were tested. The glider, “the Ukraine” was the first un-powered prototype constructed. Following the glider, Prototype 1, “The Lizard” was tested. The repaired and revised version of Prototype 1 yielded Prototype 2, the “Flappy Bird”. Lastly, after the unfortunate loss of Prototype 2, the final Prototype 3, the “Beluga” was constructed for testing.

6.1 Ground Testing

In conjunction with the testing plan, each iteration of the aircraft was named so that they could each be subjected to applicable tests. The tests and prototypes are explained in detail below. Simultaneously, the testing plan was summarized in In conjunction with the testing plan, each iteration of the aircraft was named so that they could each be subjected to applicable tests. The tests and prototypes are explained in detail below.

Table 36: Testing Plan Summary

Test Performed	Test Objectives	Test Equipment	Data Collected	Design Application
Static Motor-Propellor Thrust Tests	Analyze flight statics and thrust production	Thrust stand, Motor and propeller	Motor thrust data, motor power draw and rpm	Used to select motor and propeller configuration
Dynamic Motor-Propellor Thrust Stand Tests in Wind Tunnel	Flight dynamic performance metrics	Thrust stand, wind tunnel,	Motor thrust data, motor power draw and rpm at given airspeeds	Used to validate motor selection in a dynamic environment
Wind Tunnel Aerodynamic Tests	Confirm aerodynamic data predicted in XFLR5	Thrust stand, wind tunnel, scale model wing	Lift generated as a function of airspeed	Validated conceptual design of wing produces ample lift
Ground Mission Test	Ensure proper wing loading and structural integrity	Payload, Test Weights, Ground Test Fixture	Wing deflection in extreme loading environments	Validation of wing structure, reasoning for changing wing structural components
Radio Transmitter Range Test	Test range distance and ensure proper radio transmission	Measuring Tool, Radio	RSSI > manufacturer recommended value	Validated use of Radio Transmitter, Receiver, and Redundancy Receiver
Glider Test	Analyze aerodynamics in practice, such as stall capabilities and stability	Glider prototype "The Ukraine", video cameras	Video evidence of dynamically and statically stable behavior	Validated Aerodynamic Design and "stiff" aircraft dynamics
Powered Flight Tests	Prove aircraft's ability to fly, find areas of improvement	Prototype 1, Prototype 2, Video cameras	Video evidence of flight. Flight speed, takeoff distance, and structural limits	Validation of flight dynamics and ability to fly AIAA DBF Missions
DBF Mockups	Improve overall mission score through repetition	Final aircraft "Beluga", Flight data recorders	Simulated competition scores. Simulated design report scores.	Proof of flight performance, ground mission performance, at the AIAA DBF Competition

6.1.1 Propulsion Test

Static thrust testing was conducted early to assist in analyzing the flight dynamics of the aircraft, as well as to produce thrust values for dynamic takeoff and steady-flight analysis. Power consumption was examined to determine battery time to depletion as well. Numerical data was also used to determine the validity of various computer simulations within MotoCalc8.

6.1.2 Wind-Tunnel Test

Wind tunnel testing was the first large-scale step into confirming aerodynamic data gathered from the XFLR5 software. Testing simulated 45 mph flight speeds, which were the goal flight speeds for the aircraft. A 1/3rd scale wing was constructed for this test, Of course, this meant that the air speed needed to be 3 times as much as the desired flight speed of 45 miles per hour to replicate flight conditions. For most accurate results, a force balance was used to measure down force on an upside-down wing specimen.

6.1.3 Ground Mission Test

Prior to each major flight test or taxi test attempt, the fuselage was loaded with max payload of 30% of the aircraft weight to ensure that the wings would be able to handle the load. As well as this, the first prototype was loaded to failure to determine the strength capabilities of the wing. This test serves to validate the testing done in Ansys on wing strength and deflection capabilities. Emphasis was put on keeping the wings flight-worthy and crashworthy after these loading tests.

6.1.4 Range Test

A range test was performed on the Frsky RX6R and XM+ radio components to verify their ability to maintain a consistent signal transmission between the transmitter and receiver. The antennas were positioned in a right-angle orientation to optimize the RF signal strength, with the primary receiver located between the wing clamps and the redundant receiver situated near the payload, clear of any carbon fiber rods that have the potential to interfere with RF signals.

6.2 Glide Tests

The first proof of concept formed was an unpowered glider with no control surfaces. This was constructed using a foam fuselage, first iteration wing-design, and a replicated tail-boom and empennage assembly. An unpowered glider was ideal for gathering an idea of full aircraft stability characteristics, such as stall, center of gravity, and also provided meaningful information on crashworthiness of the aircraft. Many tests were carried out to gain insight in each of these areas. Although numerical data was not collected, photography and videos were repeatedly analyzed to influence design and analysis decision making.



Figure 41: "The Ukraine" Glider in flight

6.3 Flight Testing

6.3.1 Prototype 1 Testing

The overall goal of prototype 1 testing was to ensure that all systems worked successfully in combination and that the aircraft followed desired characteristics in the areas of takeoff field length, speed, and maneuverability. The following shows the progression of testing:

- 1) High-speed taxi test
- 2) Takeoff to 20 feet altitude and land in a straight line
- 3) Takeoff to 30 feet altitude and make a turn maneuver, then land
- 4) Take off to 50 feet altitude and make a full oval then land.
- 5) Take off to any altitude, replicate AIAA DBF aircraft circuit, if successful, continue for 5 minutes, then land
- 6) Strenuous maneuver testing to test structural and stall capabilities.
- 7) Continue to follow Mock AIAA Competition with payloads 1 and 2 following the course.

6.3.2 Prototype 2 Testing

The goal of the second prototype was to have a completely competition ready aircraft. This meaning that this aircraft can complete missions set forth by the AIAA DBF competition multiple times over without failure. The second prototype will be flown as a competition aircraft and will participate in several mock competitions. Ground tests will be repeatedly performed to ensure that the aircraft will be well-equipped come competition time.

6.4 Check Lists

These checklists were created to ensure that proper safety and flight procedures were taken for all powered flights of the Beluga aircraft. They are inspired by a similar checklist [8] provided by the Central Massachusetts Remote Control Modelers (CMRCM) club as well as using the flight rules and procedures that are expected at the competition as stated in the rules.

Table 37: Aircraft Safety Checklists

Pre-Flight Checklist	Before Take Off
<input type="checkbox"/> Inspect aircraft exterior for damage <input type="checkbox"/> Inspect aircraft Interior for damage <input type="checkbox"/> Inspect landing gear <input type="checkbox"/> Inspect Aerodynamic surfaces for damage <input type="checkbox"/> Verify servos are secure and unobstructed <input type="checkbox"/> Control surfaces for damage <input type="checkbox"/> Verify battery voltage and check for swelling <input type="checkbox"/> Secure the battery in aircraft <input type="checkbox"/> Inspect motor and propeller <input type="checkbox"/> Verify ESC is connected <input type="checkbox"/> Inspect antenna for damages and proper arrangement <input type="checkbox"/> Verify receiver is wired and secured <input type="checkbox"/> Make sure the transmitter is programed and charged <input type="checkbox"/> Prepare the mission payload	<input type="checkbox"/> Connect Battery <input type="checkbox"/> Power on RX <input type="checkbox"/> Verify transmitter is connected <input type="checkbox"/> Verify servos are moving correctly <input type="checkbox"/> Secure mission payload <input type="checkbox"/> Close and secure doors and access points <input type="checkbox"/> Install arming Fuse <input type="checkbox"/> Verify propulsion <input type="checkbox"/> Connect Battery <input type="checkbox"/> Power on RX <div style="background-color: #800000; color: white; text-align: center; padding: 2px;">Post-Flight</div> <input type="checkbox"/> Remove arming Fuse <input type="checkbox"/> Power down RX <input type="checkbox"/> Power down Transmitter <input type="checkbox"/> Disconnect and remove batteries <input type="checkbox"/> Remove payload

6.5 Testing Schedule

Table 38: Flight-Testing Schedule of Completed Tasks

Ground and Flight Testing Schedule		
Test	Date	Objective
Propulsion Test	October 1 st , 2022	Gather propulsion data such as thrust and power consumption
Standing Glide Tests	October 23 rd , 2022	Gather idea of aircraft stability and CG
40 Foot Glide Testing	October 31 st , 2022	Examine aircraft stability with no control surfaces
Wind-Tunnel Test	November 20 th , 2022	Confirm aerodynamic lift data gathered from XFLR5
Taxi Testing	December 3 rd , 2022	Confirm aircraft structural integrity while taxing and thrusting
Mock Safety Check	December 10 th , 2022	Confirm aircraft safety for upcoming flight tests
Ground Mission Test	December 10 th , 2022	Confirm aircraft structure can withstand ground test loading case (2.5g)
Prototype 1 Flight Test #1	January 13 th , 2023	Taxi Tests, Attempt Mission 1
Prototype 1 Flight Test #2	January 27 th , 2023	Attempt Mission 1
Prototype 2 Flight Test #1	February 8 th , 2023	Attempt Missions 1 and 2
Prototype 3 Flight Test #1	February 10 th , 2023	Attempt Missions 1 and 2. Deduce flight speed, takeoff speed, takeoff and landing length. Mock competition.
WPI Internal Competition (Prototype #3)	February 18 th , 2023	Replicate AIAA competition.

7 Performance Results

7.1 Ground Testing Results

Ground tests were conducted in various locations, but primarily took place on or close to the Worcester Polytechnic Institute campus. Ground tests consisted of sub-system testing, aerodynamic testing, and full-aircraft taxi testing.

7.1.1 Range Testing Results

Institute Park was chosen for range testing due to its unobstructed sight lines. The test involved starting the radio transmitter and receiver together, then having the receiver move away from the transmitter while a servo on the receiver provided feedback on signal quality. The maximum safe operating distance was determined by measuring the distance at which there was any input lag or loss of actuation. The test resulted in a connection maintained up to 994.61ft (Fig. 42) with an RSSI of 55, indicating a safety factor of 1.55. Terrain limitations prevented further distance testing.

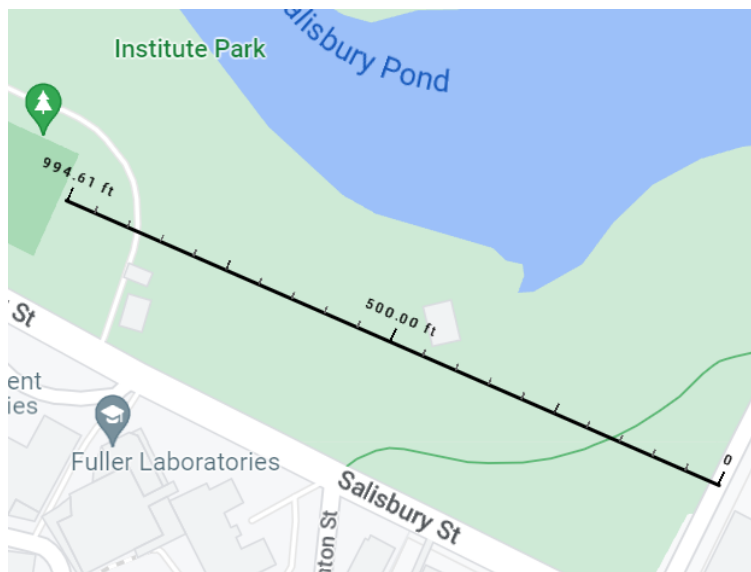


Figure 42: Range testing map at Institute Park, Worcester, MA

7.1.2 Wind Tunnel Testing Results

Wind tunnel tests on wing sections were executed to validate simulated aerodynamic performance. Due to size constraints a 1/3 scale model wing was manufactured for wind tunnel tests. Table 39 presents the lift of the wing at 0 degrees. As seen the lift generated at cruise velocity is 5.2 pounds which validates the 4308 modified airfoil shape in steady level flight. In addition, Table 40 indicates the lift generated at cruise velocity over a range of angle of attacks which again validates predicted airfoil performance calculated in section 3.4.2.

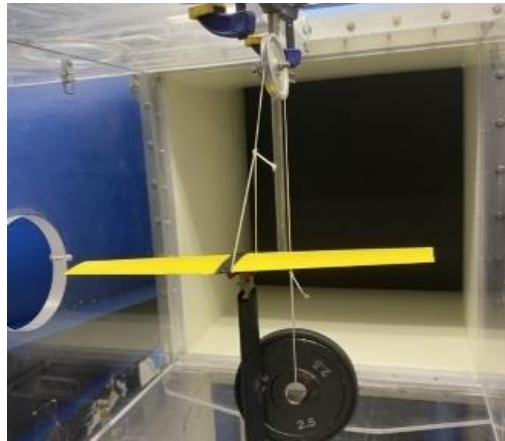


Figure 43: Wind Tunnel Testing Setup

Table 39: Experimental Lift Data at 0 AOA

0 degrees AOA	
Scale Airspeed	CL
28.8 ft/s	0.5159
38.5 ft/s	0.4752
48.1 ft/s	0.4285
52.9 ft/s	0.4242
57.7 ft/s	0.3918
60.1 ft/s	0.3756

Table 40: Lift as a function of Angle of Attack at Cruise Velocity

Varying Angle of Attack

Scale Airspeed	AOA	CL
60.1 ft/s	0	0.3756
60.1 ft/s	4	0.5547
60.1 ft/s	8	0.5909
60.1 ft/s	10	0.8364
60.1 ft/s	12	0.8899

7.2 Flight Testing Results

Flight testing results were computed from average times and distances of aircraft travel. Analysis of flight videos allowed for failure mode analysis to take place. A large portion of the iteration process was done by aggressive destructive testing of the aircraft in different loading environments. Performance of the aircraft in such maneuvers allowed for the next design to address weak points in previous prototypes. Prototype flight testing also allowed for the review of the aircraft by model aircraft professionals, who would make valuable input on the aircraft construction and flight. All flight tests were conducted at the Central Massachusetts RC Modelers Field, with the aircraft flown by AMA test pilot Randolph Holtgreffe.

7.2.1 Glider Performance – “The Ukraine”



Figure 44: Glider prototype tests of the aircraft.

Glider testing occurred in two locations: in a field or inside WPI’s Alden Hall. The standing level throw glide tests performed outside showcased the plane traveling in a straight path remaining parallel with the ground, validating the aerodynamic stability of the aircraft. The standing, upward throw glide test performed outside showcased the plane quickly traveling upward

before stalling and rolling to the left to a nosedive. The standing, downward glide tests performed outside showcased the plane yawing to the left while traveling mostly parallel to the ground. The level glide test performed inside at a height of 40ft showcased the plane traveling mostly straight and parallel to the ground, but pitched upward as the plane lost speed, stalling the plane shown in Figure 44. The final downwards glide test performed inside at a height of 40ft showcased the plane nosediving towards 15ft from the before climbing to about 22ft before stalling and crashing to the ground. Overall, all the glider tests were successful in validating all aerodynamic calculations. The tests also proved that the wings were durable in rolling collisions, while raising concerns for the alignment of the vertical stabilizer due to the aircraft veering to the left.

7.2.2 Prototype 1 Performance- “The Lizard”

Prototype 1 was tested on WPI’s rooftop field. The goal of this test was to taxi the aircraft and attempt to take off and fly a few feet off the ground. Telemetry, throttle, and controls all read well. During the taxi test it was noticed that the tail wheel was behaving oddly causing the aircraft to bank and turn seemingly at random. The aircraft was able to take off, however, only momentarily before rolling to the right and crashing on the ground. This caused a break in the fuselage of the aircraft by the tail attachment point as well as damage to the wing. Upon inspection of the aircraft, it was found that the vertical tail and rudder had sheared off during taxi, however, was still being held loosely in place by Monokote. When looking back at footage from the test it

could be seen that the tail had broken prior to take off. This is what caused the erratic movement of the rear wheel as well as the hard bank to the right once the aircraft took off.



Figure 45: Prototype one in uncontrolled roll before crashing

7.2.3 Second Prototype Performance – “Flappy Bird”

In the instance of the second flight test, all previous failure points were addressed. The rear fuselage section was modified with added support brackets, the belly of the plane was updated to 1/8 in plywood in place of 1/4 in balsa, and the vertical stabilizer was reinforced. The new wing prototype ended up being the demise of this plane, as the extreme wing deflection (shown in Figure 46) decreased aileron authority to the point that it was unable to pull out of a roll. Even after the crash landing, only a small section of the fuselage broke, along with a few spars in the left wing.



Figure 46: Prototype two showing extreme wing deflection.

A deflection test after flight confirmed that a 2.5 g load would produce deflection greater than 5 inches. This solidified the use of a D-tube with carbon-fiber supporting rods.

7.2.4 Final Aircraft Performance – “Beluga”

The final aircraft design iterates upon previous prototypes. Notably, the wing stiffness is addressed in two ways. The wing deflection was addressed by creating a box tube by wrapping 1/64” balsa sheet around the leading edge of both wings. In addition, deflection via the wing clamps were addressed by adding a carbon fiber rod which attaches through the fuselage and connects to both wings on the third airfoil rib. To maintain rules compliance the rod is not affixed to the fuselage. Further reinforcements to the tail boom connection were made by sistering 1/8”



Figure 47: Beluga in Flight

ply to the trailing edge of the fuselage where the tail piece is connected further strengthening the tail connection. Finally, an extended cowl was designed to replace the previously used top plate. This allowed for a relocation of the battery to above the wing clamps to adjust the CG. The initial test flight required small trim adjustment to all control surfaces to improve controllability, however, once electronically trimmed the aircraft performed well in level flight and in conventional attitudes in both the staging flight and payload flight.

The following aircraft performance breakdown summarizes the initial flight testing of the final model. Indicated weights are measured values. The cruise speed is estimated through analysis of the flown flight pattern and lap time achieved.

Table 41: Aircraft Performance Breakdown

Parameter	Mission 1	Mission 2	Mission 3
Takeoff Gross Weight	89.6 oz	120.00 oz	91.5 oz
Takeoff Distance	20 ft	50 ft	25 ft
Cruise Speed	66 ft/s	58.6 ft/s	63 ft/s
Lap Time	39.2 [s]	52 [s]	41.9 [s]
Flight Time	117.6 [s]	364 [s]	125.7 [s]
Max # of Laps	3	7	9

Note that lap time is estimated based off AIAA sanctioned flight path. In addition, the number of laps flown is estimated based on battery performance and lap time. Further, mission 3 performance is estimated based on predicted performance.

8 Conclusion

8.1 Summary

Design Group 2 placed 44th out of 99 teams at the 2023 Design, Build, Fly competition in Tucson, Arizona. This result was a culmination of months of planning and hard work by our team. At the start of the project in late August 2022, the team quickly divided itself into different roles which focused on different elements of the design process. Once the missions and rules were released by the AIAA, the team quickly got to work dissecting the rules and requirements in order to determine which design parameters to emphasize. After the basic aircraft characteristics were set, the team began extensive analysis to develop all components on the aircraft. This analysis is a culmination of design decisions, analysis, computer simulations, physical tests and advisor input which resulted in a conceptually sound aircraft. From these

concepts, a series of prototypes were developed and constructed in the lab. The team used various construction techniques from 3D printing PLA to laser cutting balsa wood to hand filing aluminum plates. Each iteration saw more sound construction and techniques which allowed for continuous improvement. The first had multiple issues that were made evident during the first flight attempt. After several redesigns and numerous flight tests, the team finally had a product that was ready to compete. The aircraft was shipped to the DBF flyoff competition in Tucson, Arizona and arrived late due to a shipping carrier error. As a result, the team completed the preflight tech inspection late. With two days remaining in the competition, the team attempted Mission 1 and failed due to touching down next to the runway during landing, After a reattempt, the team was able to complete Mission 1. Next, the team elected to perform the ground mission, for which the aircraft was able to carry an addition 5.5 lbs in addition to its maximum payload with a ground mission gross weight of 13 lbs. Next, the team attempted Mission 2, which involved flying with a payload. The aircraft attempted four take-offs for this mission, the first three attempts saw the aircraft barely exceed the 60ft takeoff requirement, resulting in failures. On the fourth attempt, the landing gear assembly snapped off the aircraft and rendered it inoperable. The team is satisfied with the outcome of the MQP, as 44th is the highest placement at a DBF by any WPI team to date.

8.2 Conclusions

The team considers its performance at the DBFcompetition a success; however, there is room for improvement in the future. As noted, at the competition the team passed tech inspection, completed the first flight mission and the ground mission. The aircraft has successfully completed most mission requirements in earlier mock competitions, proving its potential and airworthiness. The aircraft achieved a take-off distance of approximately 100 ft on the grass CMRCM field while carrying an electronics payload and carried the jamming antenna

without payload in these earlier competitions. In addition, an emphasis on aircraft speed was realized as seen by the cruise speed in excess of 45mph during test flights. Despite obstacles encountered at the DBF competition, the team has succeeded in designing and manufacturing an aircraft compliant with competition rules, and achieving the goals established at the beginning of the project.

8.3 Recommendations for Future Work

In the future, a greater focus on the structural components of the aircraft needs to be taken into consideration. A single, main structural member is something we considered that would have helped with the overall strength of the aircraft. At the competition, a few teams were able to apply over 750 lbs of added test weights during the ground mission by using a removable, single piece anhedral wing. An increased focus on the structural strength of the aircraft and its wings would have helped in this area.

An emphasis should be put on finding additional sponsorship or support for the DBF projects. The location of the competition needs to be taken into greater consideration, as it was found that the increased temperatures in Arizona had more of an impact on the aircraft's take-off than anticipated. We found that the use of our PLA printed parts eventually began to warp throughout the competition. Additional focus should be made on the aircraft's maneuverability, turn radius and acrobatic movement. This would have helped save time during the 360 degree turns in the flight course. Our team also put a lot of effort toward small improvements in drag reduction and weight saving.

8.4 Project Broader Impacts

Aligned with the theme of the AIAA DBF competition, the designed aircraft was intended for "Electronic Warfare" and has military implications. In response to the increasing use of small

portable UAVs in combat areas, the aircraft was designed as a counter-UAV solution, featuring a jamming antenna attachment to disrupt communication and control signals. The incorporation of such features enhances the military utility of the aircraft in hostile situations. Furthermore, the aircraft was designed with check bagged restrictions in mind, which enables the aircraft to be easily shipped via air to the United States' overseas allies. This design feature allows for convenient deployment of the aircraft to various combat zones while adhering to necessary transportation regulations. Overall, the design and engineering of the aircraft was tailored to address specific military needs in electronic warfare and transportation logistics. The aircraft's counter-UAV capability and check bagged restrictions are practical engineering solutions that offer significant military advantages.

The aircraft may also have other implications in different sectors other than the military. In the field of public health, this technology could be used for the efficient delivery of medical supplies to remote areas or disaster zones where traditional transportation methods are not feasible. The antenna on the wing tip could be used to collect data on the affected areas and transmit it back to medical professionals for analysis and response. This capability could be critical in providing timely and life-saving medical assistance. Additionally, the RC plane's search and rescue capabilities could help locate and save individuals in remote or difficult-to-access areas.

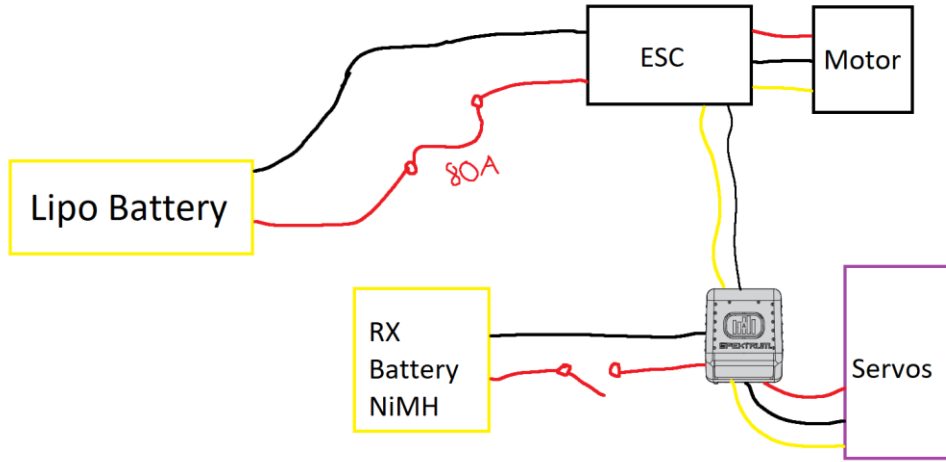
In the economic sector, the RC plane's payload capacity could be utilized for cargo delivery in areas where traditional transportation methods are not cost-effective. The antenna on the wing tip could be used to track the location of the plane during delivery, ensuring the safety and security of the cargo. The ability to deliver critical supplies efficiently and accurately could potentially open new markets for businesses and create job opportunities in areas previously inaccessible.

9 References

- [1] "2022-23 Design, Build, Fly Rules," American Institute of Aeronautics and Astronautics, 2022.
- [2] "Part 107 – Small Unmanned Aircraft Systems", Code of Federal Regulations, 15 October 2022.
<https://www.ecfr.gov/current/title-14/chapter-I/subchapter-F/part-107>
- [3] Raymer, D. P., "Aircraft Design: A Conceptual Approach," Sixth Edition, AIAA, 2018.
- [4] Lennon, A., "The Basics of RC Model Aircraft Design," Air Age Media, 1996.
- [5] "Aircraft Super Calculator, Holdfast Model Aero Club, retrieved 1 December 2022.
<http://holdfastmac.asn.au/technical-articles/supercalc/>
- [6] Fahad, E., "RC Plane Designing Calculations, Making, and Flight Test," retrieved 12 September 2022.
<https://www.electronicclinic.com/rc-plane-designing-calculations-making-and-flight-test/>
- [7] "Popular Servos (25) Database," RC Servo Specs and Reviews, retrieved 30 November 2022.
<https://servodatabase.com/>
- [8] "Winter Down-Time Aircraft Checklist." Central Massachusetts Radio Control Modelers, retrieved 5 December 2022. <https://www.cmrcm.org/>

10 Appendix

10.1 Appendix A: Wiring Diagram



10.2 Appendix B: Thrust-Drag MATLAB Code

T/W Calculations for the MQP Plane

```
clear all;
close all;
syms v
syms Speed
```

Definitions

```
W = 7; %Weight (lb) of aircraft w/ payload
S = 3.225; %Wing area (ft^2)
AR = 4.553^2/S %Aspect Ratio (ft)
e0 = 1.78*(1-0.045*AR^0.68)-0.64 %Oswald Efficiency
q = 1/2*0.0765*v^2; %dynamic pressure
C_D0 = 0.0215; %parasitic drag of plane
rho = 0.0765 %pressure
```

Fundamental T/W Equation

```
T_W = q*C_D0/(W/S)+(W/S)/(pi*AR*e0*q)
```

Simulated Thrust

```
T_sim = [5.68125    0;
5.63125          1.467;
5.575           2.934;
5.525           4.401;
5.475           5.868;
5.41875         7.335;
5.36875         8.802;
5.3125          10.269;
5.2625          11.736;
5.2125          13.203;
5.15625         14.67;
5.10625         16.137;
5.05            17.604;
5              19.071;
4.94375         20.538;
4.89375         22.005;
4.8375          23.472;
4.775           24.939;
4.71875         26.406;
4.65625         27.873;
4.6             29.34;
4.5375          30.807;
4.46875         32.274;
4.40625         33.741;
4.3375          35.208;
4.26875         36.675;
4.2125          38.142;
4.1375          39.609;
```



```

4.0625      41.076;
3.98125    42.543;
3.9         44.01;
3.8125     45.477;
3.71875    46.944;
3.625      48.411;
3.525      49.878;
3.41875    51.345;
3.325      52.812;
3.2125     54.279;
3.09375    55.746;
2.975      57.213;
2.85       58.68;
2.71875    60.147;
2.5875     61.614;
2.45625    63.081;
2.3125     64.548;
2.175      66.015;
2.025      67.482;
1.8875     68.949;
1.73125    70.416;
1.58125    71.883;
1.41875    73.35;
];

```

Measured Thrust Curve

```

T_meas =[7.06 0;
7.02 7.335;
6.97 14.67;
6.81 22.005;
6.69 29.34;
6.3 36.675;
6.15 44.01;
5.77 51.345;
5.41 58.68;
4.9 66.015;
4.39 73.35;
];

```

50% Throttle thrust values

```

T_50 =[7.06/1.8 0;
7.02/1.8 7.335;
6.97/1.8 14.67;
6.81/1.8 22.005;
6.69/1.8 29.34;
6.3/1.8 36.675;
6.15/1.8 44.01;
5.77/1.8 51.345;
5.41/1.8 58.68;
];

```

```
4.9/1.8 66.015;  
4.39/1.8 73.35;  
];
```

V_Stall

```
CL_max = 1.31;  
V_stall = sqrt(2*(W/S)/(rho*CL_max))
```

New Drag Plot

```
C_Dindf = W^2/(0.5*rho*Speed^2*S)^2/(pi*AR*e0);  
C_D0 = 0.0211;  
C_Daf = C_D0+C_Dindf;  
D_af = C_Daf*0.5*rho*Speed^2*S;
```

Thrust Curve

```
T = T_W*W;  
U = vpa(subs(T,v,58)) %calculated thrust  
% plot(Speed,D)  
fplot(D_af,[3 6.5816], '--', 'color', 'b')  
hold on  
fplot(D_af,[6.5816 100], 'color', 'b')  
ylim([0 9])  
title('Thrust-Drag Curve')  
xlabel('Air speed (ft/s)')  
ylabel('Force (lbf)')  
hold on  
% plot(T_sim(:,2),T_sim(:,1))  
plot(T_meas(:,2),T_meas(:,1), 'color', 'r')  
hold on  
plot(T_50(:,2),T_50(:,1), 'color', 'g')  
hold on  
  
% yline(8.92, 'color', 'r')  
legend({'Calculated Drag', 'Measured Thrust(100% Throttle)', '50% Throttle Thrust'}, 'Location', 'northeast')  
xlim([0.0 100])  
ylim([0.0 8])  
zlim([-1.00 1.00])  
  
legend({'', 'Calculated Drag', 'Measured Thrust(100% Throttle)', 'Measured Thrust(50% Throttle)'})  
legend('Position', [0.53961, 0.17032, 0.34353, 0.15674])
```

Thrust/Weight Value at 40mph (58 ft/s)

```
vpa(subs(T_W,v,58));
```

Actual Thrust/Weight Value

```
x = 5.41/7 %w/ payload
```

```
y = 5.41/4.9 %w/o payload
```

Power/W

```
P = 750/7 %w/ payload
```

```
P = 750/4.9 %w/o payload
```

10.1 Appendix C: Dynamic Stability MATLAB Code

```
clear all; close all; clc;
format long g
%% Given Dimensions and Variables
b = 50.64/12;
c = 8.685/12;
S = 439.8084/144;
S_t = 94.4/144;
AR_w = 5.83074266;
AR_t = 2.842207627;
W = 6.61;
h = .22;
h_ac = 0.643638457;
l_t= 20.7/12;
e = 0.951;
Jy = 514;
C_d0 = 0.0192;
M = 0.052551;
rho = 0.08071935302495548;
u_0= 704.04/12;
V = u_0;
n_H = 0.414270463;
V_H= 0.588187254;
a_t= 6.283185307/12;
a_w = 0.059/12;
dE_da = 0; %need
theta_star = 0; %need
g = 386/12;
m=W;
%
%% Static Margin
% We aim to hit a 10% static margin for static stability
%Calculated by Tyler and Nick

%% Dynamic Stability Analysis
%% Lift and Drag Stability Derivatives
a = a_w*(1+(a_t/a_w)*(S_t/S)*(1-(dE_da)));
C_Ltrim = W/(1/2*rho*u_0^2*S);
C_Lu = M^2/(1-M^2)*C_Ltrim;
C_La = a;
C_Ladot = 2*a_t*n_H*V_H*(1-dE_da);
C_Lq = (AR_w+2)/(2+AR_w*sqrt(1-M^2))*(1/2+2*(l_t/c))*a_w+2*a_t*n_H*V_H;
C_Dtrim = C_d0+(C_Ltrim^2/(pi*AR_w*e));
C_Du = 0;
C_Da = (2*C_Ltrim)/(pi*AR_w*e)*a;
%
%% Non-dimensional derivatives
C_Xu = -(C_Du+2*C_Dtrim);
C_Xa = -(C_Da-C_Ltrim);
C_Xq = 0;
C_Xadot = 0;

C_Zu = -(C_Lu+2*C_Ltrim);
C_Za = -(C_La-C_Dtrim);
```

```

C_Zq = -C_Lq;
C_Zadot = -C_Ladot;

C_Mu = 0;
C_Ma = a*(h-h_ac)-a_t*V_H*(1-dE_da);
C_Madot = -2*a_t*n_H*(V_H*l_t/c)*dE_da;
C_Mq = -2*a_t*n_H*(V_H*l_t/c);
%
%% Longitudinal dimensional derivatives
Xw = 0.5*rho*V*S*C_Xa;
Xu = 2*W/V*sin(theta_star)+0.5*rho*V*S*C_Xu;
Xq = 0.25*rho*V*S*c*C_Xq;
Xwdot = 0.25*rho*S*c*C_Xadot;

Zu = -2*(W/V)*cos(theta_star)+0.5*rho*V*S*C_Zu;
Zw = -0.5*rho*V*S*(C_Dtrim+C_La);
Zq = -0.25*rho*V*S*c*C_Lq;
Zwdot = -0.25*rho*S*c*C_Ladot;
%   Zde = -0.5*rho*V^2*S*C_Lde;
Zdp = 0;

Mu = 0.5*rho*V*S*c*C_Mu;
Mw = 0.5*rho*V*S*c*C_Ma;
Mq = 0.25*rho*V*S*c^2*C_Mq;
Mwdot = 0.25*rho*S*c^2*C_Madot;
%   Mde = 0.5*rho*V^2*S*c*C_Mde;
%   Mdp = 0.5*rho*V^2*S*c*C_Mdp;
%% Longitudinal A Matrix Variables
A11 = Xu/W;
A12 = Xw/W;
A13 = 0;
A14 = -g*cos(theta_star);
A15 = 0;
A21 = Zu/(m-Zwdot);
A22 = Zw/(m-Zwdot);
A23 = (Zq+m*V)/(m-Zwdot);
A24 = -m*g*sin(theta_star)/(m-Zwdot);
A25 = 0;
A31 = (Mu+Mwdot*Zu)/Jy;
A32 = (Mw+Mwdot*Zw)/Jy;
A33 = (Mq+Mwdot*(Zq+m*V))/Jy;
A34 = -Mwdot*m*g*sin(theta_star)/Jy;
A35 = 0;
A41 = 0;
A42 = 0;
A43 = 1;
A44 = 0;
A45 = 0;
A51 = -sin(theta_star);
A52 = cos(theta_star);
A53 = 0;
A54 = -V*cos(theta_star);
A55 = 0;
%
%% Longitudinal A Matrix

```

```

A1 = [Xu Xw 0 -g*cosd(theta_star);
      Zu/(1-Zwdot) Zw/(1-Zwdot) V+Zq/(1-Zwdot) -g*sind(theta_star)/(1-Zwdot);
      Mu+Mwdot*Zu/(1-Zwdot) Mw+Mwdot*Zw/(1-Zwdot) Mq+(V+Zq)*Mwdot/(1-Zwdot) -
      Mwdot*g*sind(theta_star)/(1-Zwdot);
      0 0 1 0];
fprintf("The Longitudinal A Matrix is:")
A1
EIGEN = eig(A1)
%
P=poly(A1); disp(P);
R = roots(P); disp(R)
[Wn,Z]=damp(R);

fprintf("Damping")
disp(Z)

fprintf("Natural Freq")
disp(Wn)
% [V, D]=eig(A1);
% disp(V)
Wd1 = Wn(2)*sqrt(1-Z(2)^2)
Wd2 = Wn(4)*sqrt(1-Z(4)^2)

%Plotting the Modes onto a real imaginary plot
N = [-1.0659 10.405;
     -1.0659 -10.405]; %short period
N2 = [-0.137 0.476;
      -0.137 -0.476]; %phugoid

figure(1)
plot(N(:,1),N(:,2),'.','Marker','+')
hold on
plot(N2(:,1),N2(:,2),'.','Marker','x')
ylabel('Imaginary part of root')
xlabel('Real part of root')
xlim([-3 2])
ylim([-20 20])
xline(0)
yline(0)
legend({'Short-period','Phugoid mode',' ',''},'Location','northeast')
hold off

figure(2)
syms t
y = e^(0.102*10.46*t)*(cosd(Wd1*t)+sind(Wd1*t))
fplot(y)
xlim([0 125])
ylim([-1.5 1.5])
title('Short-Response Mode')
ylabel('Pitch Angle (deg)')
xlabel('Time (s)')
xline(0)
yline(0)

figure(3)

```

```

h = e^(0.27*0.49*t)*(cosd(Wd2*t)+sind(Wd2*t))
fplot(h)
xlim([0 1000])
ylim([-1.5 1.5])
title('Phugoid Mode')
ylabel('Pitch Angle (deg)')
xlabel('Time (s)')
xline(0)
yline(0)

%Periods
Tsp = 2*pi/Wd1
Tph = 2*pi/Wd2

```

10.2 Appendix D: Full Aircraft Drag and Aircraft Dynamics MATLAB Code

```

%Defining design velocity for the entire aircraft

```

```

Design_velocity = 66; %ft/s (close to ~40 mph)

```

```

%FOR RC AIRCRAFT WING

```

```

t_w = 0.0877; %t/c value

```

```

x_c_max = 0.2929; %x/c maximum

```

```

e = 0.8;

```

```

AR = 6.43; %aircraft aspect ratio

```

```

%Defining the geometry of the profile in 2D

```

```

Table1 = readtable("4308_coordinates.xlsx");

```

```

%Span (or length) of the prospective element being analyzed

```

```

Span_wing = 54.64; %inches

```

```

%Defining the chordlength of the prospective element being analyzed.

```

```

Chord_wing = 8.65; %inches %Mean aerodynamic chord

```

```

S_ref = Span_wing*Chord_wing; %universal reference planform area

```

```

Wetted_Surface_Area_Wing = Wetted_Surface_Area(Table1, Span_wing, Chord_wing);

```

```

Local_Reynolds_Number_Wing = Local_reynolds_number(Chord_wing, Design_velocity);

```

```
Skin_friction_Wing = Skin_friction_coefficient(Local_Reynolds_Number_Wing);
```

```
%Form Factor representing a pressure drag contribution  
%%Replace in future with CFD or wind-tunnel testing%%
```

```
FF_wing = 1 + 0.6*t_w/(x_c_max) + 100*t_w^4;
```

```
Cd_0_wing = FF_wing*Skin_friction_Wing*Wetted_Surface_Area_Wing/(S_ref);
```

```
%%%%%%%%%%%%%%%%%%%%%%%%%%%%%%%%%%%%%%%%%%%%%%%%%%%%%%%%%%%%%%%%%%%%%%%%  
%%%%%%%%%%%%%%%%%%%%%%%%%%%%%%%%%%%%%%%%%%%%%%%%%%%%%%%%%%%%%%%%%%%%%%%%
```

```
%FOR RC AIRCRAFT BODY
```

```
t_b = 0.14;
```

```
x_c_max_b = 0.2929;
```

```
%Defining the geometry of the profile in 2D
```

```
Table2 = readtable("NACA 0014.dat.xls");
```

```
%Span (or length) of the prospective element being analyzed
```

```
Span_body = 4; %inches
```

```
%Defining the chordlength of the prospective element being analyzed.
```

```
Chord_body = 28.58; %inches %Mean aerodynamic chord
```

```
Wetted_Surface_Area_Body = Wetted_Surface_Area(Table2, Span_body,  
Chord_body)*1.2;
```

```
Local_Reynolds_Number_Body = Local_reynolds_number(Chord_body, Design_velocity);
```

```
Skin_friction_Body = Skin_friction_coefficient(Local_Reynolds_Number_Body);
```

```
%Form Factor representing a pressure drag contribution
```

```
%%Replace in future with CFD or wind-tunnel testing%%
```

```
FF_body = 1 + 0.6*t_b/(x_c_max_b) + 100*t_b^4;
```

```
Cd_0_body = FF_body*Skin_friction_Body*Wetted_Surface_Area_Body/(S_ref);
```



```
%%%%%%%%%%%%%%%%%%%%%%%%%%%%%%%%%%%%%%%%%%%%%%%%%%%%%%%%%%%%%%%%%%%%%%%%
%%%%%%%%%%%%%%%%%%%%%%%%%%%%%%%%%%%%%%%%%%%%%%%%%%%%%%%%%%%%%%%%%%%%%%%%
```

```
%FOR RC AIRCRAFT Tail (Horizontal)
```

```
%Defining the geometry of the profile in 2D
```

```
%Span (or length) of the prospective element being analyzed
```

```
Span_horz_tail = 16.38; %inches
```

```
%Defining the chordlength of the prospective element being analyzed.
```

```
Chord_horz_tail = 5.45; %inches %Mean aerodynamic chord
```

```
t_ht = (1/8)/(Chord_horz_tail);
```

```
Wetted_Surface_horz_tail = 2*Span_horz_tail*Chord_horz_tail +  
(1/8)*Span_horz_tail;
```

```
Local_Reynolds_Number_horz_tail = Local_reynolds_number(Chord_horz_tail,  
Design_velocity);
```

```
Skin_friction_horz_tail =  
Skin_friction_coefficient(Local_Reynolds_Number_horz_tail);
```

```
%Form Factor representing a pressure drag contribution
```

```
%%Replace in future with CFD or wind-tunnel testing%%
```

```
FF_horz_tail = 1 + 0.6*(t_ht)/(0.2929) + 100*t_ht^4;
```

```
Cd_0_horz_tail =
```

```
FF_horz_tail*Skin_friction_horz_tail*Wetted_Surface_horz_tail/(S_ref);
```

```
%%%%%%%%%%%%%%%%%%%%%%%%%%%%%%%%%%%%%%%%%%%%%%%%%%%%%%%%%%%%%%%%%%%%%%%%
%%%%%%%%%%%%%%%%%%%%%%%%%%%%%%%%%%%%%%%%%%%%%%%%%%%%%%%%%%%%%%%%%%%%%%%%
```

```
%FOR RC AIRCRAFT Tail (Vertical)
```

```
%Defining the geometry of the profile in 2D
```

```
%Span (or length) of the prospective element being analyzed
```

```
Span_vert_tail = 6.4; %inches
```

```
%Defining the chordlength of the prospective element being analyzed.
```

```
Chord_vert_tail = 4.35; %inches %Mean aerodynamic chord
```

```
t_vt = (1/8)/(Chord_vert_tail);
```

```
Wetted_Surface_vert_tail = 2*Span_horz_tail*Chord_vert_tail +  
(1/8)*Span_vert_tail;
```

```
Local_Reynolds_Number_vert_tail = Local_reynolds_number(Chord_vert_tail,  
Design_velocity);
```

```
Skin_friction_vert_tail =
```

```
Skin_friction_coefficient(Local_Reynolds_Number_vert_tail);
```

```
%Form Factor representing a pressure drag contribution
```

```
%%Replace in future with CFD or wind-tunnel testing%%
```

```
FF_vert_tail = 1 + 0.6*(t_vt)/(0.2929) + 100*t_vt^4;
```

```
Cd_0_vert_tail =
```

```
FF_vert_tail*Skin_friction_vert_tail*Wetted_Surface_vert_tail/(S_ref);
```

```
%%COMPILING FINAL RESULTS
```

```
%[{''}, {'Planform Area (in^2)'}, {'Wetted Area (in^2)'}, {'Reference Length'},  
{'Cd_0'}, {'Skin Friction, C_f'}];%...
```

```
A = [ Span_wing*Chord_wing, Wetted_Surface_Area_Wing, Chord_wing, Cd_0_wing,  
Skin_friction_Wing;...
```

```
Span_body*Chord_body, Wetted_Surface_Area_Body, Chord_body, Cd_0_body,  
Skin_friction_Body;...
```

```
Span_horz_tail*Chord_horz_tail, Wetted_Surface_horz_tail, Chord_horz_tail,  
Cd_0_horz_tail, Skin_friction_horz_tail;...
```

```
Span_vert_tail*Chord_vert_tail, Wetted_Surface_vert_tail, Chord_vert_tail,  
Cd_0_vert_tail, Skin_friction_vert_tail];
```

```
Results = array2table(A,...
```

```
'VariableNames',{ 'Planform Area (in^2)', 'Wetted Area (in^2)', 'Reference  
Length', 'Cd_0', 'Skin Friction, C_f'});...
```

```
'RowNames', { 'Wing', 'Body', 'Horizontal tail', 'Vertical tail'})
```

```
%TEMPORARILY ADDING ARBITRARY WHEEL Cd0 Calcs
Cd_0_typical = 1.01; % assumed from "Fluid Dynamic Drag" and will be scaled to
the planform area
```

```
%wheel radius and number of front and back wheels
r_front_wheel = 1.5; % inches
r_dragger = 0.25; % inches
```

```
front_wheels = 2; % number of front wheels
back_wheels = 1; % number of back wheels
```

```
Cd_0_landing = front_wheels*Cd_0_typical*r_front_wheel/S_ref +
back_wheels*Cd_0_typical*r_dragger/S_ref;
```

```
% ARBITRARY ENGINE Cd0 calcs
engine_frontal = 4; %in^2
Cd_0_arbitrary = 0.34;
```

```
%Scaling Cd_0 based upon that experimental data
Cd_0_engine = Cd_0_arbitrary*engine_frontal/S_ref;
```

```
Cd_0_total = Cd_0_wing + Cd_0_vert_tail + Cd_0_horz_tail + Cd_0_body +
Cd_0_landing + Cd_0_engine
```

```
hold on
[Cl, Cd] = fplot(@(x) Cd_0_total + x^2*(1/(pi*AR*e))+ 0.034*(x - 0.6)^2, [0,
1.5], 'red')
```

```
L_D_ratio = [];
i=1;
while i <=45
L_D_ratio(i) = Cl(i)/Cd(i);
i= i + 1;
```

```
end
```

```
yyaxis right  
ylabel('Lift-Drag Ratio')
```

```
xlabel('Coefficient of Lift, Cl')
```

```
plot(Cl, L_D_ratio, 'blue')
```

```
yyaxis left  
ylabel('Coefficient of Drag, Cd')
```

```
fplot(@(x) Cd_0_total + x^2*(1/(pi*AR*e)) + 0.034*(x - 0.6)^2, [0, 1.5], 'red')
```

```
hold off
```

```
%Defining the maximum coefficient of lift for the modified 4308 wing
```

```
%section
```

```
%%Will correct for finite wing effects using C = the below
```

```
C = AR/(2+sqrt(4+AR^2));
```

```
% Accounting now for body aspect ratio and also correcting for finite  
% lifting body effects
```

```
AR_body = 16/25;
```

```
C1 = AR_body/(2+sqrt(4+AR_body^2));
```

```
Cl_a_wing = C*(1.35-0.39)/12 %at angle of attack of 12 degrees
```

```
Cl_a_body = C1*(1.15-0)/12 %at an angle of attack of 12 degrees
```

```
%now Cl_max of the full body is known at 12 degrees. To get in a safer  
%margin we must find Cl_a_new that is corrected for finite wing effects on  
%the entire lifting body
```

```
%Now choosing a safety factor to avoid stall, we can find a Cl_max_full  
%that will serve our purpose
```

```
% choosing landing gear mounting angle of 10 degrees
```

```
Cl_10_deg = (Cl_a_wing)*10 + 0.39;
```

```
yyaxis left
```

```
fplot(@y) (Cl_a_wing + Cl_a_body)*y -Cl_a_body + 0.39, [0,15])
```

```
xlabel('Angle of Attack, alpha')
```

```
ylabel('Coefficient of Lift, Cl')
```

```
yyaxis right
```

```
Weight = 7; %lbs
```

```
S = (Span_wing)/12;
```

```
rho = 0.07072;
```

```
Roll_friction = 0.03;
```

```
V_takeoff = 0.7*sqrt((2*Weight)/((S*(rho/32)*0.8*Cl_10_deg)))
```

```
C_l_10_degrees = Cl_10_deg
```

```
C_d_10_degrees = (Cd_0_total + C_l_10_degrees^2*(1/(pi*AR*e)) +  
0.034*(C_l_10_degrees - 0.6)^2)
```

```
Lift = 0.5*rho*S*V_takeoff^2*C_l_10_degrees/32.2
```

```
Drag = 0.5*rho*S*V_takeoff^2*C_d_10_degrees/32.2
```

```
Thrust = 2.5;
```

```
a = (32.2/Weight)*((Thrust - Drag) - 0.015*(Weight - Lift))
```

```
%a_mean =
```

```
S_ground_roll = V_takeoff^2/(2*a)
```

```
Rate_Climb_Takeoff = ((Thrust - Drag)*V_takeoff/0.7)/(Weight)
```

```
10.2.1.1 %%Looking at parameters for cruise
```

```
V_cruise = 58.67;
```

```
Cl_1_deg = (Cl_a_wing)*1 + 0.39;
```

```
C_l_1_degrees = Cl_1_deg
```

```
C_d_1_degrees = Cd_0_total + C_l_1_degrees^2*(1/(pi*AR*e)) + 0.034*(C_l_1_degrees  
- 0.6)^2
```

```
Lift_Cruise = 0.5*rho*S*V_cruise^2*C_l_1_degrees/32.2
```

```
Drag_cruise = 0.5*rho*S*V_cruise^2*C_d_1_degrees/32.2
```

```
Lift_fullspeed_ground = 0.5*rho*S*V_cruise^2*C_l_10_degrees/32.2
```

```
Drag_fullspeed_ground = 0.5*rho*S*V_cruise^2*C_d_10_degrees/32.2
```

```
V_store = [];
```

```
Drag_comp = [];
```

```
Lift_comp = [];
```

```
V=1;
```

```
i=1;
```

```
while V < 80 %ft/s
```

```
V_store(i) = V;
```

```
Lift_comp(i) = 0.5*rho*S*V^2*C_l_1_degrees/32.2;
```

```
Drag_comp(i) = 0.5*rho*S*V^2*C_d_1_degrees/32.2
```

```
V = V+1;  
i = i+1;
```

```
end
```

```
X = [V_store;Drag_comp]
```

```
figure(2)
```

```
hold on
```

```
ylabel('Drag (lbf)')
```

```
xlabel('Velocity (ft/s)')
```

```
plot(V_store, Drag_comp, 'blue')
```

```
Table_thrust = readtable("Book1.xlsx");
```

```
thrust = table2array(Table_thrust);
```

```
Velocity = thrust(:,1)*1.4667
```

```
Thrust = thrust(:,2)/16
```

```
plot(Velocity, Thrust, 'red')
```

```
ylabel('thrust (lbf)')
```

```
xlabel('Velocity (ft/s)')
```

```
hold off
```

```
function F = Wetted_Surface_Area(Table, span, chord)
```

```
%changing the coordinates in the dat file to a usable array formatting
```

```
Coords = table2array(Table);
```

```
l = height(Table);
```

```
w = width(Table);
```

```
length = [];
```

```
i = 1;
```

```

while i < l
    y2 = Coords(i+1, 2)*chord;
    y1 = Coords(i, 2)*chord;
    x2 = Coords(i+1, 1)*chord;
    x1 = Coords(i, 1)*chord;

    %Finding the distance in between points
    length(i) = sqrt((x1-x2)^2+(y1-y2)^2);

    i = i+1;
end

%Approximating area by adding the length of all panels and multiplying by
%the span
F = sum(length)*span;
end

%%%%%%%%%%%%%%%%%%%%%%%%%%%%%%%%%%%%%%%%%%%%%%%%%%%%%%%%%%%%%%%%%%%%%%%%
%%%%%%%%%%%%%%%%%%%%%%%%%%%%%%%%%%%%%%%%%%%%%%%%%%%%%%%%%%%%%%%%%%%%%%%%
% function intakes chord in inches and velocity in ft/s to calculate the
% local part reynolds number
function R = Local_reynolds_number(chord, velocity)

%dynamic viscosity of air at sea level (A/C not performing high-altitude
%flight)
mu = 0.3766*10^-6*(1/144); %lbf*s/in^2

%Density of air at sea level conditions (nneglecting altitude change)
rho = 0.0004054385345; %lbm/in^3

%need to convert velocity to in/s

```



```
velocity = velocity*(1/12);
```

```
%reynolds number calculation taking into account the local velocity and  
%chordlength
```

```
R = rho*chord*velocity/32.2/mu;
```

```
end
```

```
%%%%%%%%%%%%%%%%%%%%%%%%%%%%%%%%%%%%%%%%%%%%%%%%%%%%%%%%%%%%%%%%%%%%%%%%  
%%%%%%%%%%%%%%%%%%%%%%%%%%%%%%%%%%%%%%%%%%%%%%%%%%%%%%%%%%%%%%%%%%%%%%%%
```

```
function Cf = Skin_friction_coefficient(Re)
```

```
if Re > 10^6
```

```
    Cf = 0.074/(Re^0.2);
```

```
elseif 10^6 > Re && Re > 5*10^5
```

```
    Cf = 0.455/((log10(Re))^2.58) - (1700/Re);
```

```
elseif Re < 5*10^5
```

```
    Cf = 1.328/sqrt(Re);
```

```
else
```

```
    print("error")
```

```
end
```

```
end
```